# Mars One


| | | | |
|---|---|---|---|
| S. Brajović | 4110501 | W.P.K.M. Mulkens | 4116895 |
| A. Flinkerbusch | 4058968 | I.V. van der Peijl | 4079272 |
| M.R. Hogenboom | 4016157 | R.M. Werner | 4110498 |
| J.G.P. de Jong | 4001532 | A. Živolić | 4110331 |
| H. Lin | 4111842 | | |


Final Report

Design Synthesis Excercise

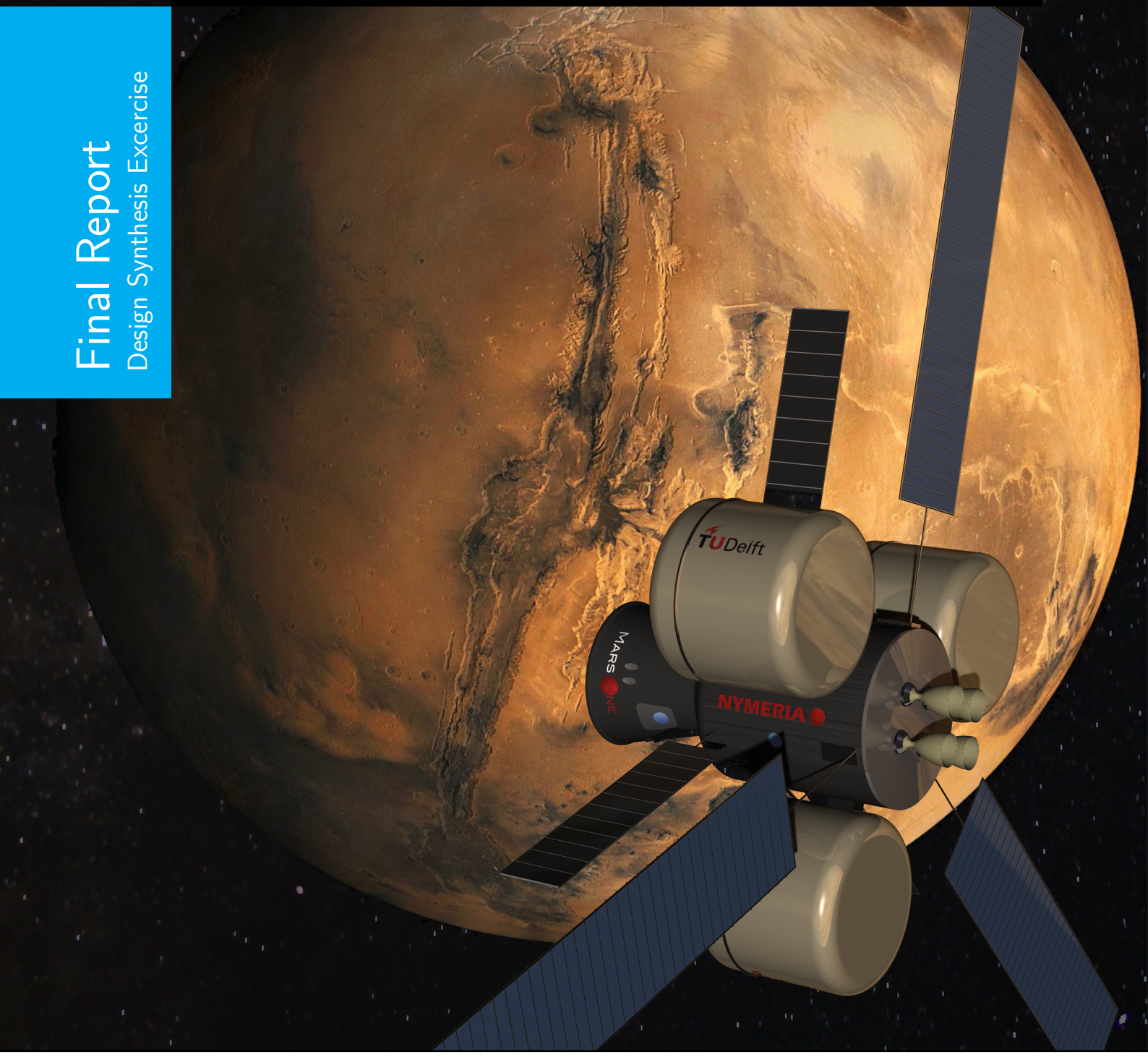



TU Delft Delft University of Technology

Faculty of Aerospace Engineering


July 2, 2013

# Preface

The Mars One initiative is determined to put the first humans on the surface of Mars. Furthermore, it aims to create a permanent human colony on Mars by providing a one-way transportation service to the red planet as early as 2023. In order to help with the realization of this, DSE group 8 aims to investigate the feasibility of such a mission and provide technical solutions which can be used to solve the most challenging issues of the manned exploration and colonization of Mars.

As discussed in the Baseline Report, the requirements and the functions of the mission itself have been specified, a literature study was done and the human and technical resources for the product have been budgeted. In the Mid-Term Report multiple design solutions were investigated and a trade-off was made to identify the optimal mission design, which was a single use transportation vehicle powered by a chemical propellant. In this Final Report the chosen design will be elaborated on in more detail within the scope of this DSE project, which is Phase A level design.

Group 8 recognizes the support of and wishes to thank head tutor ir. M. Naeije, assistant tutor Dr. ir. E. Mooij as well as the coaches, Dr. L. Guadagni and ir. J.A. Pascoe for their help and guidance provided throughout this DSE project. We also want to thank ir. M.H.J. Lemmen, ir. R. Noomen, ir. B.T.C. Zandbergen, Dr. G. Ridolfi, Dr. D. Stam, ir. K. Kumar and Dr. A. Cervone for their contribution to this report.

# Summary

The objective of this DSE Final Report is to present a feasibility study (Phase A) for both the Piloted Transfer Vehicle (PTV) and the Mars Lander (ML) that serve as the main transportation and landing system for the first manned mission to Mars (Mars One), respectively. The design concept presented in this report establishes the foundation for any further, Phase-B design efforts.

Following the definition and trade-off of multiple concepts in the Mid-Term phase, a single-use mission concept was chosen as the most feasible option to fulfill the requirements of the Mars One mission. Therefore, a more detailed design has been conducted in order to identify further design challenges and necessary subsystem designs. The required functions were analyzed and the mission design was started from the baseline design, upon which a first design iteration has been performed.

The detailed design process started by investigating an optimal interplanetary transfer trajectory, which best suits the mission requirements. Consequently, a slow, but efficient trajectory was optimized and the time of flight set to 312 days and a date of departure of the 11th of October 2026. From the velocity change required for this trajectory the needed propellant mass was estimated, which allowed for the sizing of the complete vehicle.

Following this, all the subsystems were designed in detail. This was done separately, but with consideration for the subsystems' interactions and compliance at the system level. Therefore, the subsystems had to be designed simultaneously, as they use each other's outputs as input. The chemical propulsion system was sized to allow for the chosen trajectory, with the trajectory requirements derived from crew safety, which include radiation concerns addressed by the life support system and the structural aspect of the spacecraft. To perform the atmospheric entry and landing phase, a specialized Mars Lander has been designed, which will form part of the Mars base upon arrival on Mars. Through all these subsystems, a verification and validation process is intertwined, ensuring the resulting designs have been correctly defined and perform their purpose in a satisfactory way. Great care has been put in the safety of the mission, which is reflected on in the PTV structure, life support and orbit.

Finally, the resulting final design is presented and conclusions on the design process are shown, while the development logic is explained in more detail. The total PTV mass is 24 $t$, with 120 $t$ of propellant. The ML has a mass of 4.0 $t$, giving a total system mass of 149 $t$. A detailed cost analysis of this design was also carried out, with the total cost of a cycle of three manned missions to Mars being €23.55 billion, of which €14.56 billion is development cost. The report ends with recommendations for improving the design, and further project planning for subsequent design phases.

# Contents


**1 Introduction** **1**

**2 Functional Analysis** **2**

**3 PTV Baseline Design** **4**
3.1 Sizing Approach . . . . . 4
3.1.1 Sizing iteration method . . . . . 4
3.2 Configuration . . . . . 7
3.3 Conclusion and Recommendations . . . . . 8

**4 Astrodynamic Characteristics** **9**
4.1 Assumptions . . . . . 9
4.2 Hohmann Transfer Trajectory . . . . . 10
4.3 Sensitivity Analysis . . . . . 11
4.4 Interplanetary Transfer Trajectory - Lambert's Problem . . . . . 12
4.4.1 Solution of Lambert's Problem - Porkchop Plot . . . . . 13
4.5 End-of-mission Mars orbital Maneuvers . . . . . 15

**5 PTV Propulsion System** **16**
5.1 Requirements and Design Considerations . . . . . 16
5.2 Engine Mass and Sizing . . . . . 16
5.3 Propellants . . . . . 17
5.4 Pressure Levels for the Engine and Feed System . . . . . 19
5.5 Engine Cycle . . . . . 21
5.6 Cooling Approach . . . . . 22
5.7 Engine Balance . . . . . 22
5.8 Thrust Vector Control TVC and Structural Mounts . . . . . 23
5.9 Propellant Storage . . . . . 23

**6 Environmental Control & Life Support System** **26**
6.1 Atmosphere Revitalization . . . . . 26
6.1.1 Carbon Dioxide Removal . . . . . 26
6.1.2 Oxygen . . . . . 28
6.2 Monitoring the atmosphere . . . . . 28
6.3 Food, Water & Waste Management . . . . . 29
6.4 Crew Quarters . . . . . 29
6.5 Summarizing . . . . . 30
6.6 Mars Lander ECLSS . . . . . 31
6.7 Verification & Validation . . . . . 32

6.8 Sensitivity Analysis . . . 32
6.9 Conclusion & Recommendations . . . 33

**7 Spacecraft Structural Design** **34**
7.1 PTV Structural Design . . . 34
7.1.1 Shielding against Micro-meteoroids and Orbital Debris . . . 34
7.1.2 Sizing for Pressurization Loads . . . 36
7.1.3 Sizing for Compressive Launch Loads . . . 37
7.1.4 Resistance against Vibration Loads . . . 43
7.2 Propellant Tank Structural Design . . . 43
7.2.1 Shielding against MMOD . . . 43
7.2.2 Sizing for Pressurization . . . 44
7.2.3 Sizing for Launch Loads . . . 44
7.2.4 Material Selection . . . 45
7.2.5 Thermal Property Considerations . . . 45
7.2.6 Resistance against Vibration Loads . . . 46
7.3 Summary, Conclusion and Recommendations . . . 47

**8 Thermal control subsystem** **48**
8.1 Thermal requirements . . . 48
8.2 Thermal environment . . . 49
8.2.1 Solar radiation . . . 49
8.2.2 Planetary radiation . . . 49
8.2.3 Internal heat emission . . . 49
8.3 Thermal analysis . . . 50
8.4 Passive thermal control . . . 51
8.5 Active thermal control . . . 51
8.5.1 Thermostatically controlled heaters . . . 51
8.5.2 Variable external radiation devices . . . 51
8.5.3 Thermoelectric cooling . . . 51
8.6 Conclusion and recommendations . . . 52

**9 Communications Subsystem** **53**
9.1 Layout . . . 53
9.2 Sizing . . . 53
9.3 Conclusion . . . 54

**10 Guidance, Navigation and Attitude Control** **56**
10.1 Transfer Vehicle Requirements . . . 56
10.2 Transfer Vehicle Attitude Determination and Control System . . . 57
10.2.1 Hardware sizing . . . 58
10.2.2 Sensor Selection . . . 62
10.3 Transfer Vehicle Guidance and Navigation . . . 64
10.4 Mars Lander Requirements . . . 65
10.5 Mars Lander Attitude Determination and Control System . . . 66
10.6 Mars Lander Guidance, Navigation & Control and Sensor Selection . . . 67
10.7 Conclusion and Recommendations . . . 68

**11 Power System** **69**
11.1 Power budget . . . 69
11.2 Power generation . . . 69
11.3 Solar Panels Structural Aspect . . . 71
11.4 Power distribution . . . 72
11.5 Verification and Validation . . . 72
11.6 Sensitivity Analysis . . . 73
11.7 Conclusion . . . 73

**12 ML Design** **74**
12.1 Introduction . . . 74
12.2 Mars Lander mass budget . . . 74
12.3 Atmosphere of Mars . . . 75
12.4 Flight Path Angle . . . 75
12.5 Mars Lander Structural Design . . . 76
12.5.1 Sizing for Pressurization . . . 77
12.5.2 Sizing for Compressive Launch Loads . . . 78
12.5.3 Resistance against Vibration Loads . . . 79
12.6 Heating experienced during the entry phase . . . 79
12.6.1 Verification and Validation . . . 80
12.7 ML Aerothermal Design . . . 81
12.7.1 Material Choice . . . 81
12.7.2 Aerodynamic Heating . . . 82
12.7.3 Results . . . 83
12.7.4 Interpretation . . . 83
12.8 Parachute Phase . . . 86
12.9 Thrusters . . . 88
12.10Landing Mechanism . . . 88
12.11ML Base Integration . . . 91
12.12Conclusion . . . 91

**13 Risk management and Contingency Analysis** **93**
13.1 Risk identification and mapping . . . 93
13.2 Risk mitigation . . . 97
13.3 Contingency Analysis . . . 98
13.4 Conclusion and Recommendations . . . 99

**14 Operations and Logistics** **100**
14.1 Operations and logistics . . . 100
14.2 Hardware . . . 101
14.3 Software . . . 101
14.4 Launch Schedule . . . 101
14.5 In-Orbit Assembly and Integration . . . 101
14.5.1 Rendezvous . . . 102
14.5.2 Docking . . . 102

**15 Sustainability Approach** **107**

**16 Cost and Market Analysis** **108**
16.1 Parametric Cost Estimation . . . 108
16.2 TRANSCOST Model . . . 108
16.2.1 Man-Year (MYr) Cost Definition . . . 109
16.2.2 Development Costs or Non-recurring Cost (NRC) . . . 109
16.2.3 Unit Production Costs or Recurring Costs (VRC) . . . 110
16.2.4 Ground Segment and Operations Cost . . . 111
16.2.5 Cost overview conclusions and recommendations . . . 111
16.3 Market Analysis . . . 112
16.3.1 Mars One for Investors . . . 112
16.3.2 Investors for Mars One . . . 113
16.3.3 Supporters . . . 113
16.3.4 Competition . . . 114

**17 Final Design Overview & Conclusions** **115**
17.1 Final Design Configuration . . . 115
17.1.1 PTV Sensitivity Analysis . . . 118
17.1.2 Subsystem Update . . . 118
17.1.3 Final Mission Profile . . . 119

**18 Future Developments** **121**
18.1 Production plan . . . 121
18.1.1 Manufacturing . . . 122
18.1.2 Assembly and Integration . . . 122
18.1.3 Suppliers . . . 122
18.2 Project Development . . . 123
18.3 Gantt Chart . . . 124

**A Compliance Matrix** **134**

**B Communication Flow Diagram** **138**

# Nomenclature

| Symbol | Explanation |
|---|---|
| $\alpha$ | Angular acceleration [rad/s$^2$] |
| | Thermal expansion coefficient [K$^{-1}$] |
| $\gamma$ | Flight path angle [rad] |
| | Specific heat ratio [-] |
| $\Delta$V | Change in velocity [m/s] |
| $\eta$ | Efficiency [-] |
| $\mu$ | Gravitational parameter [m$^3$/s$^2$] |
| $\theta$ | True Anomaly [°] |
| | Deviation of Z axis from the local vertical [rad] |
| $\sigma$ | Stefan-Boltzmann constant [Wm$^{-2}$K$^{-4}$] |
| | Stress [Pa] |
| $\rho$ | Density [kg/m$^3$] |
| $\phi$ | Phase angle [rad] |
| $a$ | Acceleration [m/s$^2$] |
| | Albedo factor [-] |
| $A_s$ | Surface area [m$^2$] |
| $A_t$ | Throat cross sectional area [m$^2$] |
| $c$ | Speed of light [m/s$^2$] |
| $c.g.$ | Center of gravity |
| $c_p$ | Specific heat [J/kg·K] |
| $c_{ps}$ | Center of solar pressure |
| $c*$ | Propellant characteristic velocity [m/s] |
| $C_D$ | Drag Coefficient [-] |
| $C_s$ | Solar constant [W/m$^2$] |
| $C_L$ | Lift coefficient [-] |
| $d$ | Distance [m] |
| $D$ | Drag [N] |
| | Diameter [m] |
| $E$ | Modulus of elasticity [Pa] |
| $f$ | Frequency [Hz] |
| $f_{1-3}$ | Technical development cost factors [-] |
| $f_4$ | Learning curve factor [-] |
| $F$ | Force [N] |
| | Visibility factor [-] |
| $g$ | Gravitational acceleration [m/s$^2$] |

Continued on next page

| Symbol | Explanation |
|---|---|
| $h$ | Height [m] |
| $H$ | Angular momentum [Nms] |
| $H_{EL}$ | Effort for liquid prop. engines [man·hrs] |
| $H_{VS}$ | Effort for crewed space systems [man·hrs] |
| $H_{VC}$ | Effort for crewed ballistic re-entry [man·hrs] |
| $i$ | Angle of incidence from the sun [rad] |
| $I$ | Mass moment of inertia [kg m$^2$] |
| $I_d$ | Inherent degradation [-] |
| $I_{sp}$ | Specific impulse [s] |
| $J_s$ | Solar radiation [W/m$^2$] |
| $K$ | Ballistic parameter [N/m$^2$] |
| $L$ | Length [m] |
| | Lift [N] |
| $L_d$ | Life degradation [-] |
| $m$ | Mass [kg] |
| $\dot{m}$ | Mass flow [kg/s] |
| $M$ | Moment [Nm] |
| $n$ | Mean motion of planet [°/s] |
| $p$ | Pressure [Pa] |
| $P$ | Power [W] |
| | Orbital period [s] |
| $q$ | Reflectance factor [-] |
| $r_{SOI}$ | Radius of sphere of influence [m] |
| $r_p$ | Burnout radius [m] |
| $R$ | Radius [m] |
| $R_1$ | Radius of perihelion [m] |
| $R_2$ | Radius of aphelion [m] |
| $S$ | Surface Area [m$^2$] |
| $t$ | Thickness [m] |
| $t_0$ | Epoch date [s] |
| $t_1$ | Launch date [s] |
| $t_2$ | Arrival date [s] |
| $T$ | Orbital period Planet [s] |
| | Torque [Nm] |
| | Temperature [°] |
| $T_{syn}$ | Synodic period [s] |
| $m$ | Mass [kg] |
| \$M | One million (1,000,000) U.S. dollars |
| $v_p$ | Burnout velocity [m/s] |
| $v_\infty$ | Excess velocity [m/s] |
| $V$ | Volume [m$^3$] |
| | Velocity [m/s] |
| $V_1$ | Planet velocity [m/s] |
| $V_D^{(v)}$ | Vehicle departure velocity [m/s] |
| $V_E$ | Entry velocity [m/s] |
| $w$ | Distributed load [N/m] |
| $W$ | Weight [N] |

Table 1: List of Abbreviations

| Abbreviation | Explanation |
|---|---|
| 2BMS | 2-Bed Molecular Sieve |
| AAA | Avionics Air Assembly |
| ADCS | Attitude Determination and Control System |
| AHP | Analytic Hierarchy Process |
| ALARA | As Low As Reasonably Achievable |
| AMCM | Advanced Missions Cost Model |
| BPSK | Binary phase-shift keying |
| CER | Cost Estimation Relationships |
| CMG | Control Momentum Gyros |
| DID | Deliverable Item Description |
| DSE | Design Synthesis Exercise |
| DSN | Deep Space Network |
| ECLSS | Environmental Control and Life Support System |
| EIRP | Equivalent Isotropically Radiated Power |
| ESA | European Space Agency |
| ESTEC | European Space TEchnology Center |
| FPDS | Fire Prevention, Detection, and Suppression |
| FY | Fiscal Year |
| GNCS | Guidance, Navigation and Control System |
| GPS | Global Positioning System |
| HD | High-Definition |
| HOPE | H-II Orbiting Plane |
| IRVE | Inflatable Reentry Vehicle Experiment |
| ISS | International Space Station |
| LEO | Low Earth Orbit |
| LMO | Low Mars Orbit |
| LRV | Lunar Roving Vehicle |
| LSS | Life Support System |
| MCA | Major Constituent Analyzer |
| MCC | Mission Control Center |
| MISS | Manned Interplanetary Shuttle Service |
| ML | Mars Lander |
| MMOD | Micro-Metroids and Orbital Debris |
| MRO | Mars Reconnaissance Orbiter |
| MSL | Mars Science Laboratory |
| MTR | Mid-Term Review |
| MYr | Man-Year |
| NAFCOM | Nasa-Air Force Cost Model |
| NASA | National Aeronautics and Space Administration |
| NRC | Non-recurring Cost |
| OBS | Organizational Breakdown Structure |
| PTV | Piloted Earth-Mars Transfer Vehicle |
| QPSK | Quadrature phase-shift keying |
| RAMS | Reliability, Availability, Maintainability, Safety |

Continued on next page

| Abbreviation | Explanation |
|---|---|
| RS | Reed-Solomon |
| Rx | Receiver |
| RWS | Reaction Wheel System |
| SAFE | Safe Affordable Fission Engine |
| s/c | Spacecraft |
| SE | Systems Engineering |
| SNR | Signal-to-Noise Ratio |
| TBC | To Be Confirmed |
| TBD | To Be Defined |
| TCCS | Trace Contaminants Control Subassembl |
| THC | Temperature and Humidity Control |
| TRL | Technology Readiness Level |
| Tx | Transmitter |
| TVC | Thrust Vector Control |
| UHMWPE | Ultra High Molecular Weight Polyethylene |
| USD | United States Dollar |
| VAB | Vehicle Assembly Building |
| VRC | Variable Recurring Cost |
| WBS | Work Breakdown Structure |
| WFD | Work Flow Diagram |
| WPD | Work Package Description |
| WCED | World Commission on Environment and Development |

# 1 | Introduction

The Mars One initiative is currently actively seeking funding in order to finance their project of building a Mars base and colonizing Mars. Mars One is already accepting applications from potential astronauts that shall be selected, trained for eight years, and then sent on a one-way journey to Mars as a four-person crew by 2033. The first crew of four astronauts would then build the Mars base (with equipment and habitats sent to Mars prior to their arrival) and prepare for the arrival of additional crews in subsequent years, gradually forming a Mars colony. This astronauts would pay a high price for the glory of being the first humans on Mars - they would most likely spend the rest of their lives on Mars, building the colony and performing scientific experiments and research.

The purpose of this Design Synthesis Exercise is to investigate the feasibility of the Mars One mission. In particular the purpose of this Design Synthesis Exercise is to design a Piloted-Transfer-Vehicle and Mars Lander in a detail at the Phase A level. The launcher, the in-orbit assembly and the Mars base will be designed conceptually. This report shall also provide a overview of the steps that need to be taken after this Design Synthesis Exercise.

This Final Report starts with an overview of functions that should be performed during the mission presented in a functional flow diagram in Ch. 2. Ch. 3 explains the baseline design for the PTV based on the calculations executed in the Mid-Term Report. The astrodynamics of the transfer from Earth to Mars are determined in Ch. 4. Afterwards all the subsystems of the PTV and ML will be investigated in more detail. First the PTV propulsion subsystem will be explained in Ch. 5. Secondly the environmental control and life support subsystem which keeps the crew alive will be discussed in chapter 6. After that the PTV structural design will be discussed in Ch. 7. The thermal control subsystem controls the temperature of the PTV and the ML such that the other subsystems can perform optimally, more details can be found in Ch. 8. Afterwards the communication subsystem will be elaborated in more detail in Ch. 9. The PTV and the ML also needs a guidance, navigation and control system and an attitude determination and control subsystem. These subsystems will be explained in Ch. 10. In Ch. 11 one can read the overview of the power generation and distribution. Finally some subsystems exclusive to the ML such as the parachute and the heat shield are investigated in Ch. 12. After all the subsystems are designed, some general mission characteristics are discussed. First the risks and contingencies of the mission are analyzed in Ch. 13. Then the operations and the logistics are discussed in Ch. 14. In Ch. 15 the sustainability aspects of the Mars One mission are examined. After that a cost and market analysis is performed for the complete mission in Ch. 16. Then a complete overview of the final design and some conclusions are given in Ch. 17. Finally, the last chapter will discuss the future developments of the Mars One mission.

# 2 | Functional Analysis

In this chapter the functional flow diagram of the Mars One mission will be discussed. The mission is split up into several phases(see Fig.2.1, each of which is briefly described further in the text.

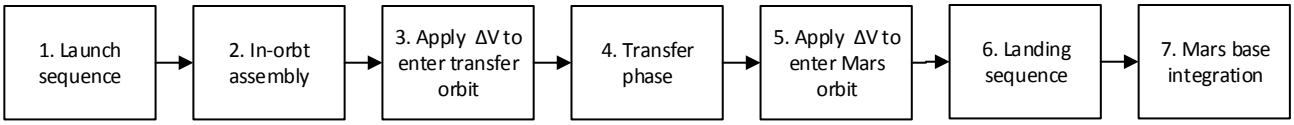


Figure 2.1: Functional flow diagram for the Mars One mission.

**Launch -** the launch phase is the first phase of the mission's functional flow diagram. It begins by the launch of the propellant modules followed by the PTV and the ML. Also in case of a failure of the launch system the crew needs to be safely returned to Earth.

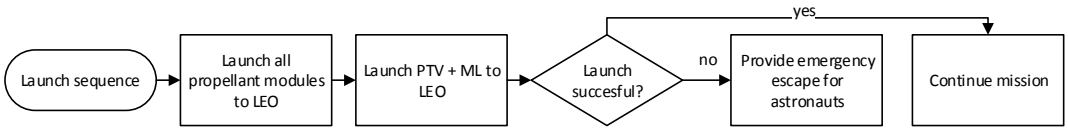


Figure 2.2: Functional flow diagram for the launch phase

**In-orbit assembly -** since the total mass needed in Earth orbit is too large for one launch, multiple launches are required. The spacecraft then has to be constructed in orbit. Firstly the propellant tanks will be launched, then the PTV and finally the ML with the crew. After all these systems are launched, they will be assembled in LEO. The process is shown in Fig.2.3

**Departure to Transfer Orbit -** the transfer phase consists out of the first burn in the parking orbit around Earth, the actual transfer and a second burn at the end of the transfer to enter into the Mars parking orbit. Before and after each $\Delta V$ applied the spacecraft is properly aligned, so that the thrust vector would point into the right direction when the engine is turned on. During the actual transfer the spacecraft floats freely through space and does not need further burns other than attitude corrections. The function of the PTV then reduces to provide

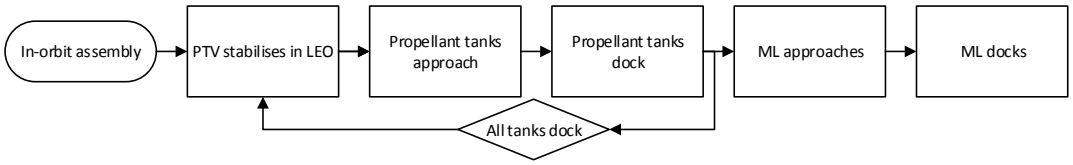


Figure 2.3: Functional flow diagram for the assembly phase

the crew with everything necessary, for example: air, food, power, shelter, communication etc. Finally, the spacecraft detaches the empty propellant tanks when possible in order to decrease the overall mass.

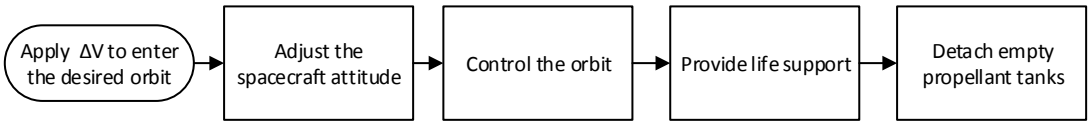


Figure 2.4: Functional flow diagram for the transfer phase

**Landing and base integration-** are parts of the functional flow diagram is the functional flow diagram for the entry, descent and landing in the Martian atmosphere. The ML will perform a ballistic entry, deploy the parachute and drop its heat shield. Finally it will deploy the wheels while thrusters are used to control the descent and touchdown. Once landed, the ML is integrated with the Mars base as shown in Fig. 2.5. The PTV is used as communication satellite after decoupling.

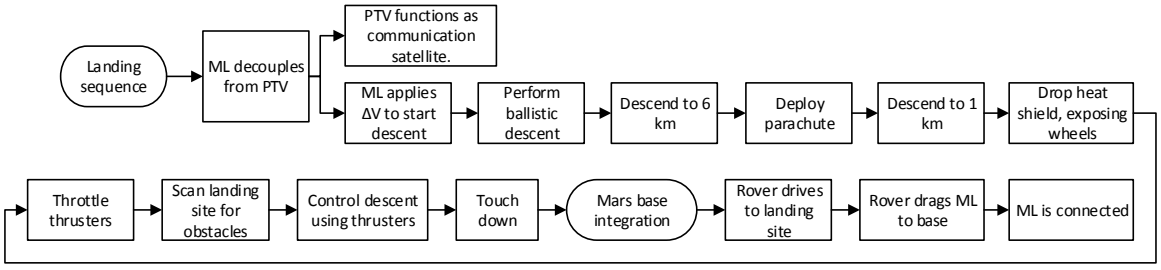


Figure 2.5: Functional flow diagram for the landing phase.

# 3 | PTV Baseline Design

For the design of most subsystems it is necessary to establish starting values for the total mass and some general dimensions of the spacecraft. These parameters are determined in this chapter in a so-called "Baseline Design" of the spacecraft. Only after all subsystems have been sized (based on the starting values) it is then possible to update the overall mass and dimensions of the spacecraft. This design update is presented as the final design of this project at the end of this report.

It would be convenient to use the concept developed in the Midterm Report as the Baseline Design, but this concept has to be adjusted since more accurate and realistic estimates of the required $\Delta V$ maneuvers have now been determined. Without taking into account the new $\Delta V$ values the final design will deviate excessively from the Baseline Design. The new $\Delta V$ values and how they are calculated is explained in Ch. 4. The change in $\Delta V$ leads to a change in propellant mass, which results in a change of the PTV's size and configuration. Also, a different type of engine is chosen, as explained in Ch. 5. The mass of this engine is decreased by more then 67 % compared to the old design, which also results in lower propellant mass needed.

## 3.1 Sizing Approach

This section explains the methods that have been applied to redesign the PTV concept. However, before the design process is initiated it is first necessary to prove that the indicated transfer method complies with the safety specification on radiation levels.

### 3.1.1 Sizing iteration method

One of the most important aspects in sizing the PTV is to try to limit the propellant mass and the number of components that have to be assembled, i.e. the number of required launches. While it is true that the launch costs are not a substantial part of the PTV's total cost, as explained in Ch. 16, the in-orbit assembly of large spacecraft modules is a complicated process as shown in Sec. 14.5. Also, attaching many large fuel tanks to a small main PTV might prove to be structurally difficult. This design therefore aims to limit the number of tanks. This is done by varying the size of the PTV's living compartment such that the necessary propellant mass will be a multiple of the payload mass limit of Space X's Falcon Heavy launcher. The Falcon Heavy rocket is selected for launching all components of the spacecraft since it has a much higher payload capacity than all presently existing launchers. Even though it is still in development right now, it is reasonable to expect that it will be ready in the next 10 years. Falcon Heavy's payload limit is equal to 53000 $kg$. The width of all compartments of the PTV is limited by the maximum diameter of the payload compartment of the Falcon Heavy (4.6 $m$). The length of the cylindrical part of the payload compartment of the Falcon Heavy is 6.6 $m$ with about 4.5 $m$ left in the cone shaped compartment. Therefore, the maximum length the propellant tanks can reach is 6.6 meters. The maximum number of fuel tanks is set to be 3,

as 3 tanks, the mass of each not exceeding 53000 $kg$, would contain the minimum amount of propellant required for the PTV size of the Mid-Term concept according to the new $\Delta V$ values. To clarify the used sizing approach a flow diagram is shown in Fig. 3.1 which indicates the followed steps.

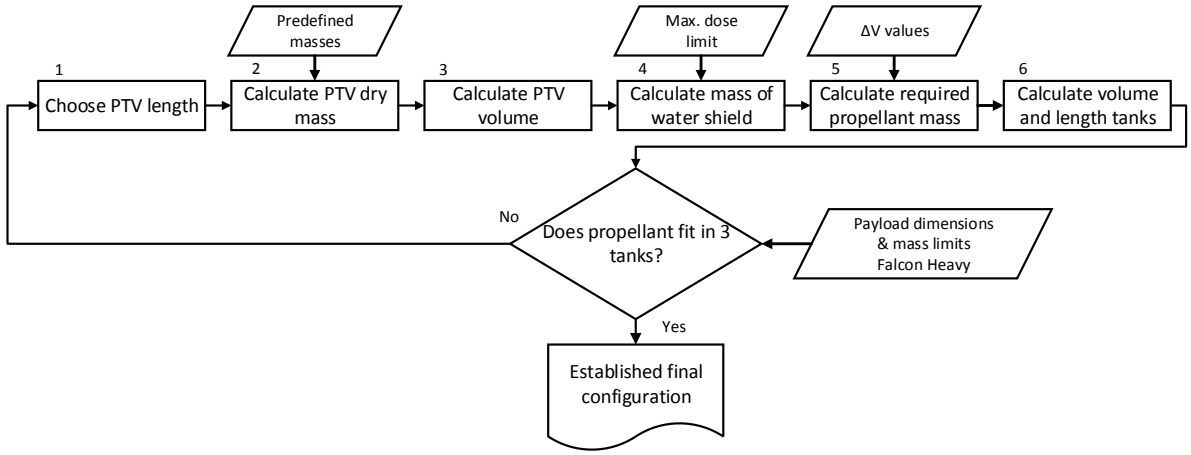


Figure 3.1: Sizing Process Flow Diagram

As can be observed in Fig. 3.1 the design process might involve iterations. The individual blocks of the flow diagram in Fig. 3.1 are now explained briefly.

**1. Choose PTV living module length:** The objective in redesigning the PTV is to allow for more living space for the crew members while keeping the required amount of propellant to a reasonable value. The PTV concept presented in the Mid-Term Review is designed is such a way that one crew member has a maximum living space of around 6 $m^3$. This does not seem to be sufficient for a travel time of 300 days. Therefore, as a first step a new length for the PTV living module is specified.

**2. Calculate PTV dry mass:** The PTV's dry mass includes components of fixed masses such as the engine, the electrical equipment or the furniture as well as components that depend on the PTV's length ($L_{PTV}$). The PTV's structural mass is based on the structural mass of the pressurized tank of the Saturn V rocket. Saturn V's tank is a good reference for the PTV's structural mass since it has been for Skylab, the first U.S. space station. In comparison to other spacecraft it is relatively simple to find its structural mass without extra components and subsystems. It has been found that this mass is approximately equal to $580kg/m$ [1]. The life support mass also varies with the length of the PTV since the water is used to shield from cosmic radiation, as explained later in the paragraph on water shield thickness.

**3. Calculate PTV volume:** The PTV's volume is calculated using the chosen PTV length and the diameter of the Falcon Heavy rocket that is planned to be used to launch the spacecraft's components. The volume follows from the simple equation for the volume of a cylinder.

**4. Calculate thickness of water shield:** Water is a very good material for shielding from cosmic radiation that does not produce secondary radiation itself [2]. It is therefore decided to use a water tank around the PTV's living module with an appropriate thickness. The limit dose of radiation that blood forming organs are allowed to receive per year is specified by [3]

Table 3.1: PTV dry mass

| | **Mass [kg]** |
|---|---|
| PTV structure mass | $L_{PTV} \cdot 580\ kg/m$ |
| Engine mass | 580 |
| Life support mass | depends on $L_{PTV}$ |
| Electrical equipment | 150 |
| Furniture | 300 |

to be 0.5 Sv. Taken a safety margin into account, it is chosen to design a radiation shield for a maximum dose limit of 0.5 Sv. According to [4] this would require a water shield with that has 20 $g/cm^2$ of mass. Using water's density at room temperature, this would result in a shield thickness of exactly 20 $cm$. This thickness will then result in a particular water volume and mass that has to be accounted for in the mass of the PTV. In addition, it has been calculated that the water needed for radiation shielding would be more than enough for consumption and hygiene throughout the journey, as discussed in Ch. 6.

**5. Calculate required propellant mass:** The propellant mass is then calculated with the $\Delta V's$ given in Ch.4 and Eq. 5.9 below. This equation is derived from the Tsiolkovsky rocket equation and accounts for a propellant tank structural mass that is equal to 10% of the total propellant mass.

$$M_{prop_{\Delta V}} = M_c \frac{e^{\frac{\Delta V}{V_{ex}}} - 1}{1.1 - 0.1 * e^{\frac{\Delta V}{V_{ex}}}} \tag{3.1}$$

In Eq. 5.9 $M_{prop_{\Delta_V}}$ is the mass of propellant needed. $M_c$ equals the mass of the structure that has to be carried by $M_{prop_{\Delta_V}}$. $V_{ex}$ is the exhaust velocity and depends on the type of engine chosen. Equation 5.9 has to be applied for every maneuver and since propellant itself is needed to carry propellant , the calculations start at the last $\Delta V$ maneuver. The following figure illustrates the order of the maneuvers and the respective $\Delta V$ needed.

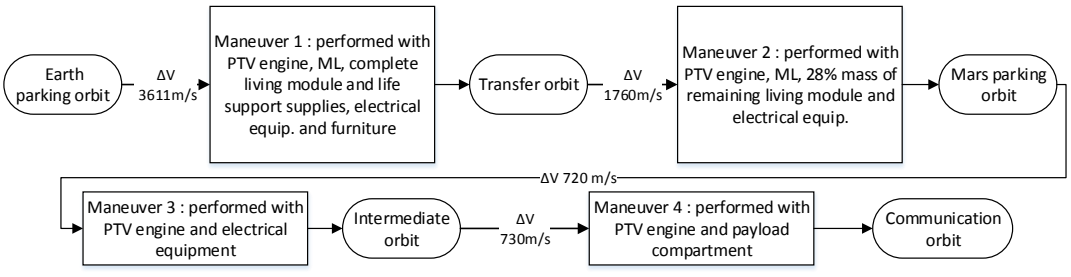


Figure 3.2: Transfer phases and required $\Delta V$ values

The last two maneuvers shown in Fig. 3.2 have to be performed in order to use a small part of the PTV as a communications relay stations, as explained in more detail in Sec. 9. With

a first $\Delta V$ the PTV is transferred into an intermediate orbit before a second $\Delta V$ propels it into the areo-stationary orbit that is required for the communications station. The plan is to discard approximately 80% of the PTV's structural mass (and other unnecessary subsystem) before these two maneuvers are performed in order to save propellant mass.

**6. Calculate Volume and size of propellant tanks** In order to calculate the required number of launches it is necessary to first determine the volume needed to store the amount of propellant calculated in the previous step. This is done using the mixture ratio and corresponding density of the fuel (liquid methane) and the oxidizer, liquid oxygen. The oxidizer-to-fuel ratio is assumed here to be 3.5:1. This assumption is valid since Liquid Methane/Liquid Oxygen injectors for potential future Mars ascent engines have been tested in 1999 with this mixture ratio [5]. The combined density of the propellant is 582.3 $kg/m^3$. The length of the propellant tank results from the calculated volume and the diameter of Falcon Heavy's payload compartment.

**7. Amount of propellant tanks** Using the mass and size limit of the Falcon Heavy it is now possible to determine how many fuel tanks, i.e. launches, are needed for each year of departure. If this number exceeds 3, as explained previously, another iteration is carried out with a smaller PTV length. This is performed multiple times until the number of launches does not exceed 3 any more. This PTV length then automatically results in a corresponding mass and size for all of the spacecraft's components. Through this method the final value of the PTV's length is found to be 5 m.

## 3.2 Configuration

Following the method outlined above, the mass and dimensions of the redesigned PTV have now been determined. The arrangement of the modules is determined so as to facilitate the fuel flow to the engine. It is decided to place the propellant tanks next to the PTV rather than stacking them in series. It is then possible to route the propellant from each tank through the PTV to the engine. In this case there is also the advantage of dumping the empty propellant tanks after the first $\Delta V$ maneuver, which saves mass and thus propellant for the second $\Delta V$ maneuver. In order to maintain the symmetrical configuration, the fuel tank needed for the last two maneuvers is placed inside the PTV. Tab. 3.2 presents the mass and major dimensions of the spacecraft's main components. The mass of the tanks includes the propellant and the mass of the ML is obtained from the ML's mass budget in Sec. 12.2. The volumes of the modules have a limit in order to fit in the launcher. Since the diameter is predefined, only the length is significant.

Table 3.2: PTV dimensions

| **Components** | **PTV** | **Engine** | **Tank2** | **ML** | **Tank** | **Total** |
|---|---|---|---|---|---|---|
| Length $[m]$ | 5 | 1.6 | 0.06 | 5 | 4.65 | 11.6 |
| Mass $[kg]$ | 25800 | 580 | 529 | 6830 | 120970 | 154710 |

## 3.3 Conclusion and Recommendations

The corrected basic PTV design has now been established for the exact $\Delta V$ values. This configuration will be the baseline for all subsystem designs. Should the total mass increase due to the mass of particular subsystems, then the design presented here has to be iterated further. This means that more propellant mass might be required. According to current calculations this baseline design contains a mass contingency of approximately 25370 $kg$ that can be launched together with the PTV and its engine on the first launch. A propellant increase is not expected to exceed this amount. In Tab. 3.2, the baseline configuration dimensions and masses can be found.

# 4 | Astrodynamic Characteristics

In order to design cost-effective, crewed, minimal risk interplanetary missions, it is essential to use Earth-Mars trajectories that minimize both energy requirements and transfer time for the astronauts. However, the transfer time and energy needed are usually inversely proportional, which presents a design issue. The transfer time is of special concern since spending a long time in interplanetary space brings health risks, as the crew will continuously be exposed to galactic cosmic rays and solar particle events that can significantly increase their chances of developing cancer and endanger their health in multiple ways.

This chapter explains how this transfer orbit design problem is addressed and crew safety taken into account. The presented result is an optimal interplanetary trajectory for the Mars One mission. As cost and safety are the main driving requirements, the trajectories which minimize the total required $\Delta V$ have been investigated and a suitable orbit has been selected for launch in 2026.

## 4.1 Assumptions

A number of assumptions have been made to facilitate trajectory calculations, while at the same time providing accurate results and valid design choices. They concern astrodynamic characteristics and radiation shielding.

**Patched Conics** For the calculations of interplanetary trajectories the patched conics assumption is used. This method of simplification is constructed by dividing space into various parts by assigning each of the $n$ bodies (e.g. the Sun, planets...) its own sphere of influence, calculated using Eq. 4.1. Whenever the spacecraft is inside the sphere of influence of a smaller body, only the gravitational force between the spacecraft and that body is considered; otherwise the gravitational force between the spacecraft and the larger body is considered. This allows the complicated n-body problem to be reduced to multiple two-body problems for which the solutions are the conic sections of the Kepler orbits, thus allowing for accurate interplanetary trajectory design [6].

$$\frac{r_{SOI}}{R} = \left(\frac{m_p}{m_s}\right)^{\frac{2}{5}} \tag{4.1}$$

**Radiation Shielding - ALARA Principle** Because this is a one-way mission radiation concerns are different than for the return mission designs typically analyzed by government space agencies such as NASA or ESA. The maximum number of safe days in interplanetary space has been estimated by different sources and amounts to 180-200 days per journey when using Aluminum shielding of at least 20 $g/cm^2$ [7]. However, this is influenced by the shielding method used (shielding material *and* shield thickness) and assumes a return mission; therefore

the upper limit is $2 \times 200$ days. On the other hand, since the Mars One mission consists of only one transfer journey, it is assumed that adequate shielding can be provided to keep radiation levels under a reasonable limit and allow for a longer journey, thus requiring less $\Delta V$. This is in accordance to the ALARA (As Low as Reasonably Achievable) principle stipulated by the International Commission on Radiological Protection (ICRP). This limit on safe transfer time for the astronauts has been set to **350 days**, therefore only faster trajectories will be considered.

**Future considerations** It is noted that if future research shows that for radiation, psychological, or any other relevant concern the transfer time needs to be reduced, it can be done so by choosing a faster trajectory with a larger total $\Delta V$ requirement.

## 4.2 Hohmann Transfer Trajectory

Considering the driving mission requirements of cost and safety, it is beneficial to choose a trajectory that is both simple and efficient. Furthermore, radiation protection requirements also directly influence the journey duration. However, considering this a one-way mission, where the total travel time is reduced to one transfer only, a trajectory with a longer transfer time can be used in order to reduce cost (as compared to conventional return missions). The most energy efficient transfer trajectory under the assumptions of circular and coplanar orbits is the Hohmann transfer (See Fig. 4.1), necessitating a travel time of 260 days but posing the lowest $\Delta V$ requirement for an impulsive transfer [6]. In this case the entire Earth-to-Mars transfer will consist of two distinct $\Delta V$ maneuvers, the first used to escape Earth orbit and enter a Hohmann transfer trajectory and the second to enter a Mars parking orbit from the Hohmann transfer trajectory. This theoretical most-efficient transfer will be used as a reference point for first order estimates and for sensitivity analysis, as due to the small inclination and eccentricity of the real orbits of both Earth and Mars (see Tab. 4.1), the actual optimal orbit will come close to the ideal Hohmann trajectory. Nevertheless, in order to obtain even more efficient orbits with higher travel time the Lambert problem approach will be used.

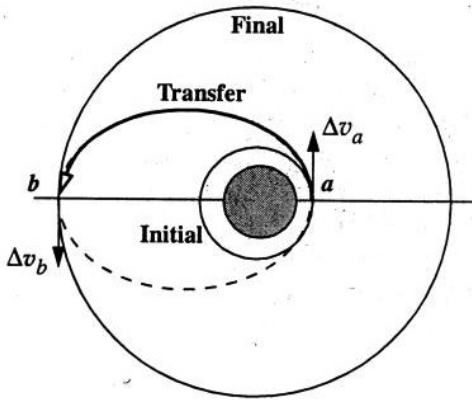


Figure 4.1: Idealized Hohmann transfer trajectory leg to an outer planet

Table 4.1: Astronomical data for the Sun, Earth and Mars [6]

| **Object** | **Radius (km)** | **Mass (kg)** | **Semimajor axis of orbit** | **Orbit Eccentricity** | **Incl. of orbit to the ecliptic** |
|---|---|---|---|---|---|
| Sun | 696 000 | $1.989 \cdot 10^{30}$ | - | - | - |
| Mars | 3396 | $641.9 \cdot 10^{21}$ | $227.9 \cdot 10^{6}$ | 0.0935 | 1.85° |
| Earth | 6378 | $5.974 \cdot 10^{24}$ | $149.6 \cdot 10^{6}$ | 0.0167 | 0.00° |

## 4.3 Sensitivity Analysis

The initial $\Delta V$ maneuver required to place the spacecraft on an interplanetary trajectory occurs in the sphere of influence of the departure planet. Considering the large scale of the entire trajectory, the size of this sphere of influence can be approximated as a point. However, any errors in position and maneuvers at this maneuver point will consequently have proportionally larger effects on the trajectory itself. This can be illustrated by considering an idealized Hohmann transfer by using Eq. 4.2 [6], which shows the variation of $R_2$ (radius of aphelion) due to the variations of $r_p$ (burnout radius) and $v_p$ (burnout velocity).

$$\frac{\delta R_2}{R_2} = \frac{2}{1 - \frac{R_1[V_D^{(v)}]^2}{2\mu_{sun}}} \left( \frac{\mu_1}{V_D^{(v)} v_\infty r_p} \frac{\delta r_p}{r_o} + \frac{v_\infty + \frac{2\mu_1}{r_p}}{V_D^{(v)}} \frac{\delta v_p}{v_p} \right) \tag{4.2}$$

Here $R_1$ is radius of perihelion, $V_D^{(v)}$ is the departure velocity of the vehicle, $\mu_1$ is the standard gravitational parameter of the departure planet, $V_1$ is the planet's speed and $v_\infty$ is the excess velocity of the vehicle.

In order to quantify the sensitivity of the trajectory to initial errors, we consider an example Earth to Mars mission, starting from a 300 $km$ parking orbit using the following values:

Table 4.2: Calculation parameters

| $\mu_{sun}[km^3/s^2]$ | $\mu_{earth}[km^3/s^2]$ | $R_1[km]$ | $R_2[km]$ | $r_p[km]$ |
|---|---|---|---|---|
| $1.327 \cdot 10^{11}$ | 398 600 | $149.6 \cdot 10^{6}$ | $227.9 \cdot 10^{6}$ | 6678 |

Furthermore, using:

$$V_1 = V_{Earth} = \sqrt{\frac{\mu_{sun}}{R_1}} \tag{4.3}$$

$$V_D^{(v)} = \sqrt{2\mu_{sun}} \sqrt{\frac{R_2}{R_1(R_1 + R_2)}} \tag{4.4}$$

$$v_p = \sqrt{v_\infty^2 + \frac{2\mu_{earth}}{r_p}} \tag{4.5}$$

and inserting this into Eq. 4.2 yields:

$$\frac{\delta R_2}{R_2} = 3.127 \frac{\delta r_p}{r_p} + 6.708 \frac{\delta v_p}{v_p} \tag{4.6}$$

This analysis shows that a variation in the burnout speed ($v_p$) of 0.01% or 1.1 $m/s$ will change the target radius $R_2$ by 0.067% or 153000 $km$. Similarly an error of 0.01% in burnout radius ($r_p$) produces an error of more than 70000 $km$, which results in the PTV completely missing the target orbit and compromises mission success.

**Conclusion** As a consequence, small errors which occur during the launch and trajectory insertion phase of the mission must be corrected by additional maneuvers during the coasting flight along the trajectory. This is important to consider when designing the propulsion system and the GNC, as it imposes additional requirements on these subsystems and will be incorporated in those designs.

## 4.4 Interplanetary Transfer Trajectory - Lambert's Problem

In order to approach the design of the interplanetary trajectory required for the Mars One mission and systematically make use of the patched conics procedure for three-dimensional trajectories, the Lambert solution is used. As the mission is to send the spacecraft from Earth to Mars in a specified time, the transfer trajectory can be approximated as a heliocentric elliptic Kepler orbit from the position of the Earth at the time of launch to the position of Mars at the time of arrival. By comparing the initial and the final velocity vectors of this heliocentric Kepler orbit with the corresponding velocity vectors for the Earth and Mars, an estimate of the required launch energy and the maneuvers needed for the capture at Mars can be obtained.

The frame of reference used for this problem is the heliocentric ecliptic frame shown in Fig. 4.2. Starting from the departure phase, firstly the state vector of the Earth (Planet 1) is obtained at departure time ($t$) and the state vector of the arrival planet at arrival time ($t+t_{12}$).

The next step is to determine the transfer trajectory of the spacecraft using the patched conic procedure, where it can be observed that the heliocentric position vector of the spacecraft at time $t$ (departure) is the same as that of the departure planet ($\mathbf{R}_1$). Similarly, the heliocentric position vector of the spacecraft is the same as that of the arrival planet ($\mathbf{R}_2$)) at time $t + t_{12}$ (arrival). Using the heliocentric position vectors $\mathbf{R}_1$ and $\mathbf{R}_2$, a Lambert problem solver can be used to obtain the spacecraft's departure and arrival velocities $\mathbf{V}_D^{(v)}$ and $\mathbf{V}_A^{(v)}$ relative to the sun. Consequently, either the state vectors $\mathbf{R}_1$ and $\mathbf{V}_D^{(v)}$ or $\mathbf{R}_2$ and $\mathbf{V}_A^{(v)}$ can be used to obtain the six orbital elements necessary to define the transfer trajectory, which are:

- $h$ - specific angular momentum
- $e$ - eccentricity
- $i$ - inclination
- $\omega$ - argument of perigee
- $\Omega$ - right ascension
- $\theta$ - true anomaly

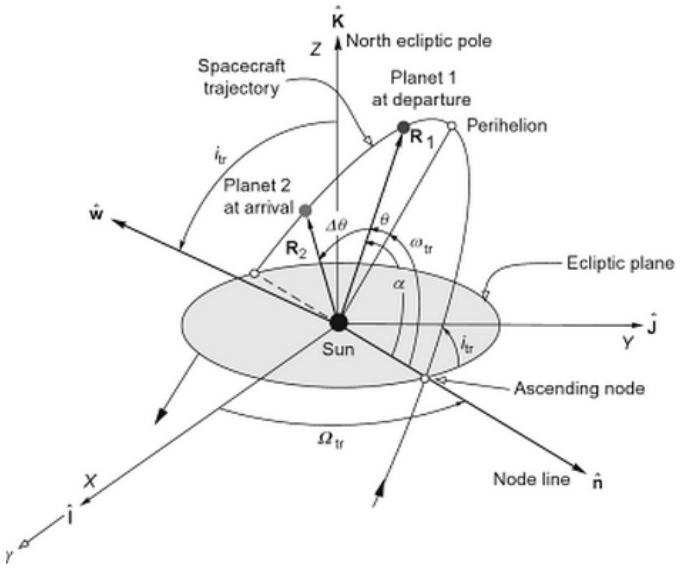


Figure 4.2: Heliocentic orbital elements of a three-dimensional transfer trajectory from Earth ($P_1$ - Planet 1) to Mars ($P_2$ - Planet 2)

### 4.4.1 Solution of Lambert's Problem - Porkchop Plot

As noted, Lambert's theorem allows for the calculation of the various possible transfer orbits along with their respective departure dates, $\Delta V$ and transfer time requirements. Consequently solving the Lambert problem for the mission period of interest, a *porkchop* plot visualization of the solutions can be created as in Fig. 4.3. The *porkchop* plot shows that the optimal launch windows open every 26 months (indicated by the crosses in Fig. 4.3) and the distinct areas of minimum $\Delta V$ requirements repeat cyclically. For the Mars One planned launch time frame of 2023+ the first launch date requiring the lowest $\Delta V$ was found as the 11th of October 2026 (first cross from the left). The launch window parameters for all three planned launches are summarized in Tab. 4.3. The relatively long travel time is justified by the low $\Delta V$ requirement and, as it is a one way mission, the crew is exposed to only one interplanetary journey, limiting radiation concerns. Additionally, the two subsequent launches can be launched 26 and 52 months afterwards, respectively (indicated by 2nd and 3rd cross from the left). Thus, the requirement of completing all three transfer journeys in the proposed 10-year timeframe and completing one transfer at least every 3 years is fulfilled.

Table 4.3: Parameters of optimal transfer trajectories for three Mars transfer missions

| **Launch Window** | **Total $\Delta V$ (km/s)** | **Transfer time (days)** | **Departure date (MJD2000)** | **Departure date (calendar)** |
|---|---|---|---|---|
| 1st | 5.371 | 312 | 9801 | 11th October 2026 |
| 2nd | 5.573 | 306 | 10554 | 4th November 2028 |
| 3rd | 5.912 | 285 | 11313 | 2nd February 2031 |

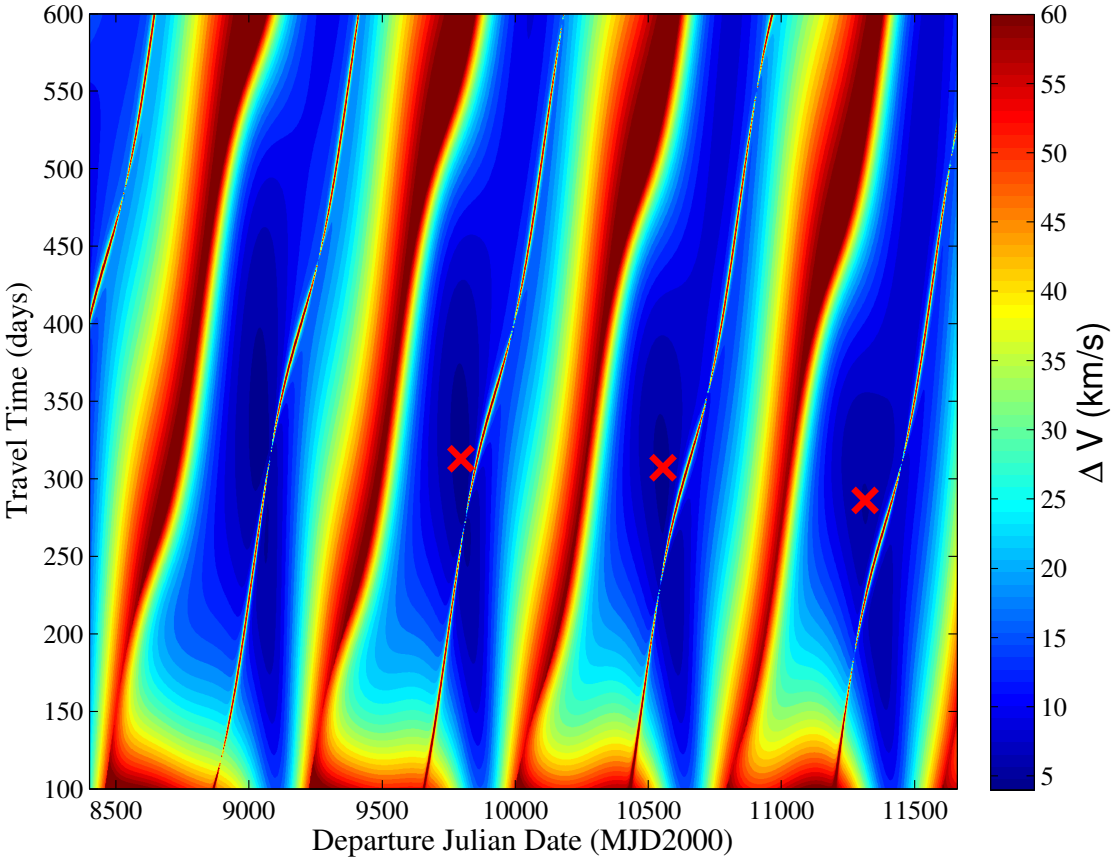


Figure 4.3: Porkchop plot of the Earth to Mars transfer launch windows from the 1st of January 2023 (8400 MJD2000) to the 3rd of November 2031 (11660 MJD2000). The minimum $\Delta V$ trajectories are indicated by the crosses

**Lambert's problem limitations** As can be seen in Fig. 4.3 there exist thin lines, which represent trajectories requiring very high $\Delta V$ values. This series of solutions of the Lambert problem are anomalies which arise due to the definition of the Lambert problem and present a weakness of the algorithm. They shows solutions for the situation where the state vectors of Earth and Mars are aligned on a line (or nearly so) on opposite sides of the Sun. In that case, due to the slight inclination of the Mars orbit, the Lambert solver computes a transfer orbit which is out of the ecliptic plane, therefore resulting in an very high $\Delta V$.

**Verification and Validation** In order to calculate the state vectors a Matlab code has been used and verified with orbital mechanics theory in accordance with [6]. To execute the computations, the TUDAT software (Copyright (c) 2010-2013, Delft University of Technology - Izzo's method Lambert targeter) was used, which was verified by the Astrodynamics and Space Missions department of TU Delft.

**Conclusion and Reccomendations** Due to cost and safety being the drivers of this mission, a relatively long transfer journey of 312 days has been selected in order to minimize the $\Delta V$ requirement and therefore the mission cost (See Fig. 4.4). With more time and resources, optimizer algorithms could be used in order to find an optimal trajectory which could have a

better relation of transfer time to $\Delta V$ needed. If it is proven that a shorter transfer time is necessary for any other issues, a different trajectory could be selected.

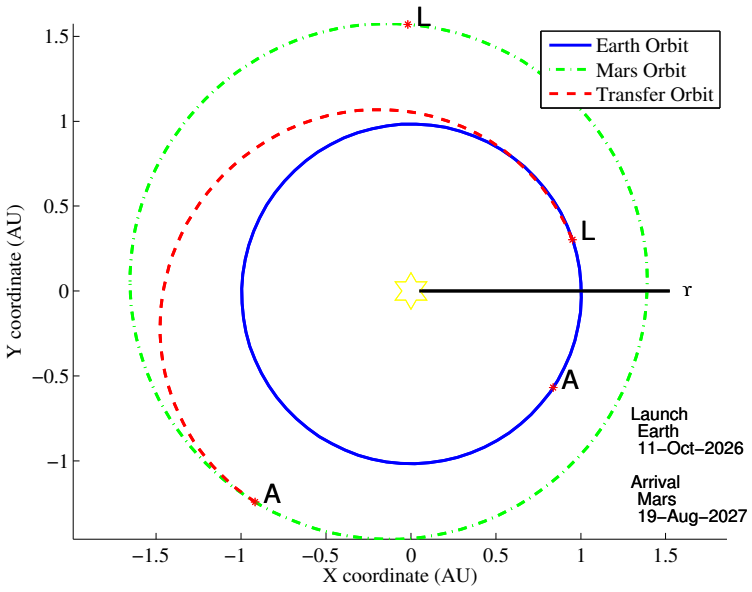


Figure 4.4: Minimum $\Delta V$ interplanetary trajectory as solved by Lambert's problem solver

## 4.5 End-of-mission Mars orbital Maneuvers

After the PTV arrives in Mars orbit, the ML is separated and descends to Mars. The PTV is meant to stay in an areostationary orbit above the base to act as a communications relay station. Before the PTV goes in to an areostationary transfer orbit, it jettisons all the unnecessary equipment left over from the mission to reduce the propellant needed. This includes the living module and the waste water previously used for radiation shielding.

The interplanetary orbit analysis performed in 4 suggests that the PTV arrives in an elliptical orbit with a semi major axis of 4500 $km$ and an eccentricity of 0.2. The areostationary orbit is a circular orbit at an altitude of 17000 $km$. To move from the parking orbit to the areostationary orbit, the altitude and the eccentricity needs to be changed. A minimum energy transfer is used for this, as travel time is not a critical concern for this operation. The total $\Delta V$ needed for increasing the ellipse until its apoapsis is at an altitude of 17000 $km$ is 0.72 $km/s$. For the second burn 0.73 $km/s$ is needed to transform the elliptical into a circular orbit.

# 5 | PTV Propulsion System

Liquid Rocket Propulsion Systems (LRPS) are the most popular form of rocket propulsion when relatively high specific impulse and high thrust levels are required. They have been researched and used extensively and have therefore reached a high technology readiness level, which translates into low cost, low risk and high reliability. Thus, a LRPS has been chosen to fulfill the propulsion requirements of the Mars One mission. In this chapter, the conceptual design and sizing of this propulsion system is presented.

## 5.1 Requirements and Design Considerations

In order to proceed with the design of the propulsion system, first the requirements for this system are analyzed. These requirements come from the chosen interplanetary trajectory, the mass of the payload being transported by the rocket, the expected mass of the complete system and the size envelope limitations of the launcher. Consequently, they will define the type, size and characteristics of the propulsion system.

**Requirements**

- $\Delta V = 5371\ m/s + 10\%$ (margin) $=\ 5901\ m/s$
- $m_p$ (Payload mass $\rightarrow$ PTV+ML) = 32,700 $kg$
- $m_{initial}$ (Initial system mass upper limit) = 150,000 $kg$
- F/W = 0.3 (Minimum thrust over weight ratio) [8]
- $D_{max}$ (Maximum diameter - envelope limitation) = 4.6 $m$

## 5.2 Engine Mass and Sizing

**Mass** From theory it can be shown that liquid rocket engine or thruster mass is closely related to the thrust level. In order to start the sizing of the propulsion system, the required thrust level is calculated using the assumed initial mass upper limit of 150,000 kg and initial F/W ratio of 0.3. This gives a required thrust of:

$$F = \frac{F}{W} \cdot W = 0.3 \cdot 150,000 \cdot 9.81 = 441.45\ kN$$

Using this result, an initial estimate for the engine mass is obtained using the mass estimation relationship for cryogenic liquid propellant engines presented in [9], which suggests as follows:

$$m_E = 0.0016 \cdot F + 36.763 = 743\ kg \tag{5.1}$$

Here $m_E$ is engine mass in kilograms and $F$ is the engine thrust in newtons, with the relation having a Standard Error of Estimate (SEE) of 11.9% . This mass estimate is grossly based on historical data and is suggested as an conservative initial estimate. It expected that by the mission timeframe of 2025+ better thrust-to-weight performances will be achieved, such as with the currently planned SpaceX Merlin 1D-Vac engine [10].

**Sizing** Besides the mass, the thrust of liquid rocket engines also influences the size of the thrust chamber and nozzle and consequently the entire engine. Using size estimating relationships for pump-fed bipropellant liquid rocket engines from [9], (based on historical data from [8]) the following sizes are obtained:

Engine Length:

$$L_E = 0.2259 \cdot F^{0.194} = 2.81\ m \tag{5.2}$$

Engine Diameter:

$$D_E = 0.0914 \cdot F^{0.2184} = 1.56\ m \tag{5.3}$$

Here it is emphasized that for the case of this first order estimate, the liquid rocket engine envelope is defined as the smallest enclosure that encompasses the rocket engine completely, i.e. for pump-fed rocket engines this includes the thrust chamber, pump system, gimbal and Thrust Vector Control (TVC) system.

## 5.3 Propellants

**Propellant Classification** Propellants for liquid rocket engines are classified in different levels. At the first level there is a distinction between *monopropellants* and *bipropellants*. Monopropellants exothermically react by themselves in a combustion chamber, usually in the presence of a chemical catalyst. They are the most simple rocket propellants in terms of operational complexity, the most popular being *hydrazine* ($N_2H_4$). However, they are limited by their in specific impulse, with hydrazine achieving an $I_{sp}$ of about 230 s. On the other hand, bipropellants are liquid propellants which give the highest performance. They combine fuel and oxidizer to obtain high $I_{sp}$ values, and as shown in [8], the smaller the exhaust-gas molecules the higher the obtainable specific impulse. This higher specific impulse usually translates into a smaller overall mass of the vehicle and is therefore beneficial to the entire mission design. However, this is not always the case, as in the example of hydrogen and oxygen, which give a high specific impulse but the density of hydrogen is so low that it requires extremely large and therefore heavy tanks for storage.

**Storage** An important consideration in choosing propellant combinations is their storability. The storage is typically not a critical issue for launch vehicles, therefore hydrogen and oxygen are often used for those applications. However, for propellants that need to be stored for a long time (300+ days in this case), *space storables* are usually a better choice. These propellants can be stored at much higher temperatures and therefore greatly reduce the requirements and complexity of the storage system.

**Toxicity** Potential hazards due to propellant toxicity and corrosiveness need to be carefully assessed for a good propellant choice. Most commonly used propellants have a certain degree of toxicity, and choosing one or the other is related to the amount of toxicity that is deemed acceptable. In the present design choice, methane and kerosene (RP-1) have been identified as significantly less hazardous than liquid hydrogen. Methane proves to be even safer than RP-1, as it is non-toxic.

Table 5.1: Liquid Bipropellant Characteristics [11], [12]

| **Propellant** | **O/F ratio** | $I_{sp}$ $[s]$ | **Fuel Density** $[kg/m^3]$ | **Ox. Density** $[kg/m^3]$ | **Fuel Storage Temp.** $[C°]$ | **Ox. Storage Temp.** $[C°]$ |
|---|---|---|---|---|---|---|
| $H_2/O_2$ | 6 | 435 | 77 | 1140 | -252.9 | -182.96 |
| $CH_4/O_2$ | 3 | 365 | 445 | 1140 | -161.6 | -182.96 |
| $RP-1/O_2$ | 2.25 | 325 | 807 | 1140 | 3 | -182.96 |

**Conclusion** The propellant of choice for this mission is $CH_4/LOX$, which uses liquid methane as fuel and liquid oxygen as oxidizer. As presented in Kokan et al. [11], and demonstrated by recent methane engine altitude tests done by NASA (See Fig. 5.1a citestonealtitude2008) and XCOR (Fig. 5.1b), methane is a promising fuel for future space propulsion applications. There is much research being done at this moment to further develop liquid methane engines from both government agencies such NASA and private enterprises (e.g. XCOR and SpaceX). Liquid methane can be stored at a temperature higher than that of the respective oxidizer (See Tab. 5.1, which means it does not suffer from severe storability issues for long duration missions such as liquid hydrogen, which needs a much lower temperature. Therefore, when using liquid methane as fuel the oxidizer storage capabilities become the limiting factor in the propulsion system design, and not the fuels storage capabilities as when using liquid hydrogen. Furthermore, liquid methane provides a considerable advantage in terms of energy density, therefore requiring much smaller tanks than liquid hydrogen, which compensates for the $I_{sp}$ advantage of hydrogen. Finally, when considering kerosene, which is a common fuel for launch vehicles, it has been found that the $I_{sp}$ advantage of methane over kerosene overcomes the advantage in density that kerosene possesses, therefore resulting in a smaller total vehicle mass when using liquid methane.

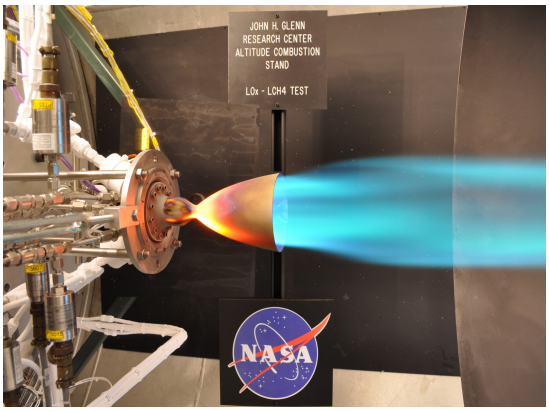


(a) Methane Engine test - John H. Glenn Research Center - altitude combustion stand [13]

(b) Field testing of XCOR Methane rocket engine [14]

**In-Situ Propellant Production (ISPP)** An additional reason for choosing methane for the propulsion system of the Mars transfer PTV is the possibility of using ISPP systems in the future to produce gaseous oxygen and methane on the Martian surface. This studies are in a preliminary phase [15] but could lead to propellant production on Mars once a Mars colony is established, which would facilitate the design of return missions.

## 5.4 Pressure Levels for the Engine and Feed System

One of the most important considerations for liquid engines is the pressure distribution. Pressure variations in the storage tanks, feed system and thrust chamber determine the propellant flow rate. Determining the pressure values is an iterative process, important to assure the required engine performance. However, space engines have no fixed design exit pressure or corresponding expansion ratios as they operate in a vacuum, meaning that there is no concerns of flow separation. Thus, space engine performance ($I_{sp}$) is independent of combustion chamber pressure.

In order to proceed with the analysis of the pressure levels, the combustion parameters for the $CH_4$/Ox were found in the TU Delft space systems engineering liquid propellant database and are shown in Tab. 5.2.

Table 5.2: Oxygen-Methane energetic properties for O/F = 3 and a pressure of 10 *bar* (frozen flow) [16]

| **Flame Temp. ($T_c$)** $[K]$ | **Molar mass ($M$)** $[kg/mol]$ | **Specific heat ratio ($\gamma$)** $[-]$ | **Charac. velocity ($c^*$)** $[m/s]$ |
|---|---|---|---|
| 3246.7 | 20 | 1.2088 | 1784.8 |

Furthermore, for the purpose of this analysis a number of assumptions were made concerning the flow thermochemistry and combustion properties:

- Frozen flow
- Isentropic flow
- Perfect gas
- One-dimensional flow
- Combustion efficiency ($\eta_c$) = 1 (this is conservative since for frozen flow $\eta_c$=1 - 1.15)
- Nozzle efficiency ($\lambda$) = 0.98

**Combustion Chamber Pressure and Nozzle Expansion Ratio** In order to understand the effect of the chamber pressure on the specific impulse (only for engines operating in a sensible atmosphere) and the size of the thrust chamber (also for space engines), Eq. 5.4 is presented [8]:

$$\dot{m} = \frac{p_c A_t}{c^*} \tag{5.4}$$

where:
$\dot{m}$ = mass flow rate $[kg/s]$

$p_c$ = chamber pressure $[Pa]$
$A_t$ = throat cross sectional area $[m^2]$
$c^*$ = propellant characteristic velocity $[m/s]$

Eq. 5.4 shows that the engine size (throat area) is directly related to chamber pressure. A higher pressure results in a smaller throat area, engine size and, consequently, lower weight. Therefore an increased thrust chamber pressure corresponds to a decreased total system mass. On the other hand, as a high chamber pressure is *not* required for the high performance of a space engine (as opposed to atmospheric engines), it is merely enough to optimize the nozzle expansion ratio to achieve a high $I_{sp}$. The optimum nozzle expansion ratio gives about 90% of the maximum theoretical $I_{sp}$ for a particular engine[8]. Using as reference an RP-1/LOx engine from [8], an expansion ratio ($\varepsilon$) of 100 and a combustion chamber pressure ($p_c$) of 0.7 $MPa$ was chosen.

**Dynamic Pressure** During the operation of the engine, the propellant flows from the tank and therefore obtains a flow velocity. The total pressure of the propellant can be approximated to be constant for a short while, which means that the static pressure drops to allow the increase of the dynamic pressure. Assuming incompressible liquid propellant, this can be demonstrated through the use of Bernoulli's equation:

$$\Delta p_{dynamic} = \frac{1}{2}\rho v^2 = \frac{1}{2} \cdot 966.25 \cdot 10^2 = 0.048\ MPa \tag{5.5}$$

where $\rho$ is the average propellant density $[kg/m^3]$ and $v$ is the flow velocity $[m/s]$ for which a typical value is 10 $m/s$ according to [8].

**Presure Drops** The goal when designing a feed line is to make the pressure drops as small as possible, but is is important to account for them as a contingency measure. As suggested by [8], for the feed system a $\Delta p_{feed} = 0.05\ MPa$ was chosen and for the injector for a throttled system a $\Delta p_{inj} = 0.3 p_c = 0.21\ MPa$. Additionally, since an ablative cooling system (See Sec. 5.6) is used, there are no cooling system pressure drops (as in the case of regenerative cooling) $\Delta p_{cool} = 0\ Pa$.

**Propellant Tank Pressure** Using the above results for combustion chamber pressure, dynamic pressure and pressure drops, the required tank pressure can be found and consequently a decision made on whether to use a pump-fed system or a pressure fed system. By using the historical data provided in [8], the required tank pressure for pressure fed systems can be found using the above results as follows:

$$p_{tank} = p_c + \Delta p_{dynamic} + \Delta p_{feed} + \Delta p_{cool} + \Delta p_{inj} \tag{5.6}$$

This gives a total tank pressure $\Delta p_{tank} = 1.008\ MPa$. This is a pressure level well within the capabilities of pressure fed systems, but considering the volume of the propellant tanks needed for this mission, a pressure-fed system would introduce a tremendous weight increase over a pump-fed system. By using a pump-fed system, the weight of the tanks can be lowered significantly by lowering the tank pressure to 0.3 $MPa$ and using a turbo pump to feed the combustion chamber.

## 5.5 Engine Cycle

From the needed pressure analysis in order to feed the rocket engine with propellant, a pump system will be used. Although more expensive and complex, this type of feed system offers significant advantages for large scale systems as compared to pressure-fed systems in terms of weight-saving on tank structural weight and therefore total vehicle weight. The three typical approaches for providing power to these pumps are as follows [8]:

- **Expander cycle** - Pumped, high pressure propellant feeds through a heat exchanger used to cool the thrust chamber structure. The exchanger heats and vaporizes the propellant, which then feeds into the turbine and then in the combustion chamber.
- **Staged-combustion** - Small amounts of fuel feed into the oxidizer flow or small amounts of oxidizer feed into the fuel flow. This mixture pre-burns to produce warm gas to drive the turbine, and afterwards enters the combustion chamber to combust completely (See Fig. 5.2).
- **Gas generator** - The fuel and oxidizer (2%-5%) feed into a separate combustor. The produced hot gases then power the turbine and exhaust overboard.

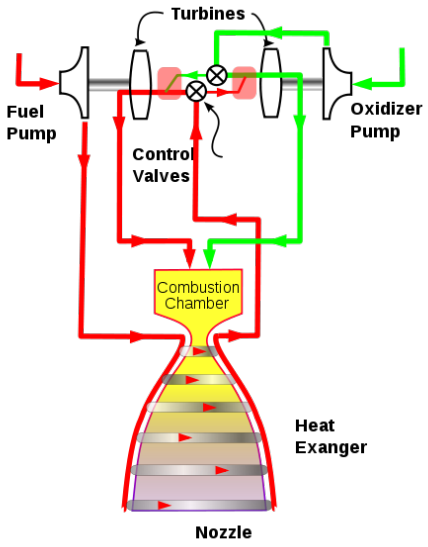


Figure 5.2: Staged Combustion Cycle (aerospace.org )

Of these presented concepts, the gas generator is the most simple but offers low performance. The remaining two are complex, but high performance solutions, with the expander cycle operating at a lower turbine inlet temperature. As a consequence, the expander cycle is able to provide less turbine power and chamber pressure than the staged-combustion system. It can be concluded that staged combustion offers the highest performance of all the approaches in return for increased complexity and cost. However, due to the large propellant mass and significant $\Delta V$ requirements of the mission, propulsion performance is crucial to reduce total costs and therefore staged-combustion will be used for the Mars One design.

## 5.6 Cooling Approach

Typical thrust chambers are designed to operate at temperatures well above the melting point of the structural materials. Therefore, it is necessary to cool them to avoid structural failure by using one of the following methods:

- **Radiation cooling** - The thrust chamber cools down through the radiation of heat into its surroundings. This is the simplest but lowest performing cooling method. It is mostly used for components that reach modest temperatures.
- **Ablative cooling** - The lining of the thrust chamber absorbs heat and ablates. This approach is used where simplicity is more important than low weight. However, the lifetime of the engine is restricted by the ablation rate of the expendable material.
- **Regenerative cooling** - Cold propellant runs through a heat exchanger which is an integral part of the thrust-chamber wall. The propellant absorbs heat being transferred to the structure, allowing the structure to maintain a lower temperature. Used with expander cycles.
- **Film cooling** - Fuel, oxidizer or coolant is injected close to the thrust chamber wall. This produces a flame with a lower temperature next to the wall. Lighter than ablative but more complex.

For the main propulsion system requiring only two relatively long burns we use ablative cooling, as it allows to reduce the system complexity and costs. This means that the engine lifetime is limited, but that is not an issue as the engine is designed to be expended after only one transfer journey. For the ADCS system and the respective small thrusters with very short burn times radiation cooling is used.

## 5.7 Engine Balance

As the propulsion system makes use of a pump to feed propellant to the engine, it is necessary to balance the system pressured and the power required by the pump with the power provided by the turbine. This process is highly iterative and therefore in this text only a rough first-order estimate will be given, which can be updated once the propulsion system components are designed in more detail. The power required for the turbo-pump is as follows:

$$p_{req} = \eta_T \cdot \dot{m}_T \cdot c_p \cdot T_i \cdot \left[1 - \left(\frac{1}{p_{trat}}\right)^{\frac{\gamma-1}{\gamma}}\right] \tag{5.7}$$

where:

$\eta_T = 0.7$ - turbine efficiency [-]
$\dot{m} = 123$ - turbine mass flow [kg/s]
$c_p = 1.4$ - specific heat of turbine drive gasses $(J/kg \cdot K)$
$T_i = 1100$ - turbine inlet temperature $(K)$
$p_{trat} = 1.5$ - turbine pressure ratio for staged combustion (-)
$\gamma = 1.2088$ - specific heat ratio (-)

Using this relation in combination with:

$$F = I_{sp} \cdot \dot{m} \cdot g_0 \tag{5.8}$$

and using the values previously obtained for the chosen propellant and oxidizer ($CH_4$/LOx) gives an estimate of $p_{req} = 8.66\ kW$.

**Propellant Mass and Tank Size** Now that the propellant has been chosen and the engine type known, an estimate of the propellant mass for the mission will can be made by using the ideal rocket equation [8]:

$$m_{prop} = \frac{m_{pay}\left[e^{\frac{\Delta V}{I_{sp}g_0}} - 1\right](1 - f_{inert})}{1 - f_{inert}e^{\frac{\Delta V}{I_{sp}g_0}}} \tag{5.9}$$

where the only new parameter is the inert mass fraction ($f_{inert}$). A typical first order estimate for space engines $f_{inert}$ from [8] is 0.1 for high-performance systems, where the lower the inert mass fraction, the higher the system performance. Furthermore, considering the initial payload mass estimate of 32,700kg (from the baseline design) and an expected $I_{sp}$ value of $CH_4$/LOx of 365 $s$ the resulting propellant mass is $m_{prop} = 257$ $t$. It must be noted that this value is only a first iteration on the baseline design values and not the final design value. The propellant mass for the final design will be presented when all the respective subsystems are sized and the total payload mass is defined.

## 5.8 Thrust Vector Control TVC and Structural Mounts

TVC systems maintain the vehicle's correct attitude for the thrust duration by rotating (gimballing) the thrust chamber or by redirecting the exhaust flow so that the thrust vector also generates a vehicle torque. Typical TVC methods include movable vanes, or the injection of other fluids in the flow. However, due to the high-performance capabilities of the PTV ADCS the propulsion system itself will rely exclusively on the ADSC for attitude control and not provide TVC capabilities in order to simplify the design.

Accounting for the configuration and mass of all the components that hold the structure together is very difficult to do at a preliminary design level. Accurate results can only be obtained when a detailed structural analysis of the system is performed after it has been designed in detail. Therefore, in order to account for the structural mounts and accompanying hardware the inert mass is increased by a contingency margin of 10%.

## 5.9 Propellant Storage

As mentioned in Ch. 3 the propellant will be stored in three external tanks. For ease of manufacturing each tank contains LOX and $LCH_4$ separated by a common bulkhead. This also enables the tanks to be emptied equally to reduce unbalances or to empty them sequentially, so that they can be jettisoned.
LOX and $LCH_4$ are cryogenic fuels, meaning that their critical temperature is below 123 $K$. Thermal control is therefore a vital part of the propellant storage. As mentioned above the pressure in the storage tanks is estimated to be 3 bar, to not unnecessarily increase the structural weight. For this pressure the vapor temperature of oxygen is 80 $K$ [17] and for methane 97 $K$ [18]. In this analysis both tank compartments are kept at the same temperature to set the temperature exchange between both compartments to zero.

To calculate the influx of energy into the tank it is necessary to consider the structure of the tank as mentioned in Ch. 7. The different layers of the MMOD shield, as described in Sec. 7.1.1, act as an insulator. Therefore the equilibrium temperature of each layer has been calculated, starting with the most outer layer. For this layer the equilibrium temperature is

defined by the energy absorbed from the sun, the energy radiated away and the energy reflected by the following layer. Also, heat is transferred through conduction by the elements connecting the different layers to each other. It has been assumed that another 20% of the total radiated energy is also transferred through conduction. This is a conservative estimation as the total area of the connection pieces is very low compared to the total area of the tank. However, as conduction is a more effective form of energy transport at the temperature range considered this still adds up to a significant amount.
For the energy transmitted by the sun it is assumed that the total energy equals the energy absorbed by the two dimensional silhouette (21.4 $m^2$) of the tank. Also, a partial reflection shield similar to the concept in [19] is used to reduce the energy received to at least 40%. To further reduce the the energy needed to keep the propellant cool an insulation layer of a thickness of 60 $mm$ is added on the inside of the tank made out of aerogel. The thermal conductivity of the aerogel is assumed to be 0.02 $W/(m \cdot K)$ [20], due to the pressure involved. It is assumed that the tanks are painted white ($\alpha$=0.14 $\epsilon$=0.94)[21], to reduce the power absorbed by the tank. Another important source of energy is the energy radiated by the PTV. The PTV dissipates a total energy of 6.6 $kW$ (See Ch. 8) over its total area. That equals an energy flux of 62.5 $W/m^2$ or around 5% of the solar irradiance at 1 $AU$.

After performing the calculations for all solar intensities along the flight path of the PTV, it is discovered that the propellant cannot be stored without an extra way of cooling. For the main part of the mission cryo coolers are considered to be used due to their relatively low weight compared to using boil off. Then the power needed for cooling can be calculated using the efficiency of cryo coolers for space applications. The coefficient of performance has been found to be 0.093 for 80 $K$.[22]. The results are plotted in Fig. 5.3. The power consumption peaks at the beginning to around 1.5 $kW$. It then suddenly drops to 375 $W$ due to external tanks being emptied and jettisoned. This value can be verified by comparing it to the power estimation given in [23] and accounting for the different sizes.

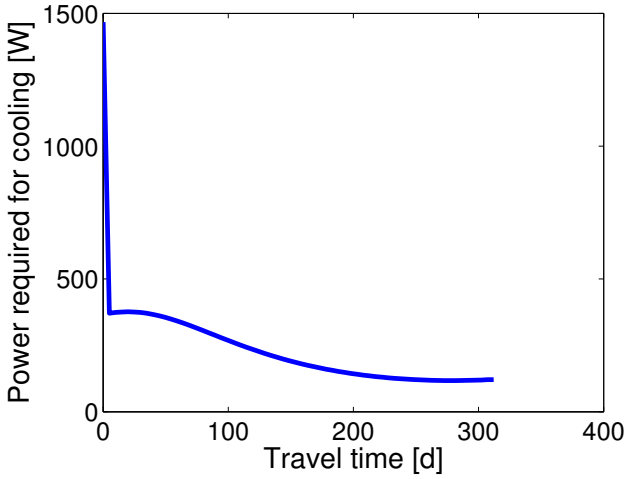


Figure 5.3: Total power required for propellant cooling

The energy needed to drive the cooling system is supplied by the PTV, therefore the cooling system cannot be used prior to docking. To keep the propellant cool during this first period of the mission, oxygen is boiled off. Above calculations suggest the heat needed to be rejected from the reservoir to be 136 $W$. For contingency this value is doubled to account for other potential sources of heat. Oxygen has a heat of vaporization of 6.8 $kJ/mol$. Per hour a total

amount of 2.3 $kg$ of oxygen is boiled off to cool the tank. The docking maneuver is expected to be completed in a few hours, for contingency a total time of 48 hours is taken to determine the extra boil off propellant. Furthermore, the tank will be cooled externally prior to the launch, so that there is no boil off occurring on ground. Therefore a total excess of oxygen of 110 $kg$ is needed to compensate boil off.

**Sensitivity Analysis** The propulsion system design depends mostly on the chosen propellant, transfer trajectory (performance), and the vehicle mass. If these inputs are not changed dramatically, the design sensitivity will not become a prominent characteristic of this subsystem, since the outputs vary approximately linearly with the inputs. However, if the inputs change considerably, such as changing from a high-trust to a low-thrust transfer trajectory, the resulting propulsion system design will change completely. Therefore, assuming there will be only minor changes in design inputs in the following design phases, the magnitude of the propulsion system sensitivity is directly related to the magnitude of the change in inputs.

**Verification and Validation** To design the propulsion system, empirical and theoretical methods from [8] have been used. They were supplemented and validated using methods presented in [9], which show a good correlation with historical data. They were both validated by applying methods to reference missions and the results were checked by consulting [24], where the obtained results were found to be within 20% of historical values.

**Conclusion and Recommendations** In this chapter the propulsion system design for the PTV has been presented. The system uses $LCH_4 + LOx$ as propellant, the propellant feed system design is operated by a turbo pump and the engine itself uses a staged combustion architecture to burn the propellant. Additionally, the system (especially the nozzle) is cooled by using ablative material, which keeps the cost and complexity to a minimum. Finally, due to the cryogenic storage needs of the propellant, cryogenic tanks will be used.

# 6 | Environmental Control & Life Support System

In order to let the astronauts survive the transfer to Mars, a Environmental Control and Life Support System (ECLSS) is necessary. Due to safety reasons, the air module consists of oxygen mixed with nitrogen, instead of pure oxygen. Oxygen is a highly oxidizing gas and nitrogen is an inert gas that is effective in decreasing the danger of the oxygen. The air of the module consists of 21 % oxygen and 79 % nitrogen and has a pressure of 101 kPa. Humans need a partial pressure of oxygen of 19.4 $kPa$ in order to breathe, and there can be a two hour emergency partial pressure of 13.4 $kPa$ [25]. A lower partial pressure will eventually result in death and thus additional oxygen and nitrogen are necessary to overcome pressure drops. Ventilation of the module air is necessary to avoid 'bubbles' of $CO_2$ around the heads of the crew members [25]. An overview of the ECLSS is given in Fig. 6.1. The dotted lines resemble the ECLSS boundary and the products of the arrows in the diagram going outside this boundary are vented in space.
In this chapter, the subsystems used for the ECLSS for both PTV and ML are explained. The chosen subsystems are already used or are being used at the International Space Station (ISS) and therefore have a technical readiness level of 9.

## 6.1 Atmosphere Revitalization

Oxygen is continuously inhaled by the astronauts and carbon dioxide is exhaled into the atmosphere, the temperature changes and the humidity increases due to human activities. In order to maintain the correct atmospheric conditions, the atmosphere is revitalized. The order of the atmosphere revitalization can be found in Fig. 6.1 and the explanation follows the same order.

### 6.1.1 Carbon Dioxide Removal

Carbon dioxide is exhaled by the crew members and has to be removed from the air and replaced with oxygen. This can be achieved via different methods. One of these methods is using $LiOH$ canisters. However, since this method requires 7 $kg$ of $LiOH$ per 4 crew members per day, it is too heavy for a long transfer time of 312 days [25].
The carbon dioxide will be separated from the air with use of a 2-Bed Molecular Sieve (2BMS) system, which consists of a $CO_2$ sorbent bed and a desiccant bed. The air from the living module is vented through the desiccant bed where the moisture of the air is removed, next it goes through the $CO_2$ sorbent bed to remove the $CO_2$. The removed $CO_2$ will go then into a Sabatier reactor, where due to a chemical reaction water is produced as explained in Sec. 6.1.2.

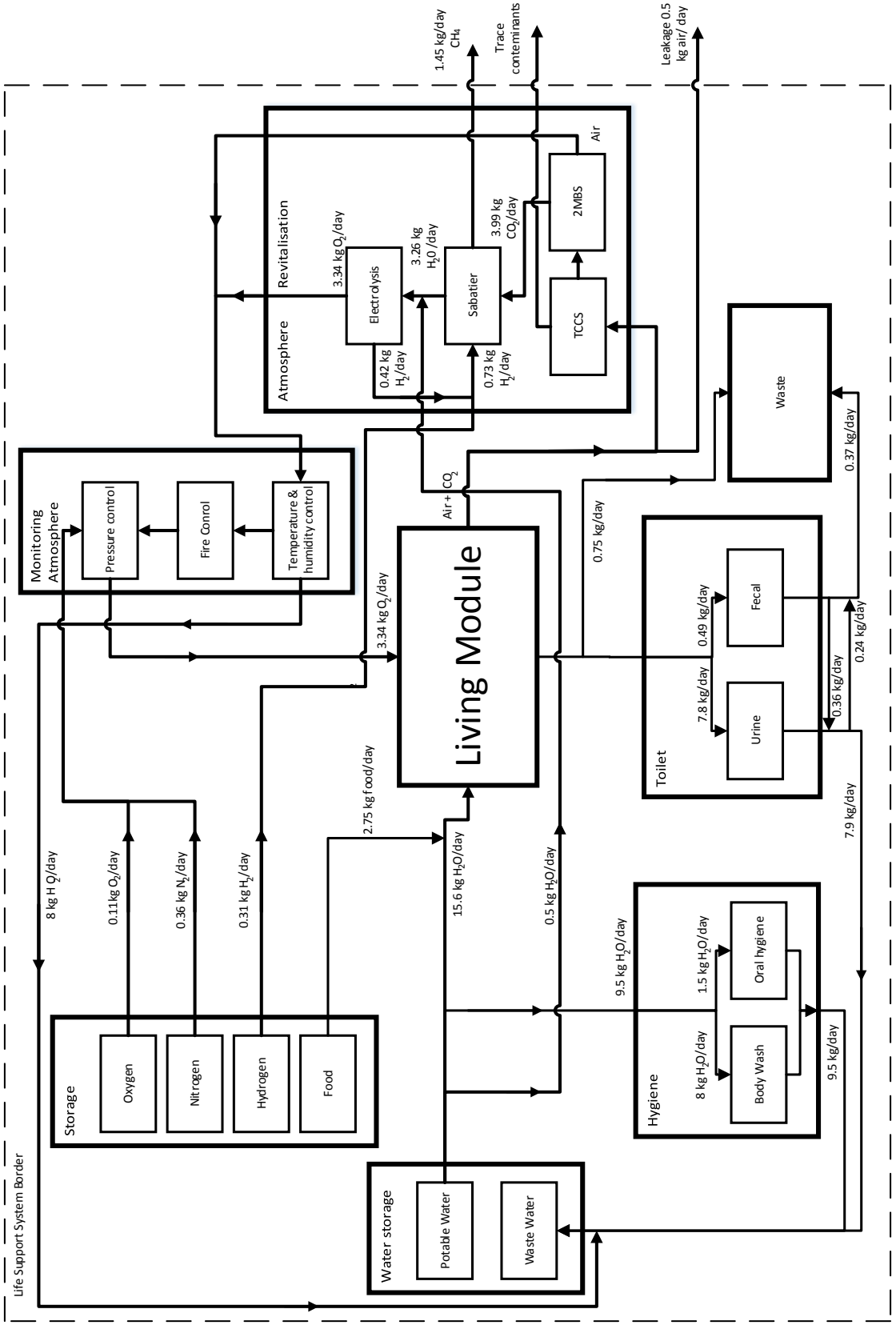


Figure 6.1: ECLSS Diagram for the PTV

### 6.1.2 Oxygen

According to NASA [26], an average person needs 0.84 $kg$ of oxygen per day. With four crew members this results in 3.36 $kg$ per day and 1041 $kg$ of oxygen per mission. It is a possibility to produce oxygen with the use of electrolysis. The electrolysis process equation for water is:

$$2H_2O \rightarrow 2H_2 + O_2 \tag{6.1}$$

As can be seen in 6.1, the ratio of water to oxygen is 2:1. This means that 2 moles of water are needed for one mole of oxygen. With the molar masses of water and oxygen, respectively 18.2 $g/mole$ and 32 $g/mole$, it can be calculated that for the entire mission 1173 $kg$ of water is needed for the production of oxygen. Since the water in the PTV is needed for shielding against cosmic radiation, it means this 1173 $kg$ of water needs to be added to the amount of water that can be used for the shielding.

Another option is bringing the oxygen needed for the entire transfer time. To decrease the volume the oxygen is stored under high pressure, which results in a higher tank mass. In this case, 90% of the oxygen mass is equal to the tank mass according to [25]. This results in 1647 $kg$ in total for the oxygen tank. The last option considered is a combination of the electrolysis reaction of water with a Sabatier reactor. The chemical reaction of this reactor is shown in Eq. 6.2.

$$CO_2 + 4H_2 \rightarrow CH_4 + 2H_2O \tag{6.2}$$

The carbon dioxide produced by the crew during the transfer time equals 1245 $kg$. With Eq. 6.2, it is found that with 229 $kg$ of $H_2$, 1019 $kg$ of water can be produced. As stated before, 1173 $kg$ of water is needed to produce the amount of oxygen needed, thus in total 133.1 $kg$ extra water is needed. As an extra product, $H_2$ is produced during electrolysis, but is also needed for the Sabatier reaction. For the entire mission, 96 $kg$ of $H_2$ is needed.
Clearly one can see that this last option is the lightest option. The electrolysis process and Sabatier reactor are both being used in the ISS and have a high reliability.

## 6.2 Monitoring the atmosphere

During the transfer to Mars, the atmosphere of the living module must be continuously monitored in order to maintain the living conditions. The air is constantly monitored by a Major Constituent Analyser (MCA) which monitors the amount of oxygen, nitrogen, carbon dioxide and methane in the atmosphere [27]. It also controls the temperature and humidity levels, detects fire and controls the pressure. Condensed water is separated from the air to maintain the desired humidity level and regulate the temperature. The fire control unit or Fire Prevention, Detection, and Suppression (FPDS) is needed to ensure the safety of the astronauts. Prevention starts already with selecting materials with low flammability, odour and off-gassing. Fire is detected with photoelectric detectors [28]. For fire suppression portable extinguishers are available for the crew. In case of a pressure drop, extra oxygen and nitrogen from the reserve tanks can be added to the living modules atmosphere in order to maintain the pressure.

The trace contaminant control sub-assembly or TCCS, which is also used in the ISS, removes trace contaminants from the living modules atmosphere with use of physical adsorption, thermal catalytic oxidation and chemical adsorption processes [29].

The Temperature and Humidity Control (THC) controls the temperature and humidity of the living module with the use of a Avionics Air Assembly (AAA) and ventilates the module using fans [26]. Humidity is removed with filters.

## 6.3 Food, Water & Waste Management

According to [4] 0.617 $kg$ of dry food is needed per person per day. This leads to a total amount of 770 $kg$ of dry food. A safety margin of 1.3 is used which leads to an amount of 1001 $kg$ food. Water is used to hydrate the food, which is included in Tab. 6.1, where the mass budget of the water is shown. As explained in Sec. 3.1 water is used for shielding against radiation. Instead of using the water in the shielding tank only, an additional amount of water could be stored in a separate tank and could be recycled during the mission. However, this would lead to an increase of systems needed to recycle water and therefore an increase in complexity and mass. Therefore, recycling of water is not used. The water used is pumped back into the water tank, where it is kept separated from the potable water by a membrane. With the length of the PTV kept in mind, it was calculated that 13823 $kg$ of water is needed in order to protect the crew against radiation. Since the crew needs 25.6 $kg$ water per day or 7987 $kg$ for the entire mission, enough water is available for the transfer and thus a safety margin is already included. The water needed for the oxygen production should be added to the 13823 $kg$ of water. An overview of the water used per day is given in Tab. 6.1.

Table 6.1: Water Use

| | Drinking & eating | Hygiene | Oxygen revitalization | **Total** |
|---|---|---|---|---|
| Water [kg/day] | 15.6 | 9.5 | 0.5 | 25.6 |

Waste management includes the management of urine, faeces and trash. Urine and faeces are collected at the toilet. This toilet is comparable to the toilet on the ISS, which uses air to flush the toilet rather than water. With use of flowing air, the liquid waste is separated from the solid waste. The liquid waste is pumped back into the waste section of the water tank, the solid waste continues to the waste container, where it will be stored for the entire mission duration.

## 6.4 Crew Quarters

In order to provide personal private space where the crew can sleep, recreate and have personal communication crew quarters are used. These quarters are comparable to the ones used in the ISS. The ISS crew quarters provide a habitable volume of 2.1 $m^3$ [30]. The crew quarters provide light and acoustic isolation and have a storage space of 0.1 $m^3$ for personal belongings. The astronaut has extra protection against radiation and solar particle events, around 9 % and 79 % respectively, due to the shielding of UHMWPE, Ultra High Molecular Polyethylene. Since no shelter for solar particle events is present in the rest of the PTV, the crew should seek shelter in their quarters in case of a solar particle event. The crew quarter cabin is shown in Fig. 6.2a. In total 4 of these cabins are needed, one for each crew member. Since only the habitable volume of the quarters was found and no other information on the dimensions is available, the outer dimensions are assumed in order to maintain the inner habitable volume. The total volume of each crew quarter is found to be 3.7 $m^3$. This provides enough volume for the materials used. According to [30], the crew quarters consists of aluminium and composite materials and

127 $kg$ of UHMWPE. With use of the known density of aluminium, it is assumed that each crew quarter has a mass of 240 $kg$. In Fig. 6.2b the configuration of the crew quarters inside the PTV is shown. The crew will lie in the crew quarters along the longitudinal direction of the PTV. The total length of a crew quarter equals 2.25 $m$, the remaining space between the quarters can be used to place electrical equipment and other life support systems.

(a) Crew Quarter of the ISS [30]

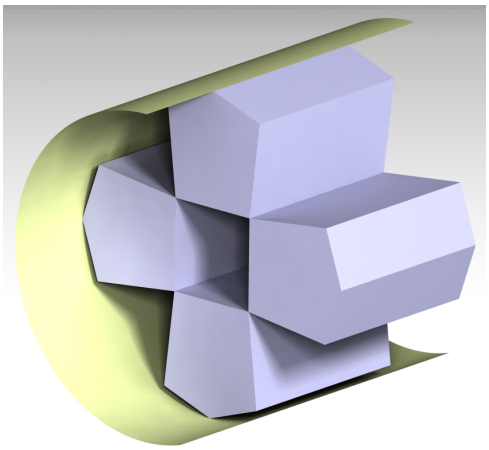

(b) Crew Quarters configuration in PTV

Figure 6.2: Crew Quarters

## 6.5 Summarizing

In Tab. 6.3 all the life support systems considered are shown, together with their masses and volumes. Since the water placed in the main water tank is used as a radiation shield, its volume and mass is not taken into account in this chapter. Also, facilities needed that are not explained above but are essential for the mission success, e.g. clothing and personal stowage are included. These masses are calculated again with use of [25]. The power requirements are explained in 11.

Table 6.2: ECLSS masses and volumes

| **Component** | **Mass [kg]** | **Volume [$m^3$]** | **Component** | **Mass [kg]** | **Volume [$m^3$]** |
|---|---|---|---|---|---|
| $H_2O$ | 97 | - | Water management | 612 | 0.7 |
| $H_2$ incl. tank | 145 | 0.021 | Waste management | 259 | 0.7 |
| $N_2$ incl. tank | 166 | | Clothing | 247 | 0.21 |
| $O_2$ incl. tank | 131 | 0.136 | Personal Stowage | 120 | 0.47 |
| 2BMS | 120 | 0.6 | Exercise equipment | 145 | 0.19 |
| TCCS | 80 | 0.6 | Medical equipment | 500 | 1 |
| Sabatier Reactor | 152 | 0.28 | Electrolysis | 150 | 0.07 |
| Food | 1001 | 5 | MCA | 100 | 0.5 |
| Food facilities | 700 | 0.5 | Crew Quarters | 960 | 14.8 |
| | | | **Total** | **5685** | **25.7** |

## 6.6 Mars Lander ECLSS

The Mars Lander (ML) is connected to the PTV and its ECLSS. When the PTV has almost arrived at Mars, it is time for the crew to enter the ML and close its hatch. The ML will detach from the PTV and therefore needs its own ECLSS from that moment onwards. The total time, from detachment from the PTV until landing on the Martian surface, will last about 5 hours. As a safety margin and because the crew will also be launched into Earth orbit in the ML, the maximum amount of time the crew can survive in the ML is 5 days. Therefore there should be oxygen present for 5 days, together with smaller oxygen tanks on the suits the crew will use in case of emergency.
Inside the Mars Lander the astronauts will wear their suits, which will protect them in case of pressure drops. When no pressure drop occurs, they will be breathing the oxygen provided by the ML. Looking at the ECLSS diagram in Fig. 6.1, some compartments of the ECLSS can be removed for the ML. The toilet, the hygiene compartment and the waste tank are not needed in the Mars Lander since the crew will wear their suit and are therefore not able to make use of these facilities. In every suit a water supply should be present, as well as a small snack, comparable to the Extravehicular Mobility Unit [31]. A water tank in the Mars Lander is present in case the landing will take more time then one day. Also, no atmosphere revitalization will take place, only $CO_2$ will be removed from the lander. This will be done with use of $LiOH$ canisters, which absorb the $CO_2$. As explained in Sec. 6.1.1, this requires 7 $kg$ of $LiOH$ for 4 crew members per day. Using these canisters during transfer would be too mass intensive, but for the relatively short period of 5 days, this will save mass compared to the systems in the PTV. All the oxygen and nitrogen needed is stored in tanks. Again, the same atmospheric ratio is used: 21 % Oxygen and 79 % nitrogen and the same loss of 0.5 $kg/day$ of air is considered. The atmosphere is constantly controlled with use of the MCA and monitored by the pressure control, fire control, and temperature and humidity control. In Tab. 6.3 an overview of the ECLS systems of the Mars lander is given.

.

Table 6.3: ML ECLSS masses and volumes

| **Component** | $H_2O$ | $N_2$ | $O_2$ incl. tank | $LiOH$ canisters | Food | MCA | Total |
|---|---|---|---|---|---|---|---|
| **Mass** [kg] | 40 | 2.7 | 15 | 35 | 13 | 100 | **205.7** |
| **Volume** [$m^3$] | 0.04 | 0.173 | 0.05 | 0.025 | 0.03 | 0.5 | **3.3** |

In Fig. 6.3, the adjusted ECLSS for the ML is shown.

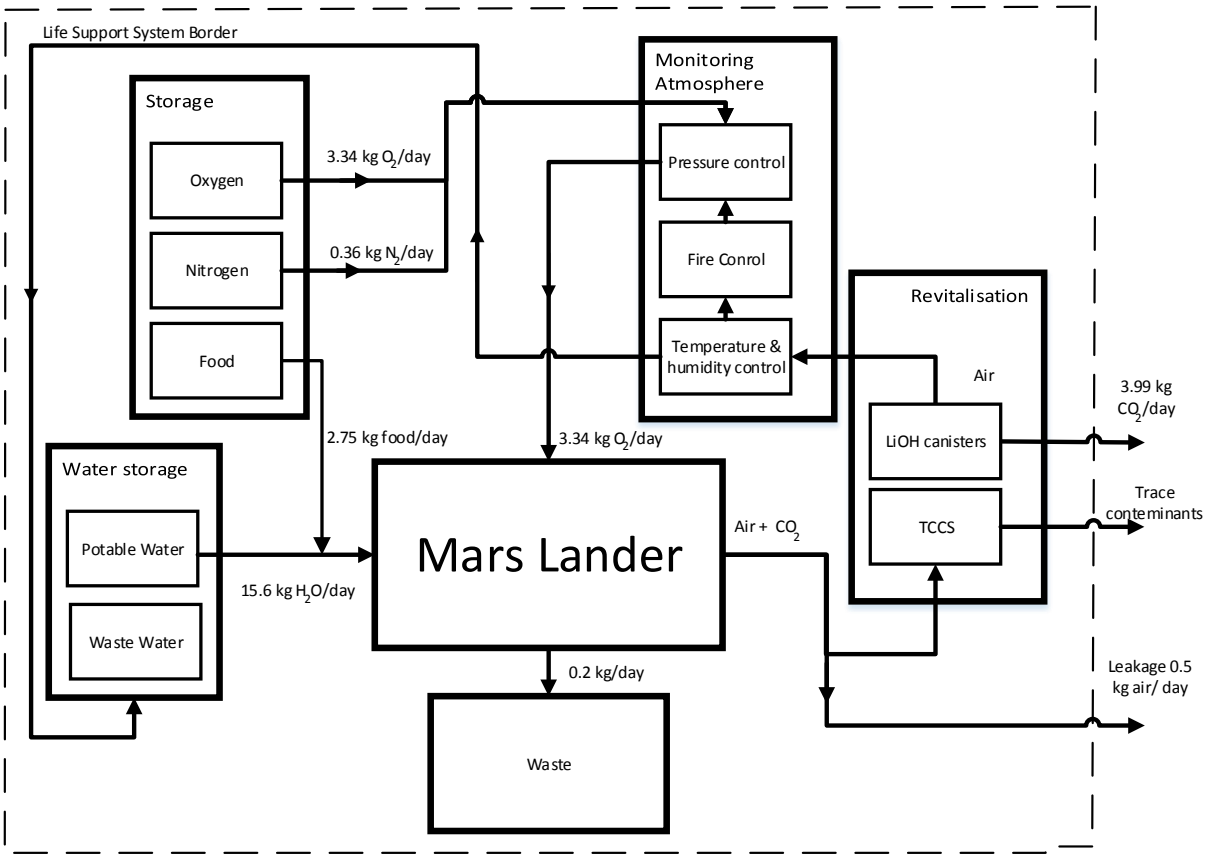


Figure 6.3: ECLSS diagram for the Mars Lander

## 6.7 Verification & Validation

The ECLSS subsystem is designed on very basic principles found in sources, as cited throughout the chapter. This is a good approach since the total design is only at phase A level. These principles can be verified with use of different literature. In the ISS, 1.72 *kg* food is provided per astronaut per day. This is including packaging and mostly not dry food, but would still require water preparation [32]. The used food mass and water available for preparation is equal to 2.3 *kg* per day per astronaut. Considering that the ISS food needs additional water, the food mass calculated is a good estimate. [33] uses the same value of 0.617 *kg* food per day.
[33] and [4] use the same value of oxygen needed per day per crew member which is also used in this chapter. Most subsystems of the ECLSS are already used on spacecrafts like the ISS. However, masses of those subsystems are often not available to validate the ECLSS mass budget. Only a rough estimation could be made of the total masses and it concluded to be in a reasonable range. This is not the case for the radiation shield: A water tank which contains the potable water and waste water has never been used before as a radiation shield. Therefore, this component cannot be validated.

## 6.8 Sensitivity Analysis

A sensitivity analysis was performed for the ECLSS. The water tank depends on the length of the living module, which depends on the number of astronauts. The water will increase with

2765 $kg$ per meter of length increase of the PTV.
If two extra astronauts are on board, extra space is needed for the crew quarters. Looking at Fig.6.2a, it can be seen that two extra crew quarters would not fit in this configuration and thus a different configuration of the crew quarters must be chosen. All supplies needed depend on a linear relation with the amount of people and travel time. Changing the number of astronauts or transfer time will thus lead to an expected linear increase/decrease of supplies masses and volumes.

## 6.9 Conclusion & Recommendations

In this chapter the ECLSS designs for the PTV and ML have been presented. The PTV uses a water radiations shield which is also be used as tank with the potable and waste water separated and thus no water recycling is used. Carbon dioxide is removed from the air with use of 2BMS, and oxygen is produced with use of a Sabatier reaction and electrolysis process and added. Crew quarters are available and provide extra protection against cosmic radiation and solar particle events. Finally, other components of the ECLSS are present: food and its facilities, medical equipment, hygiene facilities, clothing, personal belongings and exercise equipment. For the Mars Lander, a water tank is present, together with a oxygen and nitrogen tank. No atmosphere revitalisation takes place. For future designs of the PTV, it can be considered to store the water in multiple tanks which act as radiation shields to increase the redundancy of the water radiation shield.

# 7 | Spacecraft Structural Design

The spacecraft's structural integrity is essential to the mission success and the crew's safety. It is therefore important to ensure at an early stage of the design that each component's structure is able to support the maximum loads that are predicted to occur within their life cycle. This chapter discusses the sizing procedure of the most simple primary spacecraft structures. The structure of the PTV and its propellant tanks are designed first while the ML's structure will be discussed separately in the ML design section.

## 7.1 PTV Structural Design

The habitable compartment of the PTV is subjected to several load cases that are characteristic to this mission: the internal pressurization, the thermal stress due to temperature variation in space, the maximum compressive acceleration and the vibration loads during launch. However, before the main structure is designed for the critical loads it is first necessary to determine its exact size, i.e. height and diameter. For that purpose it is important to account for the size of a integral structural element: the Micro-meteoroid and Orbital Debris shield.

### 7.1.1 Shielding against Micro-meteoroids and Orbital Debris

During its transfer journey of more than 300 days it is likely that the spacecraft will be impacted by micro-meteoroids or orbital debris. Most of these objects are small, being only a few millimeters in diameter, but have very high velocities of several km per second. This means that in the event of an impact with the spacecraft the objects might perforate the main structure and cause catastrophic damage to the pressurized vessel. It is thus important to take into account an MMOD protection shield that will prevent this damage. The size of this shield will have substantial influence on the size of the PTV's main structure, which is why it is discussed before the structure is designed for critical loads.

A good example for an MMOD shield can be found on the U.S. Laboratory Module that is part of the International Space Station (ISS), as can be observed in Fig. 7.1 [34]. It uses two main versions of MMOD shields: a traditional Whipple Shield and an enhanced version, the Stuffed Whipple Shield. The concept of the Stuffed Whipple Shield is shown in Fig. 7.2. The traditional Whipple Shield configuration consists of only one bumper layer without the intermediate layers.

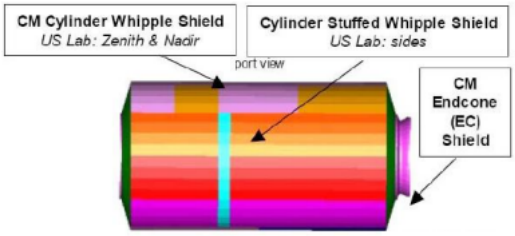


Figure 7.1: U.S. Laboratory Module MMOD Shielding [34]

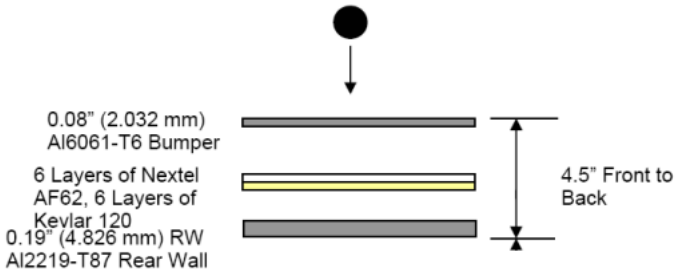


Figure 7.2: U.S. Laboratory Stuffed Whipple Shield configuration [34]

The basic principle of a Whipple Shield is to use a thin "bumper" layer with some stand-off that breaks up an MMOD projectile upon impact into a cloud of smaller debris particles whose kinetic energy is greatly reduced. The debris cloud then spreads through the stand-off gap and hits the underlying layer over a large area and thus causes much less damage than it would have without the sacrificial bumper [35]. However, it has been found that for larger and faster MMOD objects the Whipple Shield has to be improved. The improved version, called the Stuffed Whipple Shield, incorporates an intermediate shield made of multiple layers of Nextel AF62 fabric and Kevlar 120 in epoxy resin. The intermediate layers further absorb the projectile's kinetic energy and improves the performance of the original Whipple Shield. The U.S. Laboratory Module has different shielding configurations at different locations of the spacecraft because the probability of MMOD impacts coming from certain directions to the ISS can be predicted. For the Mars One Mission it is very hard to tell at this stage from what direction the MMOD might come from. Therefore it is decided to use the Stuffed Whipple Shield configuration as shown in Fig. 7.2 for the complete outer wall of the PTV as it provides better shielding performance. The thickness and material of the bumper layer is given in Fig. 7.2 from [34] and reasonable dimensions for the Nextel AF62 and the Kevlar composite can be found in [36]. The densities of the intermediate materials can be found in [37] and [38]. Using these parameters and the stand-off height shown in Fig. 7.2 the total mass of the MMOD shield can be calculated for the PTV dimensions given in Ch. 3 (4.6 m in diameter and 5 m in height). All values are summarized in Tab. 7.1.

Table 7.1: Properties of MMOD shield layers [36], [38], [37]

| **MMOD Shield Layer** | **Thickness** $[mm]$ | **Density** $[kg/m^3]$ | **Total Mass** $[kg]$ |
|---|---|---|---|
| Al6061-T6 bumper layer | 2.03 | 2710 | 399 |
| Nextel AF-62 stuffing | 4.0 | 2700 | 756 |
| Kevlar composite stuffing | 6.0 | 1350 | 566 |

The "Rear Wall" shown in Fig. 7.2 is the main structural wall whose thickness will later be determined according to critical load cases. As can be observed in Tab. 7.1 the Stuffed Whipple Shield will add an additional 1721 kg to the PTV's structure. Because the payload room's radius in the Falcon Heavy launcher is limited to 2300 mm, the shield also reduces the actual outer radius of the PTV by around 126 mm, which is the total thickness of the shield minus the 4.8 mm rear wall shown in Fig. 7.2. This makes the outer radius of the main structure 2174 $mm$. This number can now be used to size the wall thickness of the PTV main structure. The MMOD shield here is based on the shield used on the ISS. However, there is the possibility

that the spacecraft might encounter larger or faster meteoroids on its way to Mars than the ones found for the ISS in Low Earth Orbit. The Stuffed Whipple Shield proposed here then might not be sufficient to stop those projectiles. A simple solution to this problem is to increase the thickness or the stand-off between the bumper and the intermediate layers. A thicker shield will absorb more kinetic energy by breaking up a particularly large projectile into sufficiently small particles. A wider gap between the layers provides room for the debris cloud to spread out over a larger area such that their remaining kinetic energy will be less concentrated. Alternatively, there are more advanced shield configurations that have been investigated in different studies. They involve, for example, adding a Mesh Bumper shield as a second bumper. More information can be found in [39].

### 7.1.2 Sizing for Pressurization Loads

For a manned mission it is necessary to pressurize the crew's living module to an acceptable internal pressure. According to [25] the maximum pressure that is required during a space mission is slightly above sea-level pressure, at 0.1096 $MPa$. The skin of a monocoque shell is very efficient in carrying such pressure loads, which is why this structural configuration is chosen for the PTV. It is important to note that the PTV requires a surrounding water tank for radiation shielding such that the structure consists of two hollow cylinders as shown in Fig. 7.3.

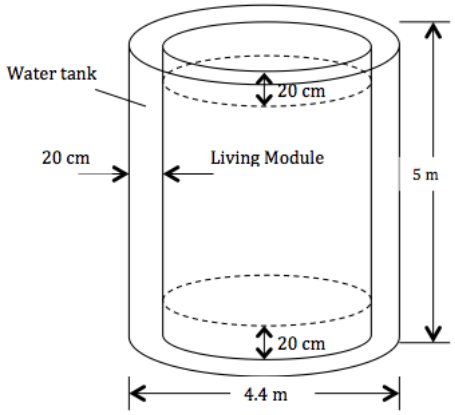


Figure 7.3: PTV Living Module Configuration

For the pressurization of he cylinders it is possible to design the PTV such that only the outer cylinder carries the pressure load. The inner cylinder only needs to be a thin-walled partition that separates the water tank from the living module. When sizing for the launch loads there is the possibility of designing the inner cylinder as a load-carrying structure as well in an attempt to save mass. This will be discussed in the next section. In the walls of the cylindrical tube the pressurization creates a longitudinal stress and a hoop stress. These stresses can be expressed as stated in Eq. 7.1 [25].

$$\sigma_{p,long} = \frac{pr}{2t}, \sigma_{p,hoop} = \frac{pr}{t} \tag{7.1}$$

The relevant parameters are: p - the internal pressure, r - the cylinder's radius and t - the wall thickness. As can be observed in Eq. 7.1 the hoop stress has twice the magnitude of the longitudinal stress and is thus more critical. The PTV's wall thickness will therefore be sized with the hoop stress. According to [25] NASA specifies the pressure safety factors for the

ultimate stress to be 2 and the yield stress to be 1.5. The ratio of the ultimate stress' safety factor to the yield stress' safety factor is 1.33. If a material's ultimate-to-yield stress ratio is lower than this number, the thickness should be designed according to the material's ultimate stress with a safety factor of 2. If the ratio is higher, then one must design for the yield stress with a safety factor of 1.5. It is thus appropriate to define the properties of some commonly used materials at this point.

Table 7.2: Material Properties [40], [41]

| | **Al 2219-T851** | **Al 6061-T6** | **Al 7075-T73** | **Steel 17-4PH** | **Ti-6Al-4V** |
|---|---|---|---|---|---|
| Ultimate Tensile Strength $[MPa]$ | 430 | 290 | 460 | 860 | 900 |
| Yield Tensile Strength $[MPa]$ | 320 | 240 | 390 | 690 | 830 |
| Young's modulus $[MPa]$ | 72000 | 68000 | 71000 | 196000 | 110000 |
| Density $[kg/m^3]$ | 2850 | 2710 | 2800 | 7860 | 4430 |
| Average Price $[US\$/kg]$ | 5.5 | 7.55 | 13.00 | 9.20 | 110.00 |

The metals shown in Tab. 7.2 are considered to be the most suitable options for this application as they are commonly used for primary structures in aerospace applications. The Aluminum alloys are very lightweight, steel has a particularly high tensile strength, and Titanium has very good high-temperature properties and a very high specific strength [41].

Using the respective safety factors the required wall thickness for each material is calculated using Eq. 7.2.

$$t = k \cdot \frac{pr}{\sigma_{des}} \tag{7.2}$$

where t is the thickness, p is the internal pressure, $\sigma_{des}$ is either the ultimate or the yield tensile stress (as discussed before) and k is the corresponding safety factor. Tab. 7.3 summarizes the required thickness that has been calculated for the selected materials.

Table 7.3: Required wall thickness for a internal pressure of 0.1096 $MPa$ for selected materials

| **Material** | Al 2219 | Al 6061 | Al 7075 | Steel 17-4PH | Ti-6Al-4V |
|---|---|---|---|---|---|
| Thickness [mm] | 1.14 | 1.66 | 1.04 | 0.58 | 0.53 |

The required thickness for supporting the highest expected pressure loads have now been established. Tab. 7.3 shows that for all materials the required thickness to withstand the pressure loads is less than the thickness required for the rear wall of the MMOD shield, as shown in Fig. 7.2. However, pressure is not the only load case that has to be accounted for. Another critical load case is the maximum compressive load during launch that could lead to buckling of the cylindrical tube.

### 7.1.3 Sizing for Compressive Launch Loads

The maximum acceleration that the PTV will experience during its lifetime is expected during launch. The plan is to use Space X's Falcon Heavy rocket to launch most of the spacecraft's

components, but since this launcher has not been built yet so it is only possible to use the manual of the Falcon 9 launcher as a reference. It is expected that the maximum load factor of -6 g given in Falcon 9's user guide is not going to be exceeded significantly. Also, none of the launchers given in [40] exceeds 6 g in magnitude (most of the load factors are significantly lower). It is therefore decided to size for a maximum compressive load of -6 g. [42].

**Buckling stress of monocoque cylinder:** The critical buckling stress of an unpressurized monocoque cylinder with radius r is given in [25] to be:

$$\sigma_{crit} = 0.6\eta\gamma\frac{Et}{r} \tag{7.3}$$

where E is the elastic modulus, t is the thickness, $\eta$ is the plasticity correction factor and $\gamma$ is the correlation factor between theory and experiment. $\eta$ is assumed to be 1.0 if the stress is below the material's proportional limit (see [25]) and $\gamma$ is assumed to be 0.5 for compressive and bending loads. Eq.7.3 has to be compared to the normal and bending stress that is imposed on the structure in order to design for the thickness.

**Maximum normal stress:** The maximum normal stress imposed on the PTV during launch originate from the total weight of the PTV itself and the experienced bending moment. It can be expressed as:

$$\sigma_{max} = \frac{P}{A} + \frac{Mc}{I} \tag{7.4}$$

where P is the normal force in [N], A is the structure's cross-sectional area, M is the maximum bending moment due to the lateral load factors, c is the cross-section's maximum distance to its neutral axis, and I is the structure's cross-sectional area moment of inertia. The normal stress in addition to the longitudinal pressure stress from Eq. 7.1 must not exceed the critical buckling stress from Eq. 7.3. This can be expressed as:

$$\sigma_{max} = 1.4\left(\frac{P}{A} + \frac{Mc}{I}\right) - 1.5\left(\frac{pr}{2t}\right) \leq 0.6\eta\gamma\frac{Et}{r} \tag{7.5}$$

where p is the maximum pressure difference expected during launch (which is assumed to be equal to the internal pressure specified earlier) and 1.5 and 1.4 are the design factors specified for inertia loads and compressive pressure stress [25].

For a thin-walled circular hoop the area A and the moment of inertia I can be simplified as:

$$A = 2\pi rt, I = \pi r^3 t \tag{7.6}$$

Combining Eqs. 7.4, 7.6 and 7.1 (as explained before) it is possible to solve directly for the respective wall thickness of the cylinder:

$$t = \sqrt{\frac{r}{0.3E}\left[1.4\left(\frac{P}{2\pi r} + \frac{M}{\pi r^2}\right) - 1.5\left(\frac{pr}{2}\right)\right]} \tag{7.7}$$

Eq. 7.7 shows the general formula for calculating a cylinder's thickness that is required to support the normal force P and the bending moment M. In the following it is discussed how P and M are obtained

**Normal force P:** Since no extra load is imposed on the PTV, the normal force is assumed to be the weight of the PTV itself times the maximum axial compressive load factor of -6 g:

$$P = -n_x W_{PTV} \tag{7.8}$$

where W = 253098 $N$ is assumed to be the total weight of the PTV as specified in the Baseline Design (mass times 9.81 $m/s^2$) and $n_x$ is the axial load factor.

**Bending moment M:** To determine the bending moment it is appropriate to idealize the structure as a uniform beam. The bending moment is caused by the weight of the PTV (which is distributed along its length) and the maximum lateral load factor, and also depends on the way the "beam" is supported in the launcher's payload compartment. Falcon 9's user guide states that the customer is allowed to specify the payload attach fittings. According to an example in [25] a common and efficient way to fix the payload is to use so-called "trunnions" that support the payload such that it can be simplified as a beam supported as shown in Fig. 7.4.

Figure 7.4: Payload support during launch

It is assumed that the PTV's weight is uniformly distributed along its length such that the maximum bending moment in the beam as show in Fig. 7.4 is given by:

$$M_{max} = \frac{n_{yz} w L^2}{8} \tag{7.9}$$

where $w$ is the distributed weight in $[N/m]$, $n_{yz} = 2g$ is the lateral maximum load factor specified in [42] and L $[m]$ is the length of the PTV.

Before actually applying this design approach and the above mentioned equations, the structural configuration needs to be specified. At this point it is possible to define different configurations. These are discussed in the following.

### Design configuration options

Two different options are investigated as structural configurations. The masses obtained with each configuration will later be compared to conclude which one is the most efficient.

#### 1. Design monocoque cylinder as only structural component:

This configuration takes the most straightforward approach using only the outer cylinder as the load-carrying component.

The skin thickness in this case is simply calculated with Eq. 7.7. The result is summarized for the selected materials in Tab.7.4.

As can be observed in Tab. 7.4, for all materials the wall thickness needed to support the launch loads is higher than the thickness needed to support the pressure loads (given in Tab. 7.3). Therefore, if the structure is indeed designed as a simple monocoque then the wall thickness have to assume the values given in Tab. 7.4. But first the a different structural configuration is considered.

Table 7.4: Required thickness for single monocoque cylinder to withstand maximum compressive launch loads

| **Material** | **Al2219** | **Al6061** | **Al7075** | **Steel 14-4PH** | **Ti-6Al-4V** |
|---|---|---|---|---|---|
| Thickness $mm$ | 6.08 | 6.21 | 6.12 | 3.69 | 4.92 |

**2. Design outer cylinder with stiffener reinforcement**

In order to reduce structural weight, stringers are commonly applied to support compressive loads. This structural configuration is shown in Fig. 7.5.

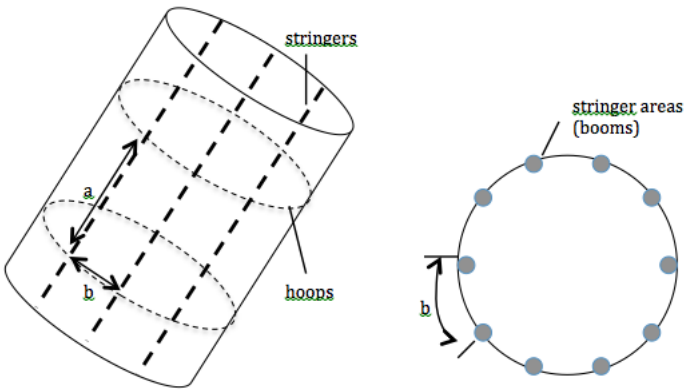


Figure 7.5: Stringer configuration and booms

The design configuration shown in Fig. 7.5 aims to maintain the skin thickness that is required for the outer cylinder to withstand the pressure loads by adding stringers to carry the compressive launch loads. The critical loads that are important for the design with stringers are described below.

**Column Buckling Load:** The use of stringers leads to two buckling limit loads that cannot be exceeded by the maximum applied normal stress. The first limit load is the Euler column buckling load which is expressed by:

$$F_{crit} = \frac{\pi^2 EI}{L^2} \tag{7.10}$$

where L is the length of the propellant tank and I is the moment of inertia given by the booms. Dividing the Euler column buckling load by the cross-sectional area gives the critical stress. It is first explained how the moment of inertia I is obtained in this case.

**Idealization of structure cross-section with booms:** In a Phase A analysis it is common practice to idealize the stingers' cross-sectional areas as "booms" and assume that they carry all normal stresses (thus disregarding the skin's cross-sectional area). The booms are treated as areas located at certain distances from the structure's neutral axis without specifying their exact dimensions. Their cross-sectional area and moment of inertia are calculated with:

$$I = \sum_{i=1}^{n} A_i d_i^2 \tag{7.11}$$

where $A_i$ is the cross-sectional area of boom i and $d_i$ is the distance of boom i to the neutral axis of the cylinder's cross-section. If a constant stringer pitch is applied then the distance $d_i$ for boom i is given by:

$$d_i = r \sin \alpha_k, k = 1, 2, ..., n/2 \tag{7.12}$$

As it is assumed that the tank has a perfect circular cross-section, a uniform distribution of stringers with a constant stringer pitch will lead to the same I about both x and y axis, so a bending moment can be supported around both axes.

### Skin Buckling Load

The second limit load is the skin buckling loads. Local skin buckling might occur in the walls between the stringers even though the stringers themselves do not buckle. The skin buckling is expressed by:

$$\sigma_{cr} = \frac{k\pi^2 E}{12(1-v^2)} \left(\frac{t}{b}\right)^2 \tag{7.13}$$

where t is the skin thickness that is needed to withstand the pressurization stress, b is the pitch between two stringers, v is the material's Poisson's ratio and k is a geometric coefficient that relates to the aspect ratio a/b (see Fig. 7.5 of one skin panel as well as how the stringers are constrained between two ends. As it is expected that the stringers are fixed to the hoops in the cylinder as shown in Fig. 7.5, it is reasonable to assume that the ends are clamped. The aspect ratio of the skin panel depends on how many hoops are used in the structure. In order to save mass it is decided to use a maximum of 3 hoops, which would result in:

$$a = \frac{L}{n_{hoop} + 1} = \frac{4650mm}{4} = 1162.5mm \tag{7.14}$$

The stringer pitch b is then varied by changing the number of stringers while keeping a constant. A graph is given in [43] that determines the value of k for different attachment types and aspect ratios a/b.

The maximum stress imposed on the structure is again given by Eq. 7.4. After selecting an arbitrary number of stringers and a certain boom area the maximum stress is calculated using Eq. 7.4. This imposed stress is then compared to the column buckling load obtained from Eq. 7.10 (and dividing the load in [N] by the cross-sectional area of the booms) as well as the skin buckling load from Eq. 7.13. If either the imposed load exceeds either the column buckling load or the skin buckling load a higher number of stringers must be used. The required number of stringers and their total mass is calculated for the selected materials and shown in Tab. 7.5.

Table 7.5: Required number of stringers and total mass of stringers for selected materias

| **Material** | Al2219 | Al6061 | Al7075 | Steel 17-4PH | Ti-6A-4V |
|---|---|---|---|---|---|
| Req. number of stringers | 264 | 178 | 296 | 401 | 584 |
| Tot. mass of stringers [kg] | 564 | 362 | 622 | 2370 | 1940 |

As can be observed from Tab. 7.5 the lowest number of stringers and lowest additional mass is achieved with Al6061 despite the superior stiffness properties of the other materials. This is explained by the fact that the skin thickness of Al6061 required to withstand the pressure loads is higher than that for other materials. The structure's skin buckling load increases with the square of the skin thickness, so a thick wall will have a very strong impact on the required number for stringers. After the results for all three design configuration are it is investigated in the following which one of them - and with what material - gives the most efficient structure.

### Configuration and Material Selection

In the following it is investigated which of the two stated design options leads to the most lightweight structure. The structure's mass is the most important trade-off factor since mass savings in the PTV's dry mass will lead to a decrease in propellant mass, which might in turn lead to a decrease in the number of required tank launches. The materials cost is unsubstantial in comparison since for this mission the development cost is estimated to be in the order to billions of USD. Fig. 7.6 shows the total mass of the structure for the three design configurations and the selected materials.

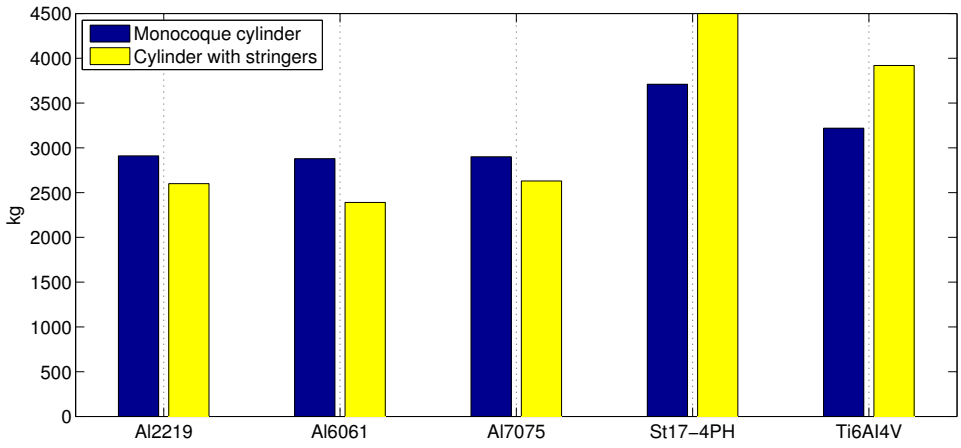


Figure 7.6: Total structural mass [kg] for different design configurations and materials

As can be observed from Fig. 7.6 the lowest mass is achieved with the cylinder + stringer configuration using Al6061. This design uses 178 stringers and has a total mass of 2390 kg. It is therefore decided to use this particular configuration and material for the PTV's main structure. It is however necessary to prove that this design will not fail due to other loads such as thermal loads or vibration loads.

**Thermal Property Considerations:** Although Aluminum alloy 6061 has a rather high coefficient of thermal expansion of 22.9E-6 [40] this value is considered acceptable since, according to Ch. 8, the temperature experienced by the PTV will stay within the maximum limits of 187 K to 308 K if black paint is used. This would result in a maximum thermal expansion stress of [41]:

$$\sigma = E\alpha\Delta T = (72000MPa)(22.9E-6)(121) = 192.5MPa \tag{7.15}$$

This level of thermal stress is acceptable as it is well below Al6061's tensile yield stress of 240 $MPa$. Also, the maximum temperature of 308 K (35°C) is only slightly above room

temperature and will thus not significantly affect the strength of the material. Also, according to [44] the Al6061-T6 alloy has good fracture fracture toughness at a very low temperature of $-196°C$, so it is reasonable to assume that at the minimum predicted temperature of $-86°C$ for this application it will also retain most of its strength properties.

### 7.1.4 Resistance against Vibration Loads

Another critical load case are the vibration loads that occur during launch. According to [42] the natural frequency of a structure installed in Falcon 9's payload compartment should have a fundamental bending mode of more than 10 Hz and a fundamental axial mode of more than 25 Hz so the designed structure needs to be able to meet these requirements. The equations for calculating the fundamental bending frequency of a beam as shown in Fig. 7.4 is given in [25] to be:

$$f_{n,bend} = 1.57\sqrt{\frac{EI}{mL^3}} \tag{7.16}$$

where E = 72 000 $MPa$ is the elastic modulus, I is the cross-sectional moment of inertia, m = 25800 $kg$ is the total mass of the tank and L = 5 $m$ is the total length of one tank (as specified in the PTV baseline design). For Eq. 12.16 to be valid it is again assumed that the PTV can be idealized as a uniform beam. For the chosen Al6061 material this results in a fundamental bending frequency of 354.5 $Hz$, which is well above the specified lower limit frequency of 10 $Hz$. The designed structure therefore meets the launcher's bending frequency requirement. For the axial frequency it is necessary to make an assumption that the mass is approximately uniformly distributed since the PTV is not a structure that carries a certain heavy payload at its free end. According to [25] the fundamental axial bending mode in this case can be expressed as:

$$f_{n,ax} = 0.25\sqrt{\frac{AE}{mL}} \tag{7.17}$$

where A is the beam's cross-sectional area. Using the chosen Al6061 material this would result in a fundamental axial frequency of 121.7 Hz, which is well above the specified lower limit frequency of 25 Hz. The designed structure therefore also meets the launcher's axial frequency requirement.

## 7.2 Propellant Tank Structural Design

Due to the large spacecraft mass and high $\Delta V$ involved, this mission requires a lot of propellant that has to be stored in tanks. These tanks also have to be designed to withstand the predicted critical loads. Due to the mass of the propellant and the pressurization requirements, the tanks must withstand a higher pressure and a higher compressive load than the PTV.

### 7.2.1 Shielding against MMOD

Similar to the PTV main module the propellant tanks have to be shielded against micro-meteoroids and orbital debris impact. It is decided to use the same Stuffed Whipple Shield configuration as shown in Fig. 7.2 for the reasons discussed in Sec. 7.1.1. For a tank with a height of 4.65 m and a outer diameter of 2.3 m (see Ch. 3) the shield would add a total of 1720 kg.

### 7.2.2 Sizing for Pressurization

As explained in Ch. 5 the propellant tanks require an internal pressure of 3 $bars$ (0.3 $MPa$). To withstand the hoop stress associated with this pressure the structure's wall thickness is again calculated with Eq. 7.2, the material's design limit strength and the corresponding safety factor (as explained in detail in the PTV structural design). The results for the selected materials are shown in Tab. 7.6 below.

Table 7.6: Required propellant tank wall thickness for a internal pressure of 0.3 MPa for selected materials

| Material | Al2219 | Al6061 | Al7075 | Steel 17-4PH | Ti-6Al-4V |
|---|---|---|---|---|---|
| Thickness [mm] | 3.13 | 4.53 | 2.86 | 1.59 | 1.46 |

As can be observed in Tab. 7.6 due to the tank's higher internal pressure it also requires a thicker skin than the PTV that is only pressurized with 0.1096 MPa (see Tab. 7.3). However, similar to the PTV it is expected that the launch loads will require a higher thickness.

### 7.2.3 Sizing for Launch Loads

As explained before the maximum expected compressive launch load is given by [42] to be -6 g. Since the tank consists of a single cylinder it will have to carry the total normal force P and maximum bending moment M. As specified in the Baseline Design chapter, the total mass of 1 tank is equal to approximately 40300 $kg$. According to the associated weight P and M are calculated with Eqs. 7.8 and 7.9.For the propellant tanks it is possible to consider two design configurations: a monocoque cylinder and a cylinder reinforced with stringers. The results for both configurations are shown in the following.

#### Monocoque Cylinder

For a monocoque cylinder Eq. 7.7 can be used to calculate the required thickness directly. The required thickness for the selected materials are summarized in Tab. 7.7.

Table 7.7: Required propellant tank wall thickness for a maximum compressive load of -6 g

| Material | Al2219 | Al6061 | Al7075 | Steel 17-4PH | Ti-6Al-4V |
|---|---|---|---|---|---|
| Thickness [mm] | 6.89 | 7.03 | 6.93 | 4.17 | 5.57 |

As can be observed from Tab. 7.7 and Tab. 7.6 the wall thickness the structure requires to resist buckling under the given maximum launch load is much higher than those required for pressurization. Using any of the selected materials would lead to a relatively high mass.

#### Propellant Tank Reinforced with Stringers

As can be observed from Tab. 7.8 Al6061 again requires the lowest number of stringers and also the smallest mass despite its low E-modulus compared to the other materials. This result has been discussed in the section on PTV sizing. Even though Al6061 now seems to be the lightest option, it is still important to evaluate the total mass of the structure (stringers + skin) when trying to choose the best material.

Table 7.8: Required number of stringers and mass for selected materials

| Material | Al2219 | Al6061 | Al7075 | Steel 17-4PH | Ti-6Al-4V |
|---|---|---|---|---|---|
| Req. number of stringers | 112 | 86 | 120 | 138 | 182 |
| Tot. mass of stringers [kg] | 222.6 | 162.6 | 234.4 | 756.6 | 562.4 |

### 7.2.4 Material Selection

The total structural mass is shown in Fig. 7.7 for both the monocoque cylinder with the skin thickness values given in Tab. 7.7 and the cylinder with the required number of stringers and skin thickness values given ign Tab. 7.6. It is important to note that the mass of the propellant tank *without stringers* is determined by multiplying the total mass of the skin by a factor of 2.5 to account for additional elements such as structural lugs, feed-system fittings, stress concentrations at tank knuckles or weld efficiencies. The use of this contingency factor is explained in [8].

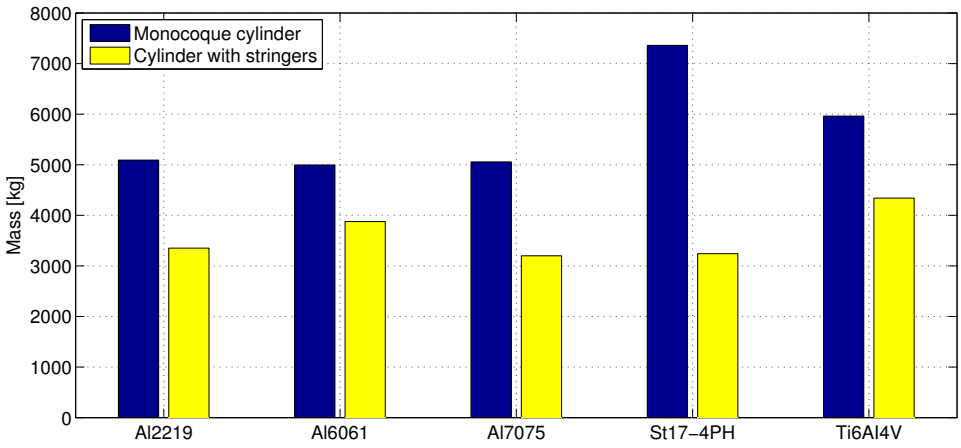


Figure 7.7: Total mass for monocoque cylinder and stringer configuration

As can be observed in Fig. 7.7 the lowest structural mass is achieved by using Al7075. Therefore, this material will be used. Also, using the stringer configuration results in a mass decrease of more than 1000 kg, so for all materials it is more efficient to use the stringer configuration than the monocoque structure. It is therefore decided to use the wall thickness designed for pressurization and reinforce it with stringers for the launch loads. For Al7075 this would result in a total mass 3200 kg for each tank. However, it is still necessary to prove that this design will be able to resist all the other predicted load cases.

### 7.2.5 Thermal Property Considerations

As explained in Sec. 5.9, the cryogenic propellant has to be stored at a constant temperature. the thermal management system of the propellant tank is therefore designed such that cyclic thermal loads due to severe temperature differences are avoided. The thermal expansion stresses are thus assumed to be negligible.

### 7.2.6 Resistance against Vibration Loads

Apart from the pressure loads and the launch loads it should also be proven that the structure of the propellant tank is above the specified vibration frequency during launch. The tank's fundamental bending and axial frequencies that result from using Al7075 are determined with Eqs. 7.16 and 7.17 to be 352.2 Hz and 115.8 Hz, respectively. These are well above the specified frequencies of 10 Hz and 25 Hz in [42]. It is therefore proven that the designed tank structure is able to provide resistance against the launch vibration loads.

### Verification and Validation

**Verification of methods of analysis:** The approach for designing the structural components follows well established methods for Phase A structural sizing, and no numerical methods (e.g. FEM models) were used for the analysis. The conventional meaning of verification, where numerical results are verified with analytic results, are therefore not applicable. Therefore, for verification it is only possible to calculate some values manually using the equations mentioned above. In this case the moment of inertia of the cylinder's cross-section has been calculated for one material including all booms and the skin thickness. With Eqs. 7.10 and 7.13 it was then verified that the maximum stress from Eq. 7.4 does not exceed these limits. As expected, the manual calculations yield the same result as the one obtained from the a model in MATLAB program.

**Validation of Results:** The results obtained for the structural dimensions of the PTV and the propellant tanks can be validated with values found in literature. In the book *Human Spaceflight Mission Analysis and Engineering* (Larson, 2000) [25] an example was given where a lunar crew module's structure is sized for pressure and buckling stability. To support pressurization a thickness of 1.61 mm is calculated, which is very similar to the values obtained for the Mars One PTV in 7.3. In that example the structure is designed as a monocoque cylinder made of Al6061 as material, so a skin thickness of 2.57 mm is calculated to withstand a compressive launch load of -3.2 g. Since the maximum launch load of the Falcon 9 is approximately twice in magnitude, the skin thickness obtained for Al6061 as shown in Tab. 7.4 also seems reasonable. The results obtained for the PTV's skin thickness is therefore assumed to be validated. The stiffener structure of the propellant tank also appears to be reasonable as the space shuttle's external tank also uses integral stringers [45].

### Sensitivity Analysis

It is important to investigate how a change in dimensions or total mass of the PTV or the propellant tanks influences the structural mass. The results for both the PTV and the propellant tank are summarized in Tab. 7.9 and 7.10 below.

Table 7.9: PTV Structural mass increase with increase in total mass and length

| Changed variable | additional number of stringers | mass increase [kg] | % increase in mass |
|---|---|---|---|
| 50% increase in total mass | 16 | 125 | 5 |
| 50% increase in length | 4 | 1340 | 56% |

Table 7.10: Tank Structural mass increase with increase in total mass and length

| Changed variable | additional number of stringers | mass increase [kg] | % increase in mass |
|---|---|---|---|
| 50% increase in total mass | 14 | 27 | 0.8% |
| 50% increase in length | 2 | 1605 | 50% |

## 7.3 Summary, Conclusion and Recommendations

The primary structures of the PTV and its propellant tanks have now been established. The final results are summarized in Tab. 7.11.

Table 7.11: Final PTV structural properties

| | **Propellant tanks** | **PTV main module** |
|---|---|---|
| Material | Al 7075-T73 | Al 6061-T6 |
| Wall thickness [mm] | 2.86 | 1.66 |
| Number of stringers | 120 | 178 |
| Total structural mass [kg] | 3200 | 2390 |
| Total estimated material cost [USD] | 41 600 | 17 900 |

In conclusion, both PTV main module and the propellant tanks will consist of a cylindrical structure reinforced with stringers. All relevant properties are shown in Tab. 7.11. This chapter only discussed the design of the primary PTV structures for the most prominent load cases. However, there are many other structural aspects that are beyond the scope of this project but will have to be considered in more detailed design phases. These include:

- Protection of structure against corrosion
- Account for stress concentrations in special locations
- Consider special mounting structures for specific subsystems or instruments
- Design structural interface to docking systems

The items mentioned above should be investigated in a Phase B design as they are also essential for ensuring structural integrity.

# 8 | Thermal control subsystem

In this section the thermal control subsystem will be discussed in more detail. In all engineering fields it is known that certain subsystems, parts or elements work better at a certain temperature range. The thermal control subsystem provides and controls this desired range of temperature such that other subsystems are protected from dangerous temperature differences and can work more efficiently.

## 8.1 Thermal requirements

First the thermal requirements of other subsystems and components of the spacecraft should be determined such that the thermal control subsystem can be properly designed. An overview of the temperature range of different components for spacecraft can be seen in Tab. 8.1 .

Table 8.1: Overview of the operating temperature range of different components of spacecraft [40] [21] [46] [47]

| **Component** | **Temperature range** (°C) |
|---|---|
| Electronic equipment | -10 to 40 |
| Batteries | -5 to 5 |
| Liquid oxygen and methane propellant | -153 to -174 |
| Microprocessors | -5 to 40 |
| Bearing mechanisms | -45 to 65 |
| Solar cells | -160 to 100 |
| Reaction wheels | -10 to 40 |
| Star trackers | 0 to 30 |
| Gyros | 0 to 40 |
| Antennas | -100 to 100 |
| Solid-state diodes | -60 to 95 |
| Crew | 18 to 27 |

As can be seen in Tab. 8.1 the ranges all differ and also the width of the range differs significantly. Some components, such as the antennas, can withstand large temperature variations, other components, such as the batteries, only a variation of a few degrees. Therefore, some components require a more accurate thermal control system.

## 8.2 Thermal environment

### 8.2.1 Solar radiation

One of the main concerns of the thermal environment is the solar radiation. It can be divided into two parts; the direct solar radiation and the indirect solar radiation. The direct solar radiation can be calculated with the following formula. In this formula $P$ is the total power output from the Sun, which is equal to $3.8 \cdot 10^{26}$ $W$.

$$J_s = \frac{P}{4\pi D^2} \tag{8.1}$$

Applying this formula for Earth and Mars a solar radiation of 1371 $W/m^2$ and 591 $W/m^2$ was found, respectively [21].

The indirect solar radiation, also called the planetary albedo, is the solar radiation from the Sun reflected by a planet. The albedo contribution to the total solar radiation can be computed with Eq. 8.2.

$$J_a = J_s a F \tag{8.2}$$

In this equation parameter $a$ stands for the albedo factor of the nearby planet and $F$ is the visibility factor. The visibility factor depends on the altitude and the bearing angle between the local vertical and the rays of the Sun. According to [21] the visibility factor can be assumed to be 0.1 for both Earth and Mars. The average albedo factor is equal to 0.15 for Mars and 0.34 for Earth [21]. With these numbers the planetary albedo was determined to be 8.9 $W/m^2$ for Mars and 46.6 $W/m^2$ near the Earth.

### 8.2.2 Planetary radiation

The planets themselves do not only reflect radiation, but also produce and radiate their own heat. Both Mars and Earth radiate all their heat in the infrared part of the spectrum. This planet radiation also influences the thermal control of the ML and PTV. According to [21] the heat rate due to planetary radiation of Mars and Earth can be assumed to be respectively 145 $W/m^2$ and 237 $W/m$ [21].

### 8.2.3 Internal heat emission

The spacecraft itself also produces some heat which influences the thermal control subsystem. This heat can be produced by other subsystems like the power or propulsion subsystem. For example the batteries can generate some significant heat and the engine will also radiate heat. Finally the crew themselves will dissipate heat due to their body temperature. It was computed that the heat dissipated by the PTV through the skin equals 6.6 $kW$ and equals 2.95 $kW$ for the ML. This was calculated by applying the formula for heat radiation [21].

$$q_{radiated} = \epsilon \sigma A T^4 \tag{8.3}$$

In Eq. 8.3 parameter $\epsilon$ is the emittance factor of the skin material, $\sigma$ the Stefan-Boltzmann constant, $A$ is the spacecraft's total area and $T$ is the temperature. For this calculation a cabin temperature of 20°C was assumed. The 6.6 $kW$ and 2.95 $kW$ heat dissipated by respectively the PTV and ML were validated with the numbers estimated by [48]. They estimated the maximum internal heat produced by the equipment of a manned deep space vehicle to be approximately 14 $kW$ and an additional 1 $kW$ is generated by the crew itself [48].

## 8.3 Thermal analysis

The best way to analyze and design the thermal control subsystem is to determine the temperature limits that the spacecraft will experience. There are two limits that should be determined, namely the extreme cold case and the extreme hot case. The extreme hot and the extreme cold case can be determined with the following formula.

$$\sigma T^4 = \left(\frac{\alpha}{\epsilon}\right)\left(\left(\frac{A_s}{A_{s/c}}\right)J_s + \left(\frac{A_p}{A_{s/c}}\right)J_a\right) + \left(\frac{A_p}{A_{s/c}}\right)F_{12}J_p + \frac{Q}{\epsilon A_{s/c}} \tag{8.4}$$

In Eq. 8.4 is parameter $\alpha$ is the absorbance factor, $A_s$ and $A_p$ are the projected areas of the spacecraft in the directions of the Sun and the planet respectively, $A_{s/c}$ is the spacecraft's total area, $J_p$ is the radiation intensity and $Q$ is the internal heat. Finally $F_{12}$ is the view factor.

A Matlab code was developed to determine the two extreme temperatures of the PTV and the ML using Eq. 8.4. It was found that the extreme hot case will occur during the parking orbit around Earth and when the spacecraft is placed between the Sun and the Earth. The extreme cold case will occur when the PTV and the ML are in orbit around Mars and in eclipse with the Sun. The code was iterated several times to determine the best $a/\epsilon$ factor such that the difference between the extrema are as low as possible and in the desired range.

The optimal $a/\epsilon$ factor was determined to be around 2.5. If an cupric oxide coating is used as finishing surface for the ML, the ML will experience a heat range of 356 $K$ to 424 $K$. For the PTV the temperature will vary between 300 $K$ and 370 $K$ if cupric oxide is used as finishing surface. The cupric oxide coating can easily be placed on other materials like aluminum and copper and has an absorption factor of 0.36 and an emittance factor of 0.15 [49]. Another advantages of the cupric oxide is that it can withstand high temperatures. According to [50] the cupric oxide can withstand a temperature of 600 degrees Celsius. This is in particular beneficial for the entry phase of the ML.

The temperatures when a cupric oxide coating is used, are too high for the crew temperature requirements and also for the other component temperature requirements, therefore the cabin of the PTV and ML should be sufficiently cooled. The best way to do this is to make use of radiators. Radiators are also used in the Space Shuttle Orbiter and the ISS. They use a liquid, such as water, to dissipate the heat. With the same Matlab program based on Eq. 8.4 it was computed that the radiators should remove 10.2 $kW$ of heat for the PTV. For the ML the radiators should remove 10 $kW$ of heat. With Eq. 8.3 for the radiation heat one is able to compute the required radiator size. For the radiators an emittance factor of 0.92 was assumed, because the radiators are covered with a black paint [40]. The temperature of the radiator ($T$) was assumed to be equal to the temperature of the crew cabin. With Eq. 8.3 is was then determined that a total area of 49.1 $m^2$ for the radiators is required. According to [25] the required power of the radiators can be neglected and the mass per square meter is equal to 8.5 $kg$ [25]. So the mass of the radiators for the Mars One mission equals 417 $kg$. With these radiators the temperature range can be brought in the desired range for the crew, namely the maximum temperature inside the crew cabin will be equal to 20°C. However as can be seen in Tab. 8.1 this is still not within the desired range of every component, therefore more components are needed for the thermal control subsystem.

## 8.4 Passive thermal control

There are two types of thermal control, namely active and passive. The passive use a combination of $a/\epsilon$ factors to get the desired temperature. The cupric oxide coating mentioned earlier is an example of passive thermal control. This cupric oxide coating is however not enough, it does not give a temperature range which is narrow enough for all the subsystems. The reaction wheels for example need a range of $-10°$C to $40°$C degrees. To achieve such a specific range more layers of material can be used to insulate the component. However such components should be designed in a more detailed design phase.

## 8.5 Active thermal control

Not all thermal requirements for every component can be achieved with passive thermal control, some temperature ranges are so specific that they need active thermal control. For example the thermal requirement of the crew compartment states that the temperature should lie between $18°$C and $27°$C, which is very hard to achieve with only passive thermal control. Therefore the ML and PTV will also need active thermal control.

### 8.5.1 Thermostatically controlled heaters

Thermostatically controlled heaters are simple active thermal control devices which are frequently used in the past by several different spacecraft. They are often applied to maintain the desired temperature of specific components like batteries and fuel lines, especially when the spacecraft is in eclipse and the components even need more heat. They can be switched on and off every moment, so they allow for accurate thermal control.

### 8.5.2 Variable external radiation devices

Variable external radiation devices are mechanical devices who change the $a/\epsilon$ factor of a certain surface. A very simple variable external radiation device is a bimetallic fin system where there can be switched between two different materials with two different $a/\epsilon$ factors. Similar concepts are pinwheels and louvre systems. The pinwheels are not longer used frequently in the space industry and louvre systems are relatively expensive according to [21]. So at first sight these systems are probably not the best active thermal control systems for the Mars One mission.

### 8.5.3 Thermoelectric cooling

"Thermoelectric devices use the principle that if current flows in a circuit of two dissimilar metals, then heat is developed at one end and absorbed at the other.[21]" So in the space industry they are mainly used to cool certain components and just as the thermostatically controlled heaters they can be switched on and off and they provide accurate thermal control.

**Sensitivity analysis** The mass of the spacecraft, which is one of the most important parameters in the aerospace industry, does not directly influence the thermal control subsystem as can be seen in Eq. 8.4. The only main parameters that influence the thermal control subsystem are the spacecraft's total area and the projected areas. If the dimensions of the PTV will be increased by 25%, the temperature of the PTV without radiators will vary between 289 $K$ and 364 $K$. It is noticed that the difference with the original case is not that high, so only a few modifications, such as resizing the radiators, will be needed.

**Verification and validation** The complete Matlab program was validated with an example given in [21]. This example calculates the extreme hot case and the extreme cold case temperature for a spherical satellite orbiting Mars. The numbers of the example, such as the absorptance factor, emittance factor, radius and internal heat, were used as input and the same extreme hot case temperature of 325 $K$ and the same extreme cold case temperature of 210 $K$ was found.

## 8.6 Conclusion and recommendations

In this chapter the thermal control subsystem was discussed in more detail. It can be concluded that the PTV and the ML will experience a wide range of temperatures and that the thermal control subsystem should be designed such that the thermal requirements are met. To meet the thermal requirements a cupric oxide coating will be used for both vehicles. To cool the spacecraft down when they are close to the Earth, where the temperature is higher, the active controllable radiators shall be used. According to [40] the weight of the total thermal control subsystem can be estimated to be 4.5% of the total dry mass of the spacecraft and the cost can be estimated to be approximately 4% of the total spacecraft cost [40]. The power needed for the thermal control subsystem is estimated to be 5% of the total spacecraft power [51]. In a later more detailed design phase the active thermal control devices should be designed for each component which has a very specific thermal requirement. After that a more detailed estimation of the power, mass and costs of the thermal control subsystem should be performed.

# 9 | Communications Subsystem

The communications subsystem forms an essential part of the mission. Not only is it necessary for communicating with the crew and to coordinate the mission but also to transfer the video streams, documenting the first humans on Mars. As it is planned to partially fund the mission by marketing it as a TV show, it is necessary to have a high communication link time per day.

## 9.1 Layout

During the first transfer the PTV will contact Earth directly through existing ground stations, for example the NASA Deep Space Network (DSN), or use a relay satellite on the same heliocentric orbit as the Earth but with a shifted true anomaly. After the ML is released from the PTV in Mars orbit, the PTV jettisons the living module and moves to an areostationary orbit above the Mars base. As the remaining part of the PTV, here called PTVsat, contains all necessary equipment for communication it then serves as a communication satellite, to relay the base traffic. With each new mission a new PTVsat is injected into Mars orbit, increasing the bandwidth as well as the reliability. The other relay satellite in heliocentric orbit ensures communication during periods when Mars is in between the areostationary satellites and Earth or the Sun. The difference in true anomaly needed to bridge these periods is very small ($<1°$), due to the relatively large distances. However, increasing the true anomaly further, decreases the maximum possible distance between either communication point and also decreases the disturbances by the sun. The difference in true anomaly has been chosen to be 60°. At 60° the stable L5 Lagrange point is located, which allows the spacecraft to stay at this point without additional station keeping efforts. An overview of the communicational flow for the Mars base can be found in Fig. B.1 and for the PTV in Fig. B.2.

## 9.2 Sizing

To appropriately cover the events in the Mars base it was assumed to use at least four HD camera feeds. With an increase for each extra PTV. According to [52] a data rate of around 40 $Mbit/s$ is required. During the flight to Mars the number of feeds can be reduced to two ($\approx 20$ $Mbit/s$) due to the smaller space aboard the PTV. The allocated power for the communication system is 1200 $W$ accounting for losses in the communication system, a transmissive power of 800 $W$ is achievable [53]. After the PTV arrives in its desired areostationary orbit, the transmissive power can be increased to 2800 $W$, due to the higher available power. It has been chosen to not use a transmissive power of more than 2800 $W$ to account for the aging effects of the solar arrays and to be able to design a lighter communications system. Due to size limitations an antenna size of 5.5 $m$ has been chosen, which will be deployed after the first $\Delta V$ in space and the tanks have been jettisoned. The data connection before jettisoning the tank will be ensured by a small auxiliary antenna that is later used for the communications link between the Mars

base and the PTVsat.
This communication system has an antenna of 1 $m$ diameter and a transmissive power of 10 $W$. Due to the low altitude of the areostationary orbit of 17000 $km$ a, in terms of data rate, sufficient communications link can be established with this configuration. The performance of this link is deliberately chosen to be higher than necessary to account for possible bad weather conditions on Mars. For the, in comparison short range, communication between Earth and the heliocentric satellite an antenna with a diameter of 2 $m$ is used. To estimate the mass of the communications system, the Boeing 601 Horizons [54] has been used as a reference satellite, due to its similar communication system parameters. The estimation then was carried out by assuming that 5% of the satellite's dry mass are allocated to the communications system. On [55] 5% is the highest fraction found for the communications subsystem mass, equaling a total mass of 130 $kg$.

The mass of the communication system installed in the Mars lander is estimated using a small satellite as a reference , again due to the similar performance parameters. Therefore, the mass is estimated to be 20 $kg$ [55]. It is assumed to use components available from satellite manufacturers as the communication link is designed to be achievable using standard components. The 5.5 $m$ fold able antenna dish, however, needs to be developed specifically for this mission. As fold able antennas of similar size have been used in other missions [56]

## 9.3 Conclusion

Performing a link budget analysis on the aforementioned communication links produces the link budgets as seen in Tab. 9.1. The given values assume a receiving station with the same antenna and efficiency (as that of the relay satellite). This is a worst case scenario as the DSN on Earth have a significantly higher gain. For the PTV (first column, Tab.9.1) a maximum data rate of 35.6 $Mbit/s$ can be achieved at the maximum distance. This is enough to fulfill the requirements of submitting at least 2 HD video streams, with a contingency for interference. The excess data rate is also enough to be used for housekeeping data traffic and personal data communication (depending on the delay phone or e-mail services). After arriving at Mars and increasing the power of the transmitter (second column, Tab.9.1) the maximum data rate for the maximum distance increases to 81 $Mbit/s$. This data rate would allow to increase the number of HD video streams to 6 and still have enough bandwidth for communications, housekeeping and extra contingency. For each consecutive PTVsat the data rate doubles, enabling to increase the number of HD video streams. The link budget in the third column Tab.9.1 shows the link between the heliocentric satellite and Earth. The maximum achievable data rate is 457 $Mbit/s$, which is enough to fulfill the data handling for all 3 PTVsats.

The Mars base link budget seen in the fourth column 9.1 shows a maximum achievable data rate of 35547 $Mbit/s$. This value is higher than the data that can be handled by the PTVsats but taken that this data can be transmitted without too much effort (10 $W$ of transmissive power) it is feasible to utilize. Also, due to the high bandwidth the link offers enough reserves for bad weather conditions.

**Verification and Validation** The methods used in this chapter are entirely based on the methods as presented in [57]. It can therefore be assumed that the methods are verified. For the weight estimation reference satellites as mentioned on [55] and on [54] have been used. The aimed at data rate over the given distance can not be validated directly using a reference satellite, as such a system does not exist. However, it is possible to extrapolate the performance of the Mars pathfinder communication subsystem [58] to match the requirements. The differences then are $< 10\%$, therefore validating the results.

Table 9.1: Link Budgets

| **Item** | **PTV to heliocentric satellite** | **PTVsat to heliocentric satellite** | **heliocentric satellite to Earth** | **Mars base /ML to PTVsat** | **comments** |
|---|---|---|---|---|---|
| Frequency $[GHz]$ | 8.4 | 8.4 | 8.4 | 8.4 | X-band |
| Tx Power $[W]$ | 800 | 2800 | 200 | 10 | |
| Antenna diameter $[m]$ | 5.5 | 5.5 | 2 | 0.5 | |
| Antenna efficiency [%] | 55 | 55 | 55 | 55 | Conservative Assumption [57] |
| Antenna gain $[dBi]$ | 51 | 51 | 42 | 30 | [57] |
| Receiver Antenna Gain $[dBi]$ | 51 | 51 | 67[1] | 42 | [1][59] |
| EIRP $[dBW]$ | 80 | 86 | 65 | 40 | |
| Distance $[km]$ | $2.94 \cdot 10^8$ [1] | $3.65 \cdot 10^8$ [2] | $8.5 \cdot 10^7$ [3] | $3.4 \cdot 10^4$ [4] | [1] Maximum Distance to Earth for transit + 10%<br>[2]Maximum Distance to Sat at 60°<br>[3]Distance to Earth + 10%<br>[4]Twice the Altitude of the areostationary Orbit |
| Free space loss $[dB]$ | -260 | -262 | -250 | -181 | |
| Received power $[dBW]$ | -129 | -127 | -118 | -99 | |
| Rx system noise temperature $[K]$ | 135 | 135 | 135 | 135 | [40, table 13-10] |
| Rx system noise $[dBJ]$ | -207 | -207 | -207 | -207 | |
| Rx power noise density $[dB/Hz]$ | 78 | 81.8 | 89 | 108 | |
| Required bit SNR $[dB]$ | 2.7 | 2.7 | 2.7 | 2.7 | [57, BPSK,QPSK,RS,Viterbi] |
| Maximum data rate $[Mbit/s]$ | 35.66 | 81 | 457 | 35547 | |

# 10 | Guidance, Navigation and Attitude Control

This chapter deals with designing the Guidance, Navigation and Control (GNC) and Attitude Determination and Control System (ADCS). These two subsystems are closely related and are therefore designed together. The GNC system is important to determine the right trajectory, and provide information on where the spacecraft currently is with respect to other celestial bodies and how to achieve the preferred orbit. The ADCS, on the other hand, is important for determining the orientation of the spacecraft at any given moment and for establishing how to achieve the desired attitude.

First of all the the ADCS design process for the PTV will be described step by step. To begin with the ADCS requirements will be identified based on which the type of attitude control can be chosen so that the components can be sized accordingly. In addition to this, the types of sensors used on board for attitude determination will be discussed and chosen. This is also a first step in designing the GNC system since these sensors are the main source of information based on which the GNC determines the current orientation. The same procedure will afterwards be applied to the ML.

## 10.1 Transfer Vehicle Requirements

First of all, general requirements will be defined.

1. The spacecraft needs to know its orientation with respect to the Sun at any given time since solar panels are used to provide the power and they need to be rotated towards the Sun.

2. The spacecraft needs to know its orientation with respect to Earth and Mars in order to know when to transfer from one orbit to another

3. The spacecraft needs to know the acceleration achieved after starting the thrusters so that it can be determined whether they were burning for long enough or how far has it turned.

4. The pointing accuracy shall be $< 0.1°$. Throughout the mission, the spacecrafts attitude needs to be corrected continuously to keep the antenna pointing in the desired direction. The antenna will, however, be designed so that it rotates independent of the PTV so that there is no need to change the attitude of the entire PTV for the purposes of communicating. However, the fact that in-orbit assembly is required influences the spacecraft pointing accuracy as well resulting in a high accuracy. [60],

5. The slew rate shall be $0.25°/s$. The slew rate is the second parameter that is used for designing the ADCS. In the Mars One mission there is no need to have a very high slew

rate [60] so it is decided that the ADCS will be designed for a low to medium slew rate of $0.25°/s$.

## 10.2 Transfer Vehicle Attitude Determination and Control System

Having determined the PTV requirements for the ADCS, the type of attitude control can be defined accordingly. The main parameter for determining this is the pointing accuracy of $< 0.1°$. To enable this it is necessary to use 3-axis stabilization. This control type can be realized by using reaction or momentum wheels. Most spacecraft nowadays rely on using a reaction wheel system (RWS) to perform the 3-axis stabilization. However, an alternative way to do this is by using a more complicated control momentum gyroscope (CMG) system. The main reason for considering this is that the assembled Mars One spacecraft weighs approximately 125 $t$ and the CMGs are mostly used for large vehicles [40], including the ISS [61]. The following Tab. 10.1 summarizes the advantages and disadvantages of both options.

Table 10.1: Comparison of RWS and CMG [62]

| | **Reaction Wheel System** | **Control Momentum Gyros** |
|---|---|---|
| Advantages | Well known technology | Used on larger spacecraft |
| | Easily implemented into the GNC system | High power efficiency |
| | Lighter for a given momentum storage | Ability to generate large torques |
| Disadvantages | Power consuming | Complex actuation and software |
| | Torque range from 0.01 to 1 $Nm$ [40] | Few options on the market |
| | Unfeasible for some size/slew values | Space consuming and heavy |

It is first of all important to ensure the reliability and safety of the spacecraft, even if it implies a slightly higher cost, in order to not endanger the whole mission. This is why the CMGs (Fig.10.1) will be used for attitude control. While this system is very complex, especially taking into account that it is a single-use PTV, reference data shows that bigger vehicles (ISS and Skylab) such as the Mars One spacecraft also use CMGs [60] [61] and some data states that combinations of certain slew requirements and high moments of inertia cannot even be achieved with the RWS [62].

Single- and double-gimbal CMGs can be chosen with the main difference being that a single-gimbal provides control about one axis while the double-gimbal controls the spacecraft about two axes. In order to provide control about three axes three double-gimbal CMGs will be used, with one of them being used for back up, a configuration similar to that of the Skylab [60]. It was decided to use this since three double-gimbal wheels would save more volume than 4 single gimbal wheels and considering the small amount of space that is available for astronauts this, is very important. In addition to the CMGs the ADCS will contain thrusters that will be used to desaturate the stored momentum. These thrusters will also serve to correct the trajectory (according to the information provided by the GNC) for any unpredictable circumstances and adjust the attitude after entering the transfer and Mars parking orbits.

Figure 10.1: Control Momentum Gyroscope [63]

### 10.2.1 Hardware sizing

Having determined the different components of the subsystem, one can now proceed with sizing them. First of all, several parameters of the spacecraft will be determined. These parameters can be found in Tab. 10.2. Some values from the table such as the mass moment of inertia were calculated with the equations presented below. The mass moment of inertia was calculated by approximating all the spacecraft components (PTV, ML and the tanks) as solid cylinders.

In addition to this, some parameters such as the acceleration need to be estimated at this point. The acceleration is calculated once the time to reach the slew rate was estimated to be 10 $s$. This decision is based on the reference data [40] but increased by 50% for the purposes of the Mars One mission (since there are no requirements that translate into high acceleration it is decided to allow more time to reach the slew rate).

Table 10.2: Relevant ADCS design parameters

| $I_{xx}$ | $I_{zz}$ | Slew rate $[deg/s]$ | Pointing accuracy [°] | Angular acceleration $[rad/s^2]$ |
|---|---|---|---|---|
| 4.9E05 | 2.96E06 | 0.25 | <0.1 | 4.4E-04 |

In order to begin with sizing the components, first of all the disturbance torques, for which the ADCS needs to correct, need to be estimated. Taking into account that this is an interplanetary mission, there are two relevant disturbance torques that need to be accounted for: the gravity gradient and solar radiation [40].

- **Gravity Gradient**
  Torque that result from a planet's gravity field, calculated by Eq. 10.1 with relevant parameters explained in Tab. 10.3

$$T_g = \frac{3\mu|I_{zz} - I_{yy}|sin(2\theta)}{2R^3} \tag{10.1}$$

- **Solar Radiation**
  This is the torque caused by the solar radiation that the spacecraft encounters and is calculated using Eq. 10.2

$$T_{sp} = \frac{F_s}{c} A_s (1+q)(c_{ps} - c_g) cos(i) \tag{10.2}$$

Table 10.3: Disturbance torque calculation parameters [40]

| Parameter | Explanation | Value |
|---|---|---|
| $\mu$ $[km^3/s^2]$ | Gravity constant[64] | Earth: 398600; Mars:42832 ; Sun:1.3271+E11 |
| $\theta$ [°] | Maximum deviation of the Z axis from the local vertical | 1 |
| $R$ $[km]$ | Orbit radius | Earth orbit (200 $km$ alt.):6571; Mars orbit (200 $km$ alt.): 3596 [65]; Transfer orbit: 1.5E08 (worst case scenario) |
| $F_s$ $[W/m^2]$ | Solar constant | Earth:1358 [40]; Mars: 585[66]; Sun:972 (average) |
| $c_{ps} - c_g$ $[m]$ | Distance between the center of solar pressure and center of gravity | 0.5 [67] |
| $A_s$ $[m^2]$ | Surface area of the spacecraft cross section | 53 |
| c $[m/s]$ | Speed of light | 300E06 |
| q [-] | Reflectance factor | 0.5 [40] |
| i [deg] | Angle of incidence of the Sun | 0 |

It is important to note that some parameters are estimated based on the reference values normally used for such calculations (as shown in [40] and [60]). The angle of incidence of the Sun is taken to be 0 in order to account for the most extreme value of the solar radiation torque, and the cross section surface area includes not only the PTV and ML but also the tanks since the whole (assembled) spacecraft will need to be controlled with this system. The reflectance factor is taken to be an average of 0.5 and finally, the distance between the center of solar pressure and the center of mass is estimated to be 0.5 $m$. This value is generally much smaller, about 0.1 $m$ for the reference vehicles [40]. These vehicles are however satellites that are generally smaller, so the value is scaled up for the Mars One spacecraft.
Now that all the relevant parameters are defined, the disturbance torques are calculated for two cases, when the spacecraft is in Earth vicinity and when it is in Mars vicinity. The values calculated for both cases are summarized in Tab. 10.4.

Table 10.4: Disturbance torques

| | Earth orbit | Mars orbit | Transfer orbit |
|---|---|---|---|
| **Gravity Gradient** | 0.17 $Nm$ | 0.12 m $Nm$ | 5.13E-09 $Nm$ |
| **Solar Radiation** | 1.8E-04 $Nm$ | 7.7E-05 $Nm$ | 1.3E-04 $Nm$ |

**Sizing the wheels** As can be seen from Tab. 10.4 the worst case disturbance is due to the LEO gravity gradient. However, the spacecraft only spends a couple of days (3-5) in LEO, while

it spends at least 300 days in the transfer orbit. Therefore the wheels will be sized according to the average solar radiation the spacecraft will experience in the transfer orbit. Eq. 10.3 [40] describes how the momentum that is to be stored is calculated. The relevant parameters are:

- $T$- the worst case disturbance torque (LEO gravity gradient) $[Nm]$
- $P$- orbital period $[s]$
- $H_{rw}$- momentum stored $[Nms]$

$$H_{rw} = T\frac{P}{4}0.707 \tag{10.3}$$

The orbital period of the orbit can be calculated using the following equation:

$$P = 2\pi \cdot sqrt\left(\frac{a^3}{\mu_{sun}}\right) \tag{10.4}$$

Parameter $a$ stands for the transfer orbit semi major axis (1.9E011 $m$) and the $\mu_{sun}$ stands for the Sun gravity constant. These values then show that the amount of momentum stored in each wheel should be approximately 1126 $Nms$, with a safety factor of 2.

Once this is known, one can calculate the wheel's moment of inertia. First of all the mass moment of inertia ($I_{wheel}$) is calculated via:

$$I_{wheel} = \frac{H_{rw}}{\omega_{wheel}} \tag{10.5}$$

An additional parameter that needs to be defined in order to determine the moment of inertia is the wheel's angular velocity. According to different references, a usual value for a CMG spinning rate is 6600 $rpm$ ([68] and [40]). This then results in a moment of inertia of 1.63 $kgm^2$. Finally, the wheel's radius and mass need to be calculated. They are interdependent and a function of the moment of inertia as can be seen in Eq. 10.6.

$$I_{wheel} = \frac{1}{2}m_{wheel} \cdot r_{wheel}^2 \tag{10.6}$$

Therefore, there will be a trade-off between the wheel's mass and radius. Fig. 10.2 represents the relationship between these two parameters. The mass range is based on references ([40], [69]).

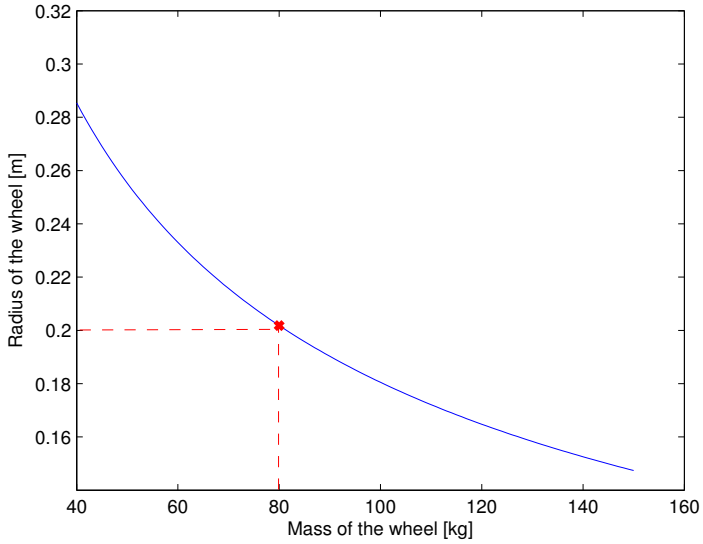


Figure 10.2: Wheel dimension-mass trade-off

Since both the mass and the volume taken by the wheel are constrained, an average value is taken for both which results in a mass of 80 $kg$ and a radius of 0.2 $m$.

**Sizing the actuators** While the reaction wheels are sized to correct for the accumulating disturbance torques, the thrusters need to be sized to account for both the momentum dumping of the reaction wheels and the performing of large maneuvers (correcting the attitude of the whole spacecraft if necessary).

First of all, the actuators will be sized so as to account for the the force necessary to perform large maneuvers. Since for this mission there are no requirements that would imply that the vehicle will have to be constantly changing attitude to point the payload in a certain direction (Ch. 9, Ch. 11), these large maneuvers refer to the attitude correction the spacecraft performs after entering a new orbit (transfer orbit and Mars parking orbit). These maneuvers in fact represent the orbit control which is not a function of the GNC system, but since these are performed by the same thrusters they will be taken into account for the sizing process. In addition to this, for the sake of contingency one larger maneuver is assumed on every 30 days in order to account for some unpredictable circumstances. The correcting force required to perform these maneuvers $F_{cor}$ is calculated by:

$$F_{cor} = \frac{I_{zz}\alpha}{d} \tag{10.7}$$

To account for the highest possible load required, the $F_{cor}$ is calculated as the force necessary to perform a maneuver around the axis with the highest moment of inertia, $I_{zz}$ and with the angular acceleration $\alpha$. With both values defined in Tab. 10.2 this force is calculated to be 562 $N$.

Finally, the force necessary to perform momentum dumping needs to be calculated and accounted for when calculating the amount of propellant needed for the ADCS. The momentum dumping will be done once a day, as is conventionally done [70]. This force is calculated by Eq. 10.8 by using the momentum stored in one wheel $H_{wheel}$, the thruster moment arm $d$ and the

burn time $t$. The burn time for momentum dumping is conventionally about 1 $s$ [40]. However to account for the high amount of momentum to be discarded the burn time will be scaled up to 2 $s$ for this mission. With the equation below this then gives a force of 164 $N$.

$$F_{dumping} = \frac{H_{wheel}}{dt} \tag{10.8}$$

Now that the total amount of thrust to be performed by the thrusters is known, the propellant mass ($M_{prop}$) required can be calculated.

$$M_{prop} = \frac{I}{I_{sp}g} \tag{10.9}$$

The parameter $I$ represents the total impulse that is the total product of all the thrust to be delivered and its corresponding burn time. Therefore, the total impulse is calculated by Eq. 10.10 where the forces exerted are multiplied by the corresponding burn duration and the number of impulses.

$$I = 64\ pulses \cdot 5s/pulse \cdot F_{corr} + 632\ pulses \cdot 2s/pulse \cdot F_{dumping} \tag{10.10}$$

Performing momentum dumping every day for 2 $s$ with two CMGs gives 632 impulses. Orbit corrections are assumed, as mentioned, to occur once a month, about 3 axes. This translates into approximately 64 impulses since 2 impulses are needed per one correction (a start and a stop impulse). The burn time for performing the maneuvers is taken to be 5 $s$ which is 66% higher than that of the reference spacecraft [40] and half the time that is allowed to reach the acceleration. Once again, the reference values are scaled up in order to account for the size of the vehicle and allow for some additional time to perform the maneuver. Finally, the last relevant parameter on which the amount of propellant still depends on is the thrusters' specific impulse $I_{sp}$ and the gravity constant.

The thrusters will be chosen based on the total amount of thrust to be produced as well as their specific impulse. Of importance when choosing the thrusters is also the nominal thrust produced and the total impulse it provides. For the Mars One mission the thruster is required to sustain a total impulse of 3.9E05 $Ns$ (according to Eq. 10.10) and have a total nominal thrust that matches $F_{cor}$ since this is the highest amount of thrust that needs to be delivered at once.

Various thrusters (from a list offered in [40]) are considered in an iteration process. Based on the characteristics mentioned above, the optimum thruster is determined to be the Ham Std/TRW mono-propellant hydrazine thruster (with specific impulse of 240 $s$, a total impulse up to 1.3+E06 $Ns$ and a nominal thrust in the range of 45-67 $N$). Using these thrusters then implies that the total number of ADCS thrusters is 12, with 2 pairs (one for redundancy) to provide torques about each axis. The thrust required per thruster of 47 $N$ and the total weight of 6 $kg$. Now all the forces predicted before can be performed with a certain burn time allowed.

Now that all the variables are known, Eq. 10.9 defines that the total propellant mass required for the ADCS is about 164 $kg$. The mass of the tank required for this amount of propellant is calculated as 10% of the total propellant mass [40] which results in 16.5 $kg$ while the required volume (with 10% contingency and a fuel density of 1080 $kg/m^3$ [71]) is 0.17 $m^3$.

### 10.2.2 Sensor Selection

Choosing the sensors, as mentioned before, represents the final step in the ADCS design and the first step to designing the GNC system. Sensors are important in order to be able to determine

the current attitude of the spacecraft. This is achieved by either using different celestial bodies as references or gyroscopes. Decisions on which sensors to use and how many of them will be made are based on the system requirements stated above.

First of all, in order to comply with the first requirement, Sun sensors will be used. These sensors will provide accurate information on the orientation with respect to the Sun (to be used by the solar panels) by measuring the amount of light or shadow on them. These sensors are very light, small and not very power consuming but need to be placed on the end of the vehicle to obtain an unobstructed view. Therefore, several of these need to be placed around the spacecraft. The number and placement of sensors is an iterative process based on previous experience [72] so the number of the sensors in this Phase-A design will be decided based on similar spacecraft. One such spacecraft is the Mars Reconnaissance Orbiter (MRO). This spacecraft is chosen since dimension-wise it is very similar to the PTV [73]. Thus, similarly to the MRO, eight Sun sensors will be used with additional eight placed as back up [74].

Sun sensors, however, cannot provide accurate information on the orientation of the vehicle with respect to the Earth and Mars. Having that this is also one of the requirements, the spacecraft will be equipped with two star trackers (one for redundancy) for accurate orientation measurements since they determine the position of the vehicle with respect to a certain star and therefore the orientation with respect to the planets can also be derived [40].

Finally, to fulfill all the requirements an Inertial Measurement Unit (IMU) is used to measure rotational and translational motion [40]. Although the IMUs require a lot of power and add to the system complexity and weight it is essential that the spacecraft is able to measure its acceleration and spin rate. For this reason an additional IMU shall also be used for contingency.

Having defined the sensors, the ADCS design for the PTV is concluded. Tab. 10.5 below summarizes the most relevant results of designing this subsystem. The power required for different components is determined from [40], as well as the mass of the sensors.

Table 10.5: ADCS design for the PTV

| | **Mass [kg]** | **Power [W]** |
|---|---|---|
| 3 Control Momentum Gyroscopes CMGs | 240 | 240 |
| 12 Thrusters | 6 | [-] |
| 16 Sun sensors | 16 | 16 |
| 2 Star trackers | 10 | 30 |
| 2 IMUs | 24 | 150 |
| Total (incl. fuel and tanks) | 477 | 436 |

An illustration of the shape and positions of the CMGs and the thrusters is shown in Fig. 10.3. Please note that the dimensions are exaggerated with respect to reality. The real dimensions, including all other subsystems, can be found in the final drawing. The thrusters will be positioned around the PTV and their places are represented with the holes seen in the PTV structure.

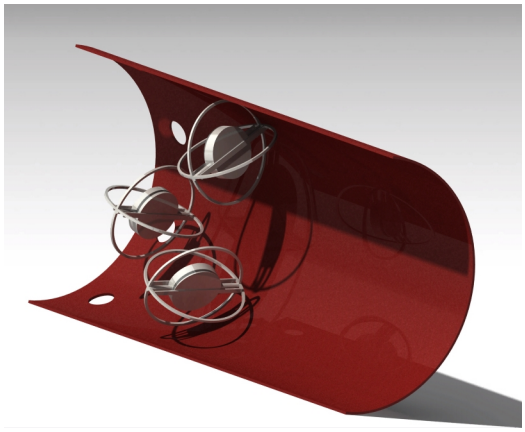

Figure 10.3: Thrusters and the CMGs placement in the PTV

## 10.3 Transfer Vehicle Guidance and Navigation

The main functions of the GNC system are to determine the PTV's position relative to other bodies and provide orbit control. This is important since the vehicle is required to perform several rendezvous with other spacecraft components (ML and the tanks) as well as the insertion into the Mars transfer and parking orbits. To determine the orbit different software systems can be used. As the mission considered is an interplanetary mission, the Deep Space Network (DSN) by JPL is the most suitable software [60]. The data obtained for orbit determination will come from the PTV's autonomous navigation system based on "Earth and star sensing". This is decided on since it is one of the few navigation methods that determines orbits for interplanetary transfers [40] as well as due to the fact that it uses star sensors that are already on board, as designed for the ADCS. In addition to this, it is decided that the PTV will be able to perform autonomous navigation without ground contact. This reduces the cost and risk of the mission [40] and increases the reliability. Also, it is common for the interplanetary missions to be autonomous in case the PTV is out of contact or communication delays are high.

Further design considers the control algorithms and the ways that the orientation is actually calculated. However, considering that this is a conceptual design phase the GNC design will be limited to sensor determination and autonomous navigation. The main GNC schematic works is shown in Fig. 10.4 in order to summarize the main principles on which this system works.

As shown in the figure, the external input is defined in the mode in which the spacecraft is flying (orbit insertion, normal etc. [40]). These external inputs in the Mars One mission are in fact commands to perform orbit insertion or correct the trajectory. The desired trajectory for the spacecraft will then be generated by the DSN based on this input. These details are afterwards forwarded to either the Guidance Logic or Control Logic.

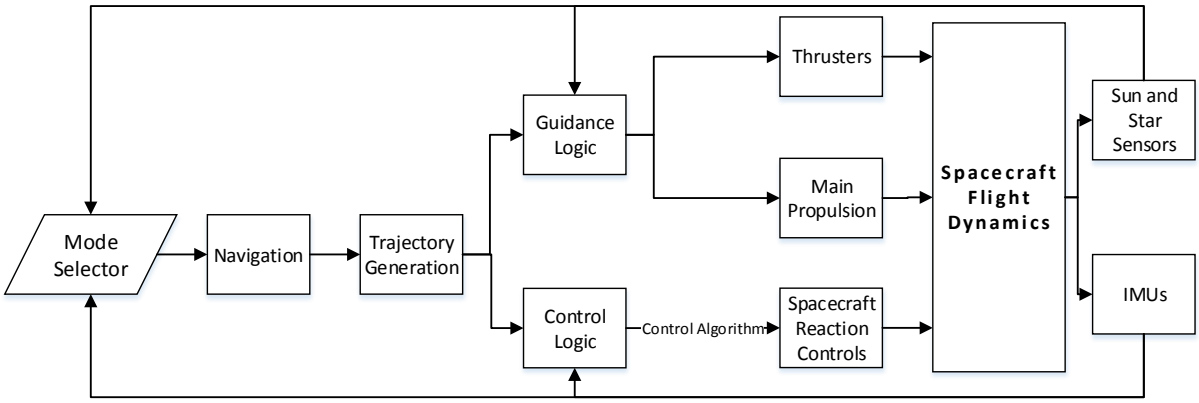


Figure 10.4: GNCS algorithm

The Guidance Logic combines it with the current estimate of the PTV's orientation (based on the sensor measurements) and guides the vehicle. After this whole process the right command is determined, processed and sent to the actuators (thrusters in this case) or the main propulsion system in order to finally perform the maneuver thereby influencing the spacecraft's flight dynamics. The Control Logic, in the meantime, combines the trajectory input with the IMU measurements of translational and rotational motion. The information is then processed through the control algorithm to command the spacecraft reaction controls and finally control the vehicle as desired.

## 10.4 Mars Lander Requirements

Once the Phase-A design of the ADCS and the GNC has been performed for the PTV, it is possible to do the same for the ML. This is done by applying the same procedure that was used for the PTV with relevant differences explained in this chapter.

The general requirements for the ML are very similar to the ones for the PTV. It is important to be able to determine the ML orientation with respect to Earth and Mars. In this case the orientation with respect to the Sun is not as relevant since batteries will be used to provide power (explained in Ch. 11). Of special importance are the precise measurements of the acceleration and rotational motion, especially for the purposes of entry and descent. When it comes to the specific ADCS requirements, the pointing accuracy can be larger with respect to the PTV since in this case there are not any solar panel requirements or in-orbit assembly maneuvers that would require very high pointing accuracy (the PTV already has a very high pointing accuracy so it will play a major part when assembling the ML and the PTV). Therefore, the system will be designed for a pointing accuracy of about 1 ° which is a medium-low defined accuracy [60]. On the other hand, the slew rate requirement will be more stringent. It is important to change the attitude of the spacecraft quickly during reentry in order to land on a specified surface. Thus, not only does the slew rate need to be higher but the entry phase in general needs precise guidance to provide landing accuracy and decrease the hazards of landing on steep or rocky terrain. The slew rate for which the vehicle will be designed is then 3 $^\circ/s$.

## 10.5 Mars Lander Attitude Determination and Control System

For the ML attitude control, reaction control wheels will be used since once again it is crucial to provide control about all three axes. Furthermore, this allows the avoidance of unnecessary complexity of the subsystem, considering that the ADCS on the ML will only be used during the separation, entry and landing phase which in total will not take longer than a few hours (about four hours for Soyuz [75]) and with the mass of the ML being just below 7 $t$ the RWS will perform as well as the CMGs [62].To enable a three axis stabilization of the system 4 wheels will be used, 3 of them orthogonally positioned to control the motion around the 3 axes and an additional wheel to provide control in case of one of the wheels failing. Also, in this case only the attitude needs to be controlled with the ADCS while the reorientation and landing will be performed using the Super Draco thrusters as explained in Sec. 12.9. Therefore no thrusters are applied.

**Hardware Sizing:** These wheels then need to be sized according to the disturbance torques that they need to correct for as well as for the slew rate requirement. First of all, the disturbance torques will be calculated just as in Sec. 10.2.1. Considering that the ADCS attitude control will only be active in the proximity of Mars, the worst case disturbance torque is the Mars gravity gradient torque of about 4.23E-04 $Nms$. However, in this case the wheel's dimensions and mass will be determined according to the torque necessary to perform a slew maneuver. This torque is calculated using Eq. 10.7 that results in 58 $Nm$ (by allowing acceleration time to be 5 $s$ since the ML has to react faster than the PTV). Then with Eq. 10.3 the momentum that needs to be stored in a wheel can be estimated. The important thing to account for is that instead of the quarter of a period that is used for the accumulated disturbance torque, the time used here is the 5 $s$ during which the vehicle will needs to provide this force and accelerate. The momentum per wheel is then estimated to be 232 $Nms$. Using some historical data, an equation to calculate a reaction wheel's mass based on the momentum stored is extrapolated in [66]. This is the Eq. 10.11 with main parameters being $M_{rw}$ - the mass of the wheel and $H_{rw}$ - the momentum stored in a wheel.

$$M_{rw} = 1.7881 \cdot H_{rw}^{0.422} \tag{10.11}$$

The mass of one wheel is then calculated to be 18 $kg$ which then implies a radius of 0.22 $m$ (similar to the PTV due to a much smaller spin rate of 5000 rpm [40]). All the relevant parameters for the ML are summarized in the following Tab. 10.6:

Table 10.6: Important Parameters for the ML Attitude Control Design

| **Parameter** | $I_{zz}$ | $I_{xx}$ | Mars Gravity Gradient Torque | Wheel Stored Momentum |
|---|---|---|---|---|
| **Value** | 11163 $kgm^2$ | 19940 $kgm^2$ | 4.2E-04 $N \cdot m$ | 232 $N \cdot m \cdot s$ |

## 10.6 Mars Lander Guidance, Navigation & Control and Sensor Selection

There is one major difference between the chosen sensors for the ML and PTV. This is the fact that in the ML case the Sun sensors are not used. This decision is made since there are no solar panels that require the exact position with respect to the Sun. Also, the star trackers will be used that provide a higher accuracy than the Sun sensors so it will be enough to use them to determine orientation with respect to the other celestial bodies. The relevant decisions with respect to the sensors and the final result of the subsystems designs are summarized in Tab. 10.7.

The requirements of the Guidance, navigation and control system for the ML are very similar to the PTV ones.It is, however, crucial to provide very accurate control and navigation throughout the landing phase. To achieve this, additional systems can be used on board such as the one used in the MSL [76], the Terminal Descent System (TDS). This will not however be discussed in further detail since the landing details and thrusters used to perform the descent on Mars will be discussed in Sec. 12.9. The main objective of this subsystem is the same as for the PTV and the scheme describing the principle in which it works can be found in Fig. 10.4.

Table 10.7: ADCS & GNC designs for the ML

| | **Mass [kg]** | **Power [W]** |
|---|---|---|
| 4 Reaction wheels | 72 | 210 |
| 2 Star trackers | 10 | 15 |
| 2 IMUs | 24 | 150 |
| Total (incl. fuel) | 106 | 375 |

**Sensitivity Analysis:** Unlike some of the other subsystems, the ADCS and GNC are not very dependent on the spacecraft itself. Reconsidering the components of these subsystems might only come as a result of a very big decrease (more than 50%) in the vehicle mass. In this case the reaction wheels could be considered for attitude control. While this change might decrease the system mass it will not bring any major changes to the spacecraft as a whole or influence any other subsystems enough to cause a change in them. Similar effect happens when changing the mass moment of inertia, no major changes will result. The only way the above presented designs would change is by changing the mission requirements but they can vary only slightly in values (pointing accuracy, slew rate). The general requirements stay the same (correcting the orbit, pointing the solar panels, determining orientation) so the overall configuration of both ADCS and GNC stay the same as well.

**Verification:** The systems presented in this chapter were designed on very basic principles since the design is only at the Phase-A level. The components were sized according to equations and reference values found in trustworthy sources as cited throughout the chapter. Since only these simple equations were used, there is no need to verify any complex numerical methods. In addition to this, the whole system was designed to meet the specific requirements (such as the pointing accuracy) so the system complies with all the requirements mentioned in Sec. 10.1. These requirements were derived from the top level requirements. This means that the system is indeed designed as necessary to enable the whole vehicle to perform its intended function.

**Validation:** Not much historical data is available to validate these results. However, all the values calculated were compared to similar spacecraft designs and concluded to be within a reasonable range. Such examples are the amount and position of the sensors that was derived from the MRO. Although the MRO is an unmanned vehicle, it is an irrelevant fact for the number of sensors. MRO was chosen for its dimensions and since it also traveled to Mars. Dimension-wise the vehicles are similar and therefore the same amount of sensors are used to make sure that they cover the whole field of view. On the other hand, to validate the type of attitude, the ISS and Skylab were used as references as they also have a very large mass and moment of inertia. This also proved to be important when sizing the wheels. Short comparison of some values for the Mars One spacecraft and the ISS is shown in Tab. 10.8. From this table it follows that the calculated values do indeed present good estimates for a conceptual design. Finally, as mentioned before, the system is designed according to the requirements derived from the stakeholder requirements. This means that the system is validated in that respect, that is - it complies with the stakeholder requirements.

Table 10.8: Mars One and ISS comparison

| | **Mars One** | **ISS[69]** |
|---|---|---|
| Mass [t] | 150 | 450 |
| Number of CMGs | 3 | 4 |
| Momentum stored [Nms] | 1126 | 4880 |
| Wheel radius [m] | 0.2 | 0.4 |
| Wheel moment of inertia [$kgm^2$] | 1.6 | 7 |

## 10.7 Conclusion and Recommendations

This chapter showed the main approach to designing the ADCS& GNC and presented the relevant references used. The end results for PTV and the ML are summarized in Tab. 10.5 and 10.7. Finally the design was verified and validated. This was, however a design at a conceptual level. This means that the values calculated are still subject to change and that further designing needs to be done. Some suggestions with respect to areas that need further investigation are presented below.

1. Define the GNC subsystem details - The hardware needs to be specified and incorporated into the PTV. Furthermore, since at this phase only off the shelf products are considered it should be determined whether or not these (both hardware and software components) need alterations to be used for the purposes of Mars One mission.
2. Investigate the additional electronics and wiring needed - These systems are very complicated and in order to enable communication between different systems additional electronics will be needed on board. When a more detailed configuration is realized this can be determined. Also the weight of these electronics and wiring needs to be calculated and added to the current estimate.
3. Determine the cost - It is important to estimate the cost of the system in order to define whether the cost percentage allocated for these subsystems is not exceeded. In succeeding design phases when the exact dimensions are specified the cost of each component (thrusters, sensors, CMGs) should be determined by contacting the supplier companies.

# 11 | Power System

All systems require electric power to operate. The power generation and distribution functions of the spacecraft are included in the power system and will be discussed in this chapter.

## 11.1 Power budget

An estimate of the power requirements of all systems is made and summarized in Tab. 11.1 In this table, five scenarios describe both standard and critical power usage moments.These scenarios are used for sizing the power generation systems. Data is derived from, and estimated based on [21], [47], [77]. The household scnerio is this bare minimum power required for the spacecraft to be operational, and fot the crew to survive. During maneuvers, such as $\Delta V$s or assembly, the second scenario is applicable.Scenarios 4 and 5 describe the power usage of the lander vehicle after decoupling, respectively during landing and after touchdown. The third scenario sums up all the crew equipment such as food heating, toilet usage amd entertainment. This peak power will probably never be reached since crew can be instructed to not use all equipment at the same time.

## 11.2 Power generation

For power generation a photovoltaic system will be used to transform sunlight into electrical energy. A nuclear power generator was considered, but rejected for possible safety issues and marketability problems.

The end of life power generated by solar panels is described by Eq. 11.1. In this equation $A$ is the area of the solar panels, $S$ the solar intensity, $\eta_{cell}$ the solar cell efficiency, $I_d$ the inherent degradation, $L_d$ the life degradation and $\theta$ the angle of incidence. The area of the solar panels will have to be sized accordingly to meet the power requirements.

$$P_{EOL} = AS\eta_{cell} I_d L_d \cos(\theta) \tag{11.1}$$

The power available is mostly affected by the solar intensity. In LEO the intensity is on average $1.36 \cdot 10^3$ $W/m^2$. In LMO, depending on the location of the planet in its orbit, this value is in between 374 $W/m^2$ in Aphelion at a distance of 1.67 $AU$ from the Sun, and 715 $W/m^2$ in Perihelion at a distance of 1.38 $AU$ from the Sun. The spacecraft will arrive when Mars is at 1.54 $AU$ from the sun, when the solar intensity equals 574 $W/m^2$. The solar intensity during the entire transfer phase is plotted in Fig. 11.1 From this figure it can be seen that the longer the mission lasts, the less power is available. To accommodate for this decrease in power, two main solutions have been defined.

Firstly, a battery system can be taken on board for use of the last hundred days. This would allow the solar panels to be smaller, lighter and cheaper, since less power is required from them.

Table 11.1: Power usage of the PTV and ML in different situations. (Sc.(Scenario) 1: Household, Sc.2: Maneuvers, Sc.3: Personal use peak, Sc.4: ML entry, Sc.5: ML landed.

| **Function** | **Sc.1 [W]** | **Sc.2 [W]** | **Sc.3 [W]** | **Sc.4 [W]** | **Sc.5 [W]** |
|---|---|---|---|---|---|
| Control | 100 | 210 | 100 | 300 | 0 |
| Guidance and Navigation | 226 | 226 | 226 | 226 | 200 |
| Computers | 200 | 300 | 200 | 300 | 300 |
| Thermal system | 200 | 200 | 200 | 400 | 200 |
| Food heating | 0 | 0 | 200 | 0 | 0 |
| Lighting | 2 | 2 | 100 | 2 | 2 |
| $CO_2$ remover | 80 | 80 | 80 | 80 | 80 |
| Air filtration | 200 | 200 | 200 | 200 | 200 |
| Electrolysis | 600 | 600 | 600 | 600 | 600 |
| Waste collection | 0 | 0 | 90 | 0 | 0 |
| Hygiene | 0 | 0 | 1000 | 0 | 0 |
| Recreational | 0 | 0 | 500 | 0 | 0 |
| Exercise equipment | 0 | 0 | 145 | 0 | 0 |
| Communications | 1200 | 1200 | 1200 | 1200 | 1200 |
| Cameras | 100 | 100 | 100 | 100 | 100 |
| 20% Contingency | 582 | 624 | 928 | 682 | 576 |
| Total | 3490 | 3742 | 5569 | 4090 | 3458 |

The specific energy of batteries generally used in space missions is around 100 $Wh/kg$ [47] and the energy density is generally around 300 $Wh/l$. If 1000 $W$[1] was needed over the duration of 100 days, this would require $1000 \cdot 24 \cdot 100 = 2.4 \cdot 10^6$ $Wh$ of energy. This would then again require $2.4 \cdot 10^6/100 = 2.4 \cdot 10^4$ $kg$ of batteries. In addition, solar panels are still needed to generate enough energy before the last hundred days. These calculated numbers are all rounded heavily in favor of the mission, and are still big. This brief canculations shows that designing the solar panels for the near-Earth phase of the mission is infeasible.

Secondly, the photovoltaic surfaces can be made larger to deliver enough power during the entire transfer. The required panel size is now calculated. For the inherent degradation a value of 0.77 is assumed and an efficiency of 0.15 [78]. A life degradation factor $L_d$ of 0.97 is assumed [78]. The angle of incidence will be kept below 1 degree. If a total power of 4043 $W$ is required at a solar intensity of 564.8 $W/m^2$, Eq. 11.1 yields a required panel size of 118 $m^2$.

Different types of solar panels are available. The choice fell on thinfilm cells, currently developed for Dutch Space [79]. These cells do not make use of high-tech technologies that allow the efficiency to climb up to 43% [80], but have an efficiency of up to 15%. The thinfilm cells are lighter and cheaper, they have a density of 0.6 $kg/m^2$ and a price of 80 €/$W$. Properties of this subsystem are shown in Tab. 11.2[2]

[1] Replacing rougly one third of the minimum power required by power generated by batteries
[2] The displayed mass is excluding the structure. The structural mass is calculated to be under 10 kg.

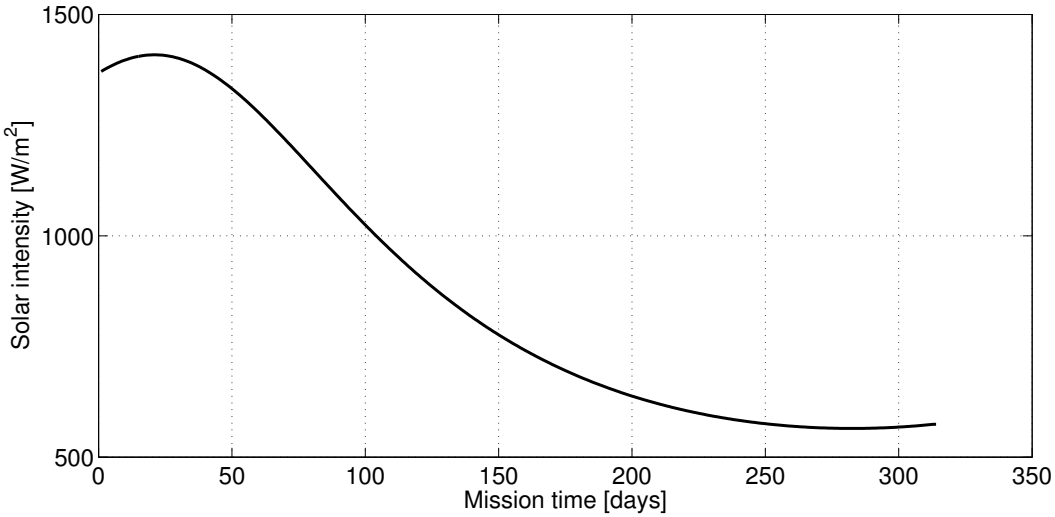


Figure 11.1: Solar Intensity as function of the mission duration.

Table 11.2: Solar array properties

| **Property** | **Value** |
|---|---|
| Solar array area [m$^2$] | 118 |
| Total array mass [kg] | 71.0 |
| Total array cost [€] | $3.2 \cdot 10^5$ |

In the beginning phase of the mission, 1.5 $kW$ of additional power is required to cool the propellant tanks (see Sec. 5.9. This required power will then slowly decrease as the solar intensity decreases and dissapear completely around day 100. This additional power requirement is no challenge since in the early mission phase more power is generated by the photovoltaic surfaces.

The entire transfer can be done with this system, apart from personal use peaks. In Earth and Mars orbit eclipses will appear, blocking all sunlight from the solar panels. Also if solar panels are not oriented properly for a brief moment, a backup source is required. Hence, a secondary (rechargable) battery cell will be implemented. This battery cell will be a Lithium Cobalt Oxide ($LiCoO_2$). This cell has a specific energy of 100 $Wh/kg$ and an energy density of 250 $Wh/l$. These numbers are high compared to other battery cells and are the main reason why this battery type was selected. Also it has a 99% charge efficiency and is available for commercial products. The main disadvantage is that extra care must be taken to not overcharge the battery, this could produce undesirable products.[47]. Tab. 11.3 summarizes some important cell properties. The driving requirement for the cell is the power it needs to deliver during entry and after landing until the ML is properly docked to to Mars base. This power is a sufficient backup for all other possible scenarios. The battery is located in the ML.

## 11.3 Solar Panels Structural Aspect

118 $m^2$ Of photovoltaic surface can be split up into three surfaces of each 39.4 $m^2$, each mounted between the propellant tanks. During launch the panels will be folded into the PTV. The panels

Table 11.3: Lithium Cobalt Oxide cell properties

| Property | Value |
|---|---|
| Total cell volume [l] | 155 |
| Total cell mass [kg] | 387 |
| Total cell capacity [kWh] | 38.7 |

can each be folded into a package of $0.4m^3$, and stored in the PTV. In orbit, the panels will expand from folded configuration to expanded configuration by inflating tubes running through the surface. After inflation, a composite laminate system consisting of a thermoset matrix resin and a fiber reinforcement in the structure will rigidize by heating, making use of solar energy. [81] Between the panels and the surface of the PTV, a space of two meters will be, bridged by a strut. This allows the panels to generate as much power as possible, lowering the chance of them being blocked by the spacecraft.

The main load on the structure will be the acceleration applied by the $\Delta$Vs. This acceleration will be around 0.3 $g$, or 2.9 $m/s^2$. It will now be calculated if this structure is capable of withstanding this load. Assuming an additional structure mass of 10 $kg$, the force applied by accelleration is $F \cdot m = 2.9 \cdot (10 + 70.9) = 89.6\ N$ This causes a bending moment at the root of the strut is equal to $M = FL/2 = 89.6 \cdot (13.1 + 2) = 678\ Nm$. One square rod of area $1cm^2$ will have a moment of inertia of $I_{xx} = bh^3/12 = 1 \cdot 1^3/12 = .0833\ cm^4$ Using Eq. 11.2, the stress can be calculated to be at max 8.14 $MPa$. These calculations are rough, but do show that loads can be easily carried by composite structures, which typically have higher failure strengths, both in tension and compression [82].

$$\sigma = \frac{yM}{I} \tag{11.2}$$

## 11.4 Power distribution

In between the power generation and power consumption, a power regulation unit (PRU) is located. This unit determines how much power is generated by the photovoltaic surfaces and also determines how much power the subsystems require. The PRU is directly connected to all systems and can convert the power to suitable voltages. Fig. 11.2 shows how the systems are connected.

## 11.5 Verification and Validation

All calculations were done in models consisting of relations and calculations based on theory taught in the Delft University of Technology aerospace engineering programme [83],[84]. All relations were carefully checked and tested with simple numbers before using them. Validation would be done by producing parts of the photovoltaic surface, and structural mechanisms and testing if they work. Also, existing satellites can do measurements on solar flux.

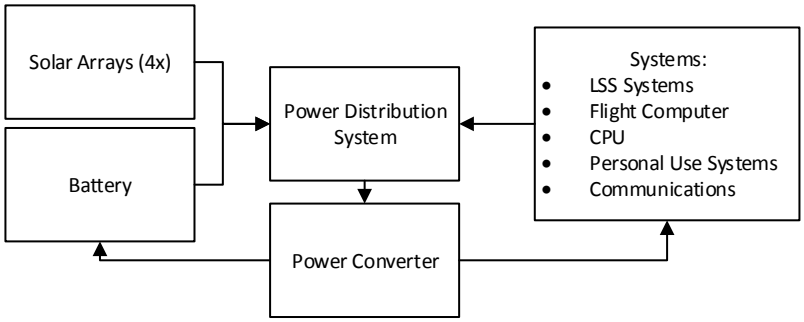


Figure 11.2: Power system block diagram

## 11.6 Sensitivity Analysis

When sizing a subsystem, it is important to consider the effects a change in the requirements will have on the design of the subsystems. If the design is not flexible enough to adjust to the change in requirements, it indicates a weakness in the design and necessitates the investigation of a contingency. This is especially important for designs where approximations or assumptions that may decrease the accuracy of the calculations are made.

For the sake of the solar arrays, a case where the total power requirements are increased by 25 % is examined. The original peak power usage of 5569 $W$ therefore becomes 6962 $W$, giving a new solar array total area, mass and cost of 146 $m^2$, 88 $kg$ and €0.4 million, respectively. Assuming three solar arrays are maintained, a new individual solar array area and folded package volume of 48.5 $m^2$ and 0.49 $m^3$ is found. The increase in the area of the arrays will increase the complexity of their unfolding process and give the need for stronger array support structures, but these increases will not affect the feasibility of the design. Similarly the cost increase is inconsequential compared to the total mission cost and there is enough space in the Falcon Heavy payload fairing for the increased package volume of the folded arrays. Therefore, it can be concluded that the solar array design concept is not very sensitive and is flexible enough to adapt to altered design requirements.

## 11.7 Conclusion

The power system for the PTV and ML were designed in this chapter. 118 $m^2$ of thin-film photovoltaic surfaces will be attached to the PTV to generate a minimum of 4 $kW$ of power when orbitting Mars. For peak use, such as maneuvers and intensive equipment use by astronauts, eclipses and the landing phase a rechargable battery cell with a total capacity of 38.8 $kWh$ is installed in the lander vehicle. The solar cells are folded into the PTV during launch, and expand by inflating tubes running through them, and then curing the composite structure. This system will be able to generate power for the entire mission, the large battery serving as extra redundancy.

# 12 | ML Design

## 12.1 Introduction

In this chapter the design of the ML will be discussed in more detail. In the previous chapters the general subsystems of the PTV and the ML were already explained, like the power budget and the life support. However the ML has some specific subsystems, that the PTV does not have, such as a heat shield, parachute and a landing mechanism. These specific ML-related subsystems will be investigated and designed in this chapter.

## 12.2 Mars Lander mass budget

In this section the mass budget of the ML will be discussed in more detail. The ML's design is based on the Red Dragon, but for the Mars One mission it needs several modifications. For the ML mass budget the dry mass of the Red Dragon is used together with the mass of the modifications needed, like the mobility system and additional life support, and the mass of the propellant, which is different. Also data from the Apollo Command Module was used to estimate the mass of some subsystems. In Tab. 12.1 an overview of the mass budget is given. With respect to sizes and dimensions, the Red Dragon's design is used as a baseline [85].

The mass of the mobility system is based on the weight of the Lunar Roving Vehicle used during the last three Apollo missions. The mass of the crew is estimated using the average mass of an Apollo astronaut [89]. The mass of the parachute system is proportionally based on the mass of the parachute system of the Mars Exploration Rover, Viking and Mars Science Laboratory (MSL) and the mass of the propellant is calculated in Sec. 12.9.

To compute the total propellant mass a Matlab program has been developed. Propellant is needed for three landing phases: entry, guidance and touchdown. The entry propellant is the propellant needed to bring the ML into the desired flight path angle ($\gamma$). The required $\Delta V$ was computed with Eq. 12.1, where the parameter $V_E$ denotes the entry velocity [90].

$$\Delta V = V_E sin(\gamma) \tag{12.1}$$

The ML also needs a certain propellant mass for steering during the landing phase, for which a model for descent guidance at Mars is presented in [91] . Using their methods of estimation a $\Delta V$ of 175 $m/s$ was found to be necessary for guidance of the ML [91]. The propellant mass necessary to perform the last phase of descent, whereby the ML is decelerated with a constant thrust from a height of 1 $km$ down to the surface, is calculated in Sec. 12.9. Assumptions have been made for the use of the SuperDraco engine which is used by the Red Dragon, and the specific impulse of this engine is estimated to be 308 $s$ with methods from [40].

Table 12.1: ML mass budget [86], [87], [88],[40]

| Component | Mass [kg] |
|---|---|
| Structure | 1700 |
| Engine | 478 |
| Propellant tank | 119 |
| Electrical equipment | 680 |
| Communications | 252 |
| Navigation | 314 |
| Heat Shield | 410 |
| Telemetry | 231 |
| Parachute system | 158 |
| Crew | 300 |
| Mobility system | 316 |
| Environmental Control | 200 |
| Life Support | 490 |
| Propellant | 1190 |
| Total mass | 6830 |

## 12.3 Atmosphere of Mars

The design of the ML depends on the environment of Mars, in particular it is heavily dependent on Mars's atmosphere. Thus before the parachute, heat shield and other subsystems can be designed Mars's atmosphere should be investigated.

The atmosphere of Mars is different from Earth's atmosphere, especially in terms of density, which is significantly lower than on Earth. For example, the air density at sea-level at the Earth is 1.225 $kg/m^3$, and according to an atmospheric model from NASA the air density at sea-level at Mars equals 0.015 $kg/m^3$. To simulate Mars's atmosphere the model provided by NASA was used, which divides Mars's atmosphere into two isothermal layers: above and below a height of 7000 $m$. The model simulates temperature, density and pressure at each altitude [92].

## 12.4 Flight Path Angle

To stay within the safety limits for the human body the $g$-loads during flight should not exceed 5 $g$. This is a requirement for the ballistic entry that prescribes the ML's maximum entry flight path angle when entering the Martian atmosphere. The maximum acceleration experienced is calculated using Eq. 12.2 [90].

$$a_{max} = -\frac{\beta sin(\gamma_E)}{2e} V_E^2 \tag{12.2}$$

Parameter $\beta$, describing the exponential decrease of the air density on Mars with increased altitude, was computed with the atmospheric model for Mars. Parameter $e$ is the Euler number. The velocity of the entry vehicle at a certain height, for instance at the height at which the parachutes are meant to be deployed, can be computed with the altitude-velocity relation (see

Eq. 12.4) [90]. The entry vehicle velocity at the parachute deployment height must be at a certain value, Mach 2 at a height of 6 $km$. Eq. 12.3 gives the height where the maximum acceleration occurs [90]. In this equation parameter $K$ stands for the ballistic coefficient.

$$h' = -\frac{1}{\beta} ln \left( \frac{\rho_0 g}{K \beta sin(\gamma_E)} \right) \tag{12.3}$$

$$\frac{V}{V_E} = exp \left( \frac{g \rho_0 e^{-\beta h}}{2K \beta sin(\gamma_E)} \right) \tag{12.4}$$

The flight path angle necessary to meet these requirements was calculated. In all cases the requirement for the entry vehicle having a velocity of Mach 2 at 6 $km$ (approximately 488.4 $m/s$) was the driving requirement for the flight path angle. The resultant flight path angle is $-2.9°$.

The flight path angle requirement implies a certain requirement for the accuracy with which a $\Delta V$ maneuver can achieve this flight path angle. The orbital velocity of the ML in Mars parking orbit Mars is 3310 $m/s$. This means that a $\Delta V$ of $3310 \cdot \sin(2.90°) = 167.5$ $m/s$ must be performed to achieve the previously obtained flight path angle. The accuracy with which a $\Delta V$ maneuver can be performed by the thrusters will determine whether a certain ballistic entry option is feasible or not. From a number of maneuvers performed by the Mars Exploration Rover's lander, it is found that orbital maneuvers can be performed with an absolute accuracy of 0.4455 $m/s$. This shows that the flight path angle can be accurately brought to within $\arcsin(2 \cdot 0.4455/3310) = 0.0154°$ of the desired angle. Although an upper limit for the flight path angle (based on the angle at which one would skip out of the atmosphere) cannot be found, it is assumed that the accuracy obtained for the flight path angle is sufficient.

**Verification & Validation** In order to validate the flight path angle the same calculation is performed for the Mars Science Laboratory mission. With parameters being a capsule mass of 2800 $kg$, an entry velocity of 6 $km/s$, and a maximum g-load during ballistic entry of 13 $g$[93], the entry flight path angle is found to be $-12.8°$, while the angle found from literature is $-15.2°$. The error is not large, and this shows that the used method is sufficient for calculating the necessary flight path angle in a Phase A feasibility study. It will, however, be necessary to use a more accurate method for calculating the required flight path angle when the design progresses into a more detailed phase.

**Sensitivity Analysis** It is convenient to conduct the sensitivity analysis with a change in the atmospheric parameters, since the atmospheric conditions are very uncertain and play an important role in Eq. 12.2, 12.3 and 12.4. If, for example, parameter $\beta$ is increased by 25%, the required entry flight path angle will be equal to $-1.9°$. This is 35% different from the original flight path angle of $-2.9°$, meaning that this aspect of the design is sensitive to change. Nevertheless, the high accuracy with which a flight path angle can be achieved implies that this will not be a large problem.

## 12.5 Mars Lander Structural Design

The Mars Lander's structural integrity is critical to the safety of the astronauts since it has to transport the crew from space onto Mars's surface with a precarious maneuver. The ML's structure must be capable of supporting whatever loads are imposed on it during landing and it also has to dissipate the high thermal energy when entering Mars's atmosphere. This section discusses the structural design of the Mars Lander. The design will consider the most important

loads predicted for the lander over one mission cycle and size the primary structure according to the highest load. In the following section the ML is designed for the pressurization loads, thermal expansion loads, compressive acceleration loads and vibration loads.

### 12.5.1 Sizing for Pressurization

The maximum pressure in the ML is assumed to be 0.1096 $MPa$, the same value as the pressure in the PTV's living module. It is decided therefore to design the ML's primary structure to be a monocoque pressure vessel. In this case the Mars Lander has the shape of a truncated cone with unequal cross-sections, and thus the equations used in Ch. 7 do not apply directly. However, a reasonable approach is to divide the cone into sections that are sized individually according to the largest cross-sectional area found in each section. The largest diameter then corresponds to the highest hoop stress in each section. This concept is illustrated in Fig. 12.1.

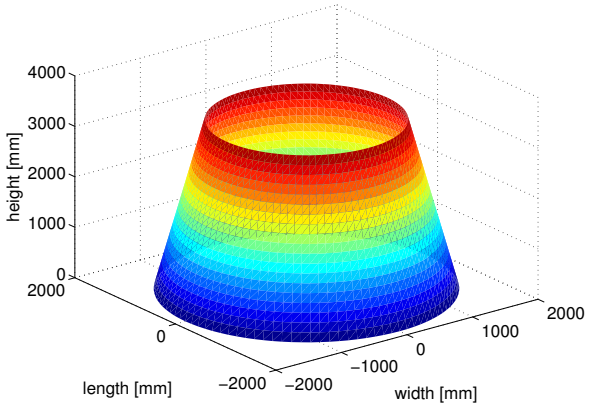


Figure 12.1: ML cone sections and dimensions

The ML cone shown in Fig. 12.1 has a bottom diameter of approximately 3700 $mm$, a top diameter of 2400 $mm$ and a height of 3350 $mm$ which follow from the ML sizing described in Sec. 12.10. The slope of the ML's side-wall is therefore inclined at an angle of 11°. The bottom diameter of each cone section can be calculated with the mentioned values. The designed structure's mass efficiency increases with the number of cone sections, but for simplicity of manufacturing it is sensible to limit the amount of sections. It is therefore decided to divide the ML into 20 small cone sections with an individual height of 167.5 $mm$. The method of sizing the thickness of a cylinder for pressurization has been explained in detail in Sec. 7.1.2 and the hoop stress has been given by Eq. 7.1. The design approach is therefore not repeated here. Tab. 7.2 with the properties of suitable materials can be found in Ch. 7. The materials shown in Tab. 7.2 are considered due to the same reasons discussed in Sec. 7.1.2.

With the design approach discussed above the wall thickness of the ML is found for every section. The required thickness for pressurization is plotted in Fig. 12.2 vs. the bottom z-coordinate of the individual cone sections.

Before the mass of the structure can be determined for the materials shown in Tab. 7.2 it is necessary to investigate other important loads that might be more critical than the pressure loads. Similar to the PTV structural design, the following section discusses the ML's structure with respect to the maximum compressive launch load.

### 12.5.2 Sizing for Compressive Launch Loads

As discussed in Sec. 7.1.3 the spacecraft's components must be able to resist a compressive load of $-6g$ during launch without buckling. The equation used to calculate the required wall thickness t has been given in Eq. 7.7. The derivation of Eq. 7.7 has also been shown in Sec. 7.1.3.

Using Eq. 7.7 and the same method described in Sec. 12.5.1 the ML's wall thickness required to withstand the maximum launch load is plotted for each of the 20 sections. Similar to Fig. 12.2 the results for all selected materials are shown in Fig. 12.3.

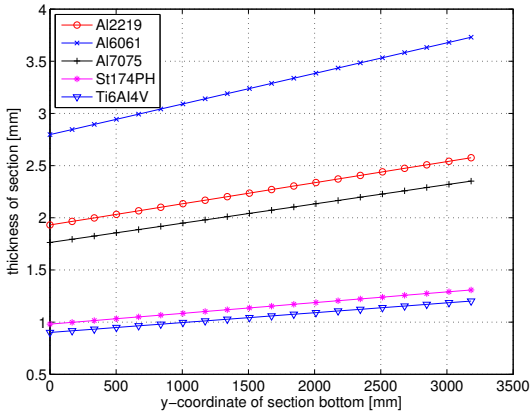


Figure 12.2: Required ML wall thickness for pressurization for selected materials

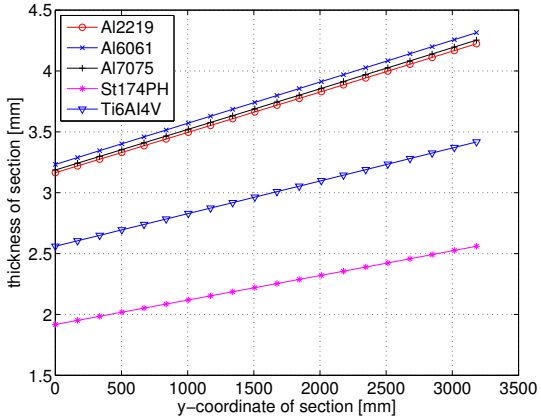


Figure 12.3: Required ML wall thickness for max. launch loads for selected materials

Comparing Figs. 12.3 and 12.2 it can be observed that for every material the wall thickness required to resist buckling is higher than the thickness required for pressurization. Each section of the ML-cone must therefore have a thickness shown in Fig. 12.3. In order to choose the most suitable material the structural weight and total cost that would result from each material have been determined. The results are shown in Figs. 12.4 and 12.5.

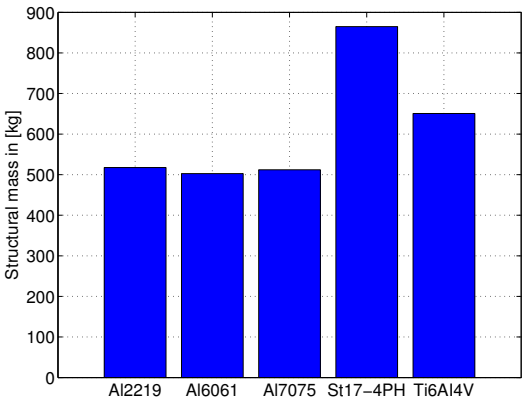


Figure 12.4: ML structural weight according to selected materials in [kg]

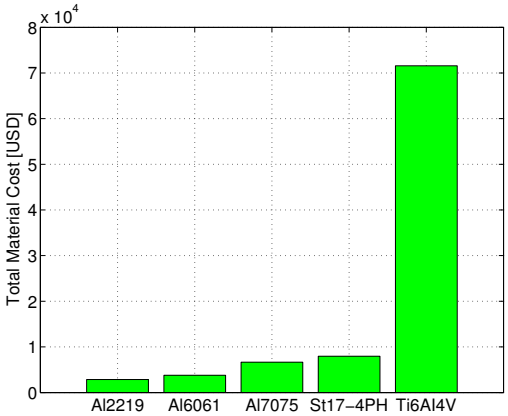


Figure 12.5: ML total material cost according to selected materials in [USD]

The mass values given in Fig. 12.4 are calculated by adding the weight of the cone's side-wall to the top and bottom surfaces that have a thickness equal to that of the adjacent side-wall

cone section. From Fig. 12.4 it can be observed that using Aluminum 6061 would again result in the lowest weight of approximately 503 $kg$. However, it is uncertain whether this material should really be used for the Mars Lander. Due to the higher temperatures predicted for the Mars Lander it is first necessary to consider the material's thermal properties.

**Thermal Property Consideration** As mentioned in the structural design chapter of the PTV the thermal expansion stress $\sigma_{thermal}$ in a material due to a temperature difference $\Delta T$ is given by:

$$\sigma_{thermal} = E\alpha\Delta T \tag{12.5}$$

where E is the material's elastic modulus, $\alpha$ is the thermal expansion coefficient of a particular material and $\Delta T$ is the expected temperature difference. The Mars Lander is expected to experience a temperature range between 229 K to 354 K, which would result in a maximum thermal stress of 197.5 $MPa$ for Al6061. This value is below the material's yield stress of 240 $MPa$, so the thermal expansion stress does not seem to contradict the use of Al6061. However, the thermal expansion coefficient of $22.9 \cdot 10^{-6}$ from [40] is the value at room temperature, so it is hard to say how $\alpha$ will change at higher temperatures as might be experienced by the Mars Lander during atmospheric entry. To ensure the crew's safety it is decided to use the Titanium-Aluminum alloy Ti-6Al-4V, which is stronger at higher temperatures than Al6061 and has a smaller coefficient of thermal expansion of $\alpha = 8.6 \cdot 10^{-6}$. The maximum thermal stress is calculated for Ti-6Al-4V to be 118.25 $MPa$, which would also give much more contingency with respect to the materials yield stress (855 $MPa$). It is therefore decided to use Ti-6Al-4V as material for the main structural shell of the Mars Lander. This design choice leads to a total structural mass of 650.7 $kg$.

### 12.5.3 Resistance against Vibration Loads

As explained in Ch. 7 it has to be proven that the structure will have higher fundamental frequencies than the lower limits specified in the launcher manual. Since the ML is cone-shaped its I and A are not constant. However, it can be easily observed that the lowest frequencies occur for the smallest area and the smallest moment of inertia, i.e. at the top of the truncated cone. If the fundamental frequencies there are higher than 10 Hz and 25 Hz, respectively, then it is proven that the vibration loads during launch will not cause any damage in any location of the structure. The method for calculating the fundamental frequencies have been explained in Sec. 7.1.4 and are thus not repeated here. Sec. 7.1.4 also gives Eqs. 7.16 and 7.17 for calculating the bending and axial fundamental frequencies for a certain cross-sectional area and moment of inertia. Using the dimensions for the smallest cross section the fundamental bending frequency is calculated to be 408.6 Hz and the fundamental axial frequency is 160.0 Hz. Thus it can be concluded that the designed ML's structure meets all the launch frequency requirements.

## 12.6 Heating experienced during the entry phase

In this section the heating characteristics of the ML during the entry phase will be discussed. Besides the g-loads it is also important to take a look into the thermal loads the ML will experience during the entry phase. Due to the high velocity the thermal loads that the entry vehicle will experience will be high. Therefore a heat shield will be used to protect the vehicle and the crew during the entry phase.

First the maximum heat rate experienced by the ML will be computed. This will be done with the following formula [94].

$$q_{conv} = k\sqrt{\frac{\rho}{r_n}}V^3 \tag{12.6}$$

In Eq. 12.6 the parameter $r_n$ is the nose radius of the entry vehicle. The nose radius of the Dragon capsule was estimated to be approximately 8.4 $m$. As a reference the nose radius of the Orion capsule equals 6.0 $m$ [95]. The parameters $\rho$ and $V$ are respectively the air density and the velocity at the maximum heat rate. The constant $k$ depends on the chemistry of the atmosphere and equals $1.9027 \cdot 10^{-4}\ Js^2/m \cdot kg^{0.5}$ for Mars [94].

To be able to compute the maximum heat rate the velocity and the air density at the maximum heat rate should be known. It was assumed that the maximum heat rate will occur at the maximum value of $\sqrt{\rho} \cdot V^3$. This can also be seen in Eq. 12.6, since $k$ and $r_n$ are constant for the same entry vehicle. Using a Matlab based software program which used the atmospheric model mentioned earlier, it was determined that the air density and velocity at the maximum heat rate are respectively $6.15 \cdot 10^{-4}\ kg/m^3$ and 3978 $m/s$ and this at a height of approximately 40 $km$.

Now that all parameters are known, the maximum heat rate can be determined. It was found that the maximum heat rate of the ML equals 121 $kW/m^2$. A graph of the heat rate as a function of the height can be seen in Fig. 12.6.

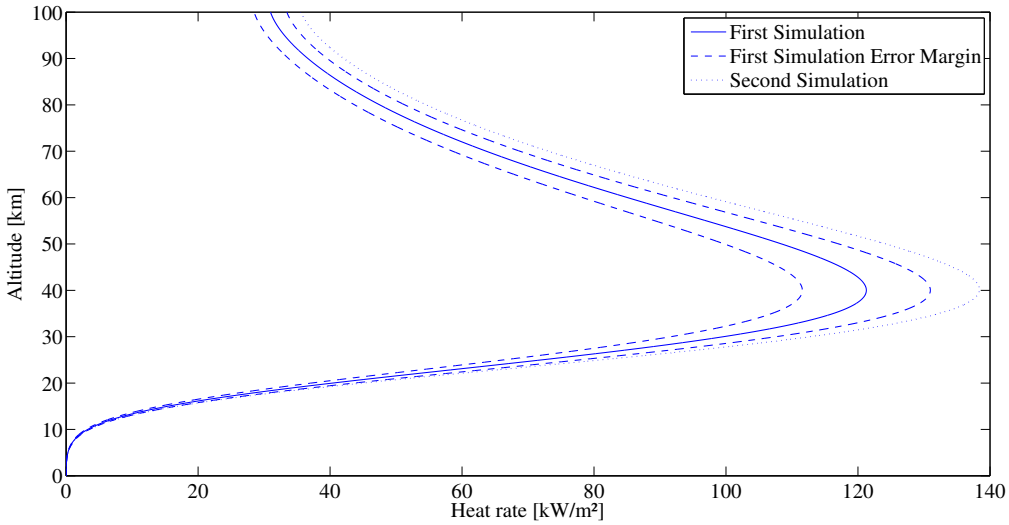


Figure 12.6: The heat rate during entry in function of the altitude

### 12.6.1 Verification and Validation

As can be seen in the graph the heat rate is rather low. As a comparison the Viking spacecraft which also entered the atmosphere of Mars from a parking orbit had a maximum heating rate of 260 $kW/m^2$ and this spacecraft is even much lighter. The ML has a very low heat rate due to several reasons. As can be seen in Eq. 12.6 $r_n$ plays an important role. The nose radius of the Dragon capsule is very high, more than eight times larger than the nose radius of the Mars Science Laboratory Capsule. Secondly the velocity of the ML during the entry is also rather

low. This can be explained by the fact that the ML goes into entry from a parking orbit around Mars, so the entry velocity is not that high as with a direct entry. The flight path angle which also influences the velocity is also very low.

Furthermore the software program which calculates the atmospheric properties has inaccuracies, due to the rough atmospheric model used (see Sec 12.3). Several assumptions were made during the derivation of the formulas for the velocity. For example the variation of the flight path angle with respect to the height was assumed to be zero. Eq. 12.6 only takes the convective heat into account and not the radiative heating, because it was assumed that the radiative heat is negligible compared to the convective heat [96]. The heat rate of the MSL simulated by [97], was used to validate the model, however there was an error of approximately 8% compared to the heat rate simulated by the [97]. Therefore there is a simulation error margin included in Fig. 12.6. Finally, Eq. 12.6 is not very accurate and there are several variations on this formula. The heat rate equation according to [98] can be seen in Eq. 12.7.

$$q_{conv} = 1.5588 \cdot 10^{-4} \sqrt{\frac{\rho}{r_n}} V^{3.04} \tag{12.7}$$

The heat rate as a function of the height according to Eq. 12.7 can also be seen in 12.6. It can be noticed that although the values for the heat rate are more or less in the same range, they are different from the first simulation. This proves that the equation for the heat rate is not very accurate and that a better estimation should be performed in a later design phase.

**Sensitivity Analysis** One should also perform a sensitivity analysis on the heat rate experienced by the ML. As can be seen in Eq. 12.6 and Eq. 12.7 the velocity is the major parameter which influences the heat rate, more than the nose radius and the air density. As sensitivity analysis the velocity was increased by 25%, the maximum heat rate in that case equals 237 $kW/m^2$. This is approximately twice as much as with the original velocity. In the later design phases one should take this into account and use a large safety margins or have a high certainty of the velocity range during the entry phase.

## 12.7 ML Aerothermal Design

Now that the heat flux that the ML will experience while entering the Martian atmosphere has been determined, the ablative heat shield that must be able to resist these loads can be designed. The material of the ablative heat shield will sublimate and the shield's thickness will shrink during the ballistic entry. How large this shield needs to be in order to keep the temperature of the ML's structure and payload within acceptable levels is now calculated. The driving requirement for the heat shield is that it must keep the temperature experienced by the crew between $25°C$ and $30°C$.

### 12.7.1 Material Choice

A number of materials are known as ablators and are candidates to be used for a Mars entry. They are known as Carbon Phenolic, SLA-561V (Super Light weight Ablator 561V), PICA (Phenolic Impregnated Carbon Ablator), Phenolic Nylon, SIRCA (Silicone Impregnated Reusable Ceramic Ablator), and AVCOAT[99] [100]. Characteristics which influence their applicability as an ablator and by which they differ include their density, specific heat, temperature of sublimation, enthalpy of sublimation, temperature of pyrolysis, enthalpy of pyrolysis, and conductivity. Although Carbon Phenolic is an excellent ablator, it also has a high thermal conductivity which

means that the heat flux experienced by the capsule may easily be conducted to the payload and structure. SIRCA is an ablative material which is often used on the back, but never on the frontal area of an entry capsule because of its inferior ablative and conductive properties, despite the ease with which it can be machined into shapes. PICA was used on the recent Mars Science Laboratory mission and because of the similarity of the landing strategy with this mission, has been selected for use as the ablative material.

In addition to the ablative material a layer of an insulator behind the ablator also helps to provide a well-functioning heat shield. Materials with low thermal conductivities which are candidates for this include Saffil (a 96% Aluminium, 4% Silica alloy), Titanium and PM-2000, an iron-chromium based alloy. The way these insulators can be applied will be investigated for all three insulators before choosing the most suitable one.

### 12.7.2 Aerodynamic Heating

When the capsule first enters Mars's atmosphere, its heat shield heats up due to aerodynamic heating. Only when the heat shield's outer layer is at a temperature high enough for sublimation does the ablation of the heat shield occur. For the entire heat shield the following heat fluxes can take place:

- At the outer surface the heat shield heats up due to convection from the air which the capsule is moving through at hypersonic speeds.
- Radiative heat heats up the outer surface of the heat shield.
- Radiative heat is emitted from the outer surface of the heat shield.
- Conduction takes place between different parts of the heat shield and from the heat shield to the inner structure of the ML (the latter should only take place to an extent which will not cause more than 5 $K$ temperature increase).
- Heat is absorbed by the process of pyrolysis, whereby material of the heat shield is charred and changes phase. This will start at the outer surface and the surface along which this occurs will move inward as more of the heat shield reaches the temperature for pyrolysis.
- Heat is absorbed by sublimation whereby material of the heat shield vaporizes, which takes place at a temperature higher than that for sublimation. This will also start at the outer surface and move inward.

The net heat flux which is left over goes towards raising the temperature of the heat shield material [101].

Predicting and understanding the interaction of a hypersonic fluid with a material which ablates and sublimates is a complex process, with many elaborate methods and programs. Because this is a Phase A study, the ablation of the heat shield due to heating from the Martian atmosphere is simplified to be able to produce a design representative enough in order to judge the feasibility of the mission. On the other hand, analyzing the heat shield as a single piece with constant properties (of e.g. temperature) is inaccurate and will likely result in excessive size requirements. In fact, the functioning of the heat shield relies on the temperature being a gradient with a high temperature on the outside in the order of thousands of Kelvin's to room temperature on the inside.

In order to analyze the behavior of the heat shield accurately, the heat shield is split up into finite elements with each element having constant properties of temperature, density, conductivity, specific heat, and the amount of charring and sublimation. The heat shield is split

up along the vertical body axis of the ML. Because this is a phase A study, a 3-dimensional finite element method to find the heat shield's behavior over the whole frontal area is deemed unnecessary. Instead, the one-dimensional approach described here is performed over the axis of symmetry, in the middle of the heat shield, where the convective heat is highest and the thickness that will be derived is interpreted as the largest one necessary over the whole heat shield [102]. Because this is a Phase A study, the effect of chemical reactions which take place in the gas in the boundary layer in front of the heat shield is neglected. Also, the concentration of free radicals of oxygen being lower (free oxygen atoms bond easily with other atoms such as those of the ablator meaning ablation takes place more easily) on Mars than on Earth (the situation for which the equations are intended) is not adapted.

The way in which heat conduction between the finite elements of the heat shield takes place is shown by the following equation[102]:

$$\rho c_p A \frac{\partial T}{\partial t} dy = \frac{\partial}{\partial y}\left(kA\frac{\partial T}{\partial y}\right) + \Delta q \tag{12.8}$$

What needs to be taken into account in the application of this equation is that the density $\rho$ and specific heat $c_p$ can change if a material is charred (after pyrolysis). The way this is applied in the model is that percentages can be applied to the amount by which a finite element is charred, and these percentages are used to calculate the element's density and specific heat. The $\Delta q$ term can be used to account for heat fluxes at the surface, heat flux due to pyrolysis in an element somewhere inside the shield, or can be set to 0 for an element which only acts as a conductor between other elements.

### 12.7.3 Results

The ablator is split up into 6 elements, and one additional element described the insulator (making for 7 finite elements). The thicknesses were fine-tuned to make the temperature of the insulator itself not increase more than 5° above 25° $C$. In order to make this happen the thickness of the ablator was decreased to 5 $mm$ and the thickness of the insulator consequently optimized. For different insulators the results were obtained as shown in Table 12.2

Table 12.2: Necessary Insulator thicknesses with 5 $mm$ PICA ablator

| | Thickness $[mm]$ |
|---|---|
| Titanium | 0.77 |
| Saffil | 2.85 |
| PM-2000 | 0.79 |

The temperatures of all the elements during ballistic entry are shown in Fig. 12.7. One can see that the temperature is lower for elements further into the heat shield, and that the maximum temperature experienced by the heat shield is that at the surface at 939 $K$.

### 12.7.4 Interpretation

The maximum temperature of the heat shield is actually lower than the temperatures for sublimation and even pyrolysis of the PICA ablative material, which are 3700 and 1973 $K$ respectively. This means that no ablation or charring actually takes place in the heat shield. Normally ablation does take place when atmospheric entry is done into Earth's atmosphere, which can be

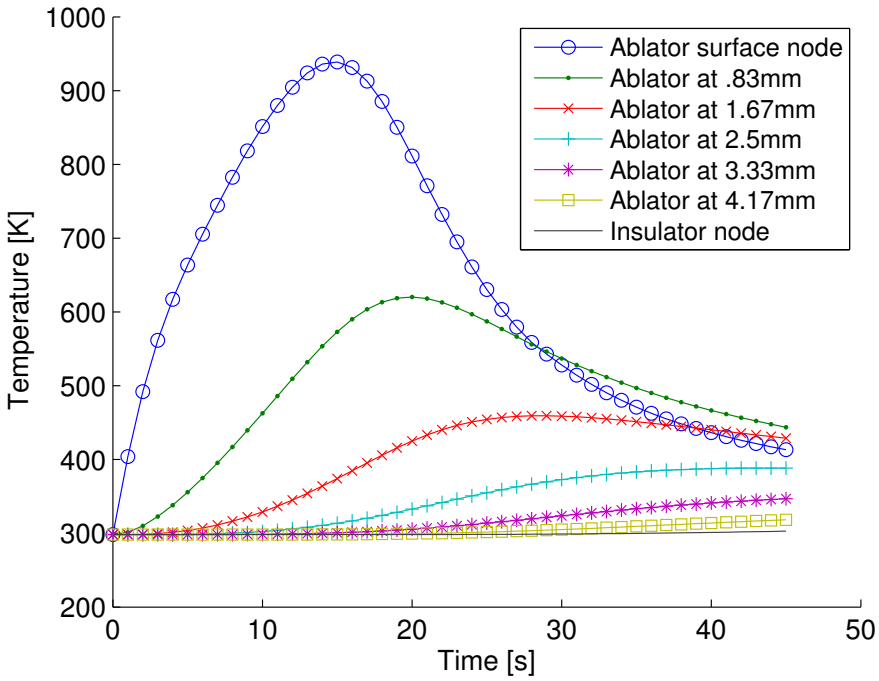


Figure 12.7: Temperatures for different nodes in the heat shield

understood to be because of the higher air density there, causing higher heat flux and higher surface temperatures.

Because no charring and sublimation take place, one could actually get rid of the entire ablator and only apply an insulator as a heat shield, whereby the better thermal properties of conductivity and specific heat of the insulator would be applied throughout all of the heat shield. However, when the above described model is applied to the case of the Mars Science Laboratory (which had an entry velocity of 5.43 $km/s$), one finds a heat shield surface temperature of 1464 $K$[103], which also suggests that no charring or sublimation took place. Nevertheless the design of the Mars Science Laboratory did incorporate a PICA heat shield, possibly in order to account for a larger than expected entry velocity or unexpected variations in the Martian atmosphere. This seems like a suitable reason for the Mars One capsule to include an ablator as well.

In order to account for unexpected variations in the Martian atmosphere and still meet the 5 $K$ requirement, the ablative layer is made slightly thicker than necessary. it is found that a large increase of air density such as it being 20 times larger only causes a 1.5% increase in ablator thickness. As an extra contingency 5% thickness is added to the ablator, leading to a final thickness of 5.25 $mm$.

Because Titanium will already be used for the main structure of the capsule, the easiest option seems to be to also use Titanium as insulator material. This will ensure that the structure only needs an extra layer of Titanium of 0.77 $mm$ to make the main structure underneath not increase its temperature by 5 $K$. Alternatively it can also be stated that the Titanium structure needs to cover the whole frontal area and needs to be at least 0.77 $mm$ thick to make the payload meet the thermal requirement, and that the Titanium itself will be able to withstand a

slightly higher temperature increase (according to the model the insulator itself will heat up by 21 $K$). The latter has been chosen. The density of PICA is 266 $kg/m^3$ and that of Titanium is 4500 $kg/m^3$.

Thus the final design of the heat shield consists of a 5.25 $mm$ layer of PICA, and the requirement that the structure of Titanium behind it should be at least 0.77 $mm$ thick and cover the whole area behind the ablator. The layer of ablative PICA weighs 14.2 $kg$ and a layer of Titanium of 0.77 $mm$ thickness weighs 37.1 $kg$.

**Verification** In order to verify that the model which has been applied in this section is indeed one which models heating during atmospheric entry, a number of checks are performed. For example, it is verified that increasing the incoming heat flux due to convection leads to an increase in internal temperature of the ML. Also, decreasing the thickness of the elements, decreasing the specific heat, increasing the air density (which increases heat due to convection), increasing the entry velocity and decreasing the nose radius of the capsule all increase the internal temperature of the ML.

**Validation** To validate that the model is accurate with respect to the real situation of aerodynamic heating during atmospheric entry, the parameters concerning the entry of the Mars Science Laboratory are inserted into the model. The parameters used are an entry velocity of 5.43 $km/s$, a heat shield of 4.5 $m$ diameter and 2.286 $cm$ thickness, a ballistic coefficient of 115 $kg/m^2$, an entry mass of 2800 $kg$, a nose radius of 1.125 $m$ and an entry angle of $-15.2°$. With the model, the peak temperature found at the outer surface is 1464 $K$. From literature this is found to be approximately 2123 $K$[103], indicating an error of approximately 45%. The error is thought to arise from the assumptions that have been made concerning the atmosphere of Mars (it has been assumed to consist of only two isothermal layers), because this is the most significant deviation from reality. Although the model produces a significant error for the outer surface temperature, it is found that this does not have a significant consequence for the internal temperature of the ML. Even if the 45% error in outer surface temperature is applied to this ML the 5 $K$ internal temperature requirement is found to be met because of the contingency that has been applied to the heat shield thickness.

**Sensitivity Analysis** The velocity with which the ML will enter Mars's atmosphere is based on the parking orbit the ML has before entering and will not change very much, because a completely different parking orbit will be necessary for this. However, the air density of the Martian atmosphere is more uncertain and likely to be different.

In order to examine the flexibility of the design, velocity with which Mars's atmosphere is entered was increased by 25%. This makes the heat flux 239 $kW/m^2$), and this large increase is explained by the heat flux being proportional to the capsule's velocity to the power 3. For the ML to be able to withstand this, it must have a PICA ablative heat shield that is 5.60 $mm$ thick (without contingency). This is just a 6.5% increase from the original thickness and shows that the heat shield design is not very sensitive to a large change in heat flux. An unexpected change of entry velocity during the mission is not expected to be a realistic phenomenon because the entry velocity of the ML is based on the parking orbit it has around Mars and needing to apply a different parking orbit doesn't seem likely. The analysis is conducted to be able to judge on the sensitivity of the design to initial requirements. Therefore, it can be concluded that possible changes in the requirements will not introduce significant problems to the heat shield design.

## 12.8 Parachute Phase

In the intermediate deceleration phase between the ballistic entry and thruster phase, the ML will deploy a parachute. In the past, several different spacecraft have applied one or more parachutes to decelerate during the entry phase. For example, the Apollo Command Module used three main parachutes during re-entry to the Earth's atmosphere and the Mars Science Laboratory used one supersonic parachute to slow down. The principle of a parachute is very simple: by unfolding a surface of a certain material the drag will be increased and the spacecraft will decelerate more quickly. Eq. 12.9 is used to calculate the drag of the parachute and entry vehicle.

$$D = 0.5 C_D \rho V^2 S \tag{12.9}$$

This equation is substituted into an equilibirum expression where drag equals weight, giving the following expression for the parachute diameter [104]:

$$D_t = \sqrt{\frac{1}{\pi C_{D_p}} \left( 2 \frac{m g_0}{\rho_0 V_f^2} - C_{D_{EV}} S_{EV} \right)} \tag{12.10}$$

As can be seen in Eq. 12.10 derived from the expression for the drag of the parachute, the drag depends on the air density, which was computed with an atmospheric model. The final velocity $V_f$ is the velocity at the end of the parachute descent phase and $g_0$ is the gravitational acceleration on the surface of Mars. The variables $C_{D_{EV}}$ and $S_{EV}$ represent the drag coefficient and area of the entry vehicle, respectively.

There is a limit to the parachute deployment Mach number, or more specifically, a limit to the parachute deployment dynamic pressure. For the MSL and the Opportunity this dynamic pressure at parachute deployment was equal to 750 $Pa$ and the Mach number was equal to 2 and 1.77 respectively [105]. Mach 2 is chosen as the velocity at which the parachute can first be deployed. For many of the cases of Mars Landers that have been found, the parachutes were deployed and jettisoned at altitudes in the order of a few kilometers above the ground. Observing the different Mars Landers that have so far been successful, a value of 6 $km$ is used as the altitude at which to deploy the parachutes, and a value of 1 $km$ as the altitude at which to discard it. After this point thrusters will be used to decelerate it further.

A preliminary design of the parachute can be made by applying formula 12.10. A relatively low drag coefficient of 0.615 was selected, equal to that of the parachute used in the Mars Science Laboratory mission, which was a disk-gap-band parachute [106]. Such a low value is required due to the supersonic velocity of the ML at the beginning of the parachute phase. With this value for the drag coefficient, the total diameter of the parachute is found to be 38 $m$. This design configuration will decelerate the ML to the velocity of 95.6 $m/s$ at the end of the parachute descent phase at 1 $km$ altitude.

In the moments following the opening of the parachute, significant g-loads will will be experienced by the crew as the drag of the ML increases. In order to keep the acceleration below 5 $g$ as stated in the requirements, a reefing parachute will be used. Reefing parachute systems work by deploying a partially folded parachute and then later cutting the cable holding it together to allow it to expand to its full size. This greatly reduces the initial shock experienced by the crew by spreading it out over two instances, thereby greatly reducing the risk of injury. The drag coefficient of the reefing and standard parachute configuration is assumed to be constant.

When released, the parachute will have an initial diameter of 26 $m$, with a total diameter of 38 $m$ when the full parachute is fully inflated 6 seconds later. During both shocks, the crew will experience 4.9 $g$ of acceleration, which fulfills the requirement. These values were found by finding the net force, and therefore acceleration, acting on the ML by summing the drag and weight of the ML with the inflated parachute.

Considering that the short time between the first and second stages of parachute deployment, it is vitally important that the parachute has time to fully inflate before the reefing cable is cut. If the inflation time is too long, the parachute could become tangled during the second deployment stage, which would result in the failure of the mission. The parachute inflation time can be calculated using the following equation [107]:

$$t_i = \frac{nD_0}{V_0^{0.9}} \tag{12.11}$$

In this equation $D_0$ represents the initial diameter of the parachute, $V_0$ is the velocity and $n$ is a constant that equals 8 for a disk-gap-band parachute. The inflation time for the initial deployment is therefore 0.79 seconds, which means that the 6 seconds between the two deployment stages is sufficient.

Table 12.3: Values for the ML parachute descent phase

| **Parameter** | **Symbol** | **Value** |
|---|---|---|
| Initial velocity | $V_0$ | 488.4 m/s |
| Final velocity | $V_f$ | 95.6 m/s |
| Initial altitude | $h_0$ | 6 km |
| Final altitude | $h_f$ | 1 km |
| Initial parachute diameter | $D_0$ | 26 m |
| Total parachute diameter | $D_t$ | 38 m |
| Parachute drag coefficient | $C_{D_p}$ | 0.615 |
| Parachute phase duration | $t_p$ | 23.7 s |
| Parachute inflation time | $t_i$ | 0.79 s |
| Parachute reefing time | $t_r$ | 6 s |

**Verification and Validation** For the design of the parachute, no analytical models were available. Instead, a numerical model was used to optimize the design using established equations from a trusted source. The numerical model was used with data from the Mars Science Laboratory [105] to check whether the outcome values are representative of a real life situation. Also, the largest parachute ever tested for a descent vehicle is 45 $m$ in diameter [108], larger than that of the ML. This shows that it is possible to use such a large parachute.

**Sensitivity Analysis** For the sensitivity analysis, the mass of the ML was increased by 25%. In order to maintain a similar final velocity, the diameter of the parachute must be increased, but not enough to increase the acceleration experienced by the crew above the 5 $g$ limit. The new reefed parachute diameter is 29.4 $m$ and the new total parachute diameter is 43 $m$. While the use of a parachute of this size is feasible, it is very large and any increase in size also increases

the risk of failure during deployment. Therefore, great care must be taken when changing any parameters that influence the diameter of the parachute.

## 12.9 Thrusters

The thrusters for the ML need to deliver a $\Delta V$-maneuver that brings the ML from its Mars parking orbit to its suborbital entry trajectory, and one which decelerates the ML during the last phase of descent until the touchdown. These are both small maneuvers which require less propellant and a smaller engine than the PTV. It has been estimated that a suitable thruster system is the "SuperDraco" engine, which SpaceX intends to use with the Red Dragon. An estimate for the specific impulse of the SuperDraco thrusters has been made at 308 $s$ [40]. Providing the ML with a $\Delta V$ of 234 $m/s$ is necessary for bringing the ML into an entry trajectory and 175 $m/s$ is estimated to be necessary for the ADCS to land the ML within the intended landing ellipse (of 7.5 km) during descent [91]. An extra component is needed for decelerating the ML with a constant thrust during the last phase of descent from 95.6 $m/s$ to zero velocity at touchdown while also working against gravity. The total propellant mass needed for these three components is calculated to be 1190 $kg$ using the Tsiolkovsky rocket equation, shown in Eq. 12.12.

$$\Delta V = V_e ln(\frac{m_1}{m_0}) \tag{12.12}$$

The last phase of descent, where the thrusters decelerate the ML with a constant thrust (calculated to be 56 kN), takes 20.4 seconds. Together with the parachute phase and the ballistic phase that last 23.7 and 46.0 seconds, respectively, the total time for entry, descent and landing will take around 90 seconds.

When calculating the time and mass that is used during the thruster descent phase the ML is assumed to have a constant mass. This is of course not exactly true as propellant is used during the descent. The amount of propellant that is actually used is therefore somewhere between two values: the amount derived assuming that the mass stays at the value found at the beginning of the thruster phase, and the amount derived with assuming the mass is equal to the value at the end of the thruster phase. The difference between these two calculations for the propellant mass is found to be 21.3 $kg$. The error in the calculated propellant mass of 381 $kg$ will definitely be less than this, and is thus not very significant.

## 12.10 Landing Mechanism

The ML will land on a set of 6 wheels which will allow the capsule to be pulled to the Mars Base by a rover. Another function of the wheels is to carry the loads experienced at the moment the ML touches down onto the Martian surface. This section shows the design of the wheels and shock absorbers are necessary to withstand the landing loads. By looking at a number of previous successful Mars rovers (Pathfinder, Spirit & Opportunity, Curiosity) it is found that Mars rovers in general have 6 wheels, so the same will be applied to the ML. This number of wheels is thought to be good for covering the rocky Mars terrain.

Shock absorbers need to be used to dampen the loads experienced when the ML touches down with a speed of 2.5 $m/s$. The main bottleneck for keeping the touchdown loads at an acceptable level are the limits that can be experienced by the crew members. The duration of the impact is not yet known, but 5 $g$ is selected as the limit for the acceleration, as this was discovered to be the maximum that humans can safely experience [25]. The shock absorber will

function as a critically damped spring and dashpot combination. Therefore, the stroke of this shock absorber, i.e. the distance that it moves, is calculated with the following equation [109]:

$$x(t) = v_0 t e^{-\sqrt{\frac{k}{m}}t} \tag{12.13}$$

In order to check that the acceleration never exceeds 5 $g$, this equation was differentiated twice to give the following expression for acceleration:

$$\ddot{x}(t) = v_0 \sqrt{\frac{k}{m}} e^{-\sqrt{\frac{k}{m}}t} \left( \sqrt{\frac{k}{m}} - 2 \right) \tag{12.14}$$

In these equations, $v_0$ is the initial velocity at impact, m is the mass of the ML, k is the stiffness of the spring and t is the time since impact. In order to find the stroke length, the optimal spring stiffness must first be selected. It is assumed that the ML initial impact will be on a minimum of 3 of its 6 wheels, meaning that the individual shock absorbers do not have to absorb all the ML loads. With this in mind, the maximum spring stiffness that gives an acceleration of under 5 $g$ throughout the duration of the impact was found in order to minimize the stroke length and, by extension, the size of the shock absorber. Therefore, the spring stiffness value of the shock absorbers is 203.2 $kN/m$, resulting in a stroke length of 9.1 $cm$. Subsequently, the shock absorbers are sized to have a length of 20 $cm$. Based on the size and stroke length the Hoerbiger SA 3/4 x 2 [110], with a mass of 1.8 $kg$, has been selected as the shock absorber to be used. For six wheels this results in a total mass of 10.8 $kg$ for all shock absorbers.

During the last phase of descent (the thruster phase) the heat shield will be jettisoned and the wheels underneath the lander are revealed. The Red Dragon capsule's underside is circular with a diameter of 3.6 $m$. If the 6 wheels are lined up in a $3 \times 2$ pattern with a minimum clearance between the wheels equal to the diameter of one wheel, a maximum wheel diameter of 60 $cm$ is found. Until now, the Mars rover with the largest wheel diameter has been the Curiosity rover, with a diameter of 50 $cm$. The width of the wheels will be 30 $cm$, based on the amount of space under the heat shield for the folded wheels. A render of the ML with the wheels deployed is shown in Fig. 12.8.

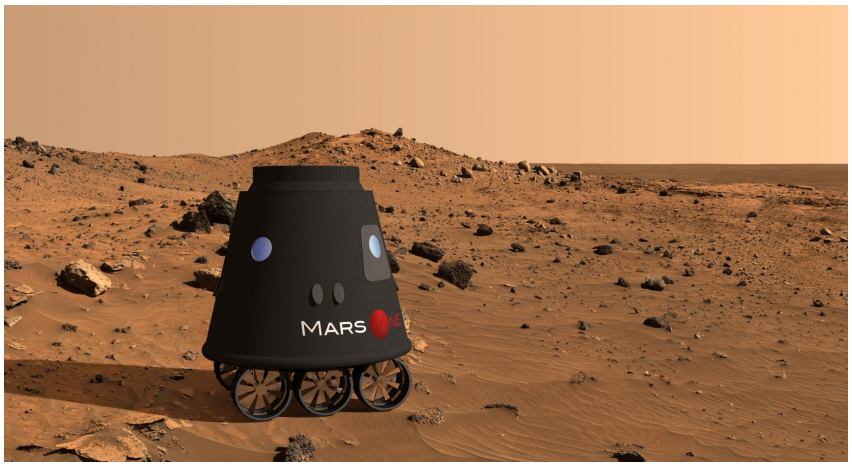


Figure 12.8: The ML wheels under ML in the deployed configuration

Aluminum 7075-T6 is used for the horizontal and vertical struts that suspend the wheels, with a Young's modulus of 71.7 $GPa$, a yield stress of 434 $MPa$ and a yield strain of 0.61%.

They are designed as hollow tubes with a thickness that is 10% of their radius and are able to withstand the impact loads of landing. The failure modes which are driving and which are designed for are that of buckling of the vertical strut and bending (until a yield tensile strength is reached) of the horizontal strut. An overshoot factor of 10 is applied to the calculations to compensate for the fact that a constant force is assumed and the force might be higher during the impact. A safety factor of 2 is also applied to ensure safety of the human payload. In order to withstand these loads the hollow cylindrical struts must have an outer radius of 10 $cm$ and an inner radius of 9 $cm$. The same sizes are used for the horizontal and vertical strut for ease of manufacturing. This results in a horizontal strut length of 5 $cm$ and a vertical strut length of 45 $cm$ below the shock absorbers. As a result of the landing, the horizontal and strut will experience a maximum stress and strain of 31.9 $MPa$ and 0.045 % respectively, while the vertical strut will experience a respective maximum stress and strain of 383 $MPa$ and 0.53 %. The stress is calculated with Eq. 12.15. All of these values are below the material yield stress and strain values, showing that the struts will not fail during landing. Also, the length of the struts were found to be small enough that they will not experience buckling during impact.

$$\sigma = \frac{My}{I} \tag{12.15}$$

Table 12.4: Design values for the wheels and shock absorbers

| **Parameter** | **Symbol** | **Value** |
|---|---|---|
| Initial velocity | $v_0$ | 2.5 m/s |
| Spring stiffness | k | 203.2 kN/m |
| Stroke length | s | 9.1 cm |
| Shock absorber length | $l_s$ | 20 cm |
| Wheel diameter | $d_w$ | 60 cm |
| Wheel width | $w_w$ | 30 cm |
| Strut outer radius | $r_{out}$ | 10 cm |
| Strut inner radius | $r_{in}$ | 9 cm |
| Horizontal strut length | $l_h$ | 5 cm |
| Vertical strut length | $l_v$ | 45 cm |

In order to provide for space under the ML in which to include the folded landing mechanism, the height of the ML is increased with 45 $cm$ with respect to the height of the baseline design, the SpaceX Dragon capsule, giving a total height of 3.35 $m$. The diameter of the bottom surface of the ML is increased from 3.6 $m$ to 3.79 $m$.

**Verification and Validation** With any design method, it is important to ensure that the results are accurate and reliable. The equations used for the structural analysis came from a trustworthy source [111] and the numbers were further verified with the use of an alternative method for the calculation of the stresses. Using Eq. 12.16, a maximum stress of 347 $MPa$ was found to act on the vertical strut. This is within 10% of the originally calculated value and falls within the safety margin, meaning that the accuracy of the structural analysis is acceptable. Despite this, the difference is large enough that more precise calculation methods will be required in the subsequent, more detailed, design phases. The final results for the spring

stiffness of the shock absorbers of the ML were validated against the results of an analysis of automotive shock absorbers and were found to be similar to representative data[112].

$$\sigma = \frac{F}{A} \tag{12.16}$$

**Sensitivity Analysis** For the sensitivity analysis of the landing phase, the mass of the ML was increased by 25%. This results in a stress and strain on the vertical strut of 479 $MPa$ and 0.67 % respectively, greater than the failure values for the chosen material. Therefore, 11 $cm$ and 10 $cm$ would have to be the new values for the inner and outer radius. Also, in order for the shock absober deflection to remain below 10 $cm$, the spring stiffness of each shock absorber would need to be increased to 232 $kN/m$. The new values for the landing struts are not significantly larger than the previous values and would therefore not have a significant impact on the total system weight or performance. Therefore, the design can considered robust and resistant to changes in the requirements.

## 12.11 ML Base Integration

Once landed, the ML still needs to connect with the Mars base, as stated in the requirement concerning the reusability of the ML. Also, the crew will not be physically strong enough to carry out demanding tasks or walk any significant distance due to the muscle atrophy associated with an extended stay in a microgravity environment. Therefore, a method of transporting the ML to the Mars base that does not require significant exertion from the crew members is required.

Prior to the first manned mission to Mars, multiple unmanned missions will be sent. These missions will scout a suitable base location, deliver supplies and materials and construct the base [113]. Two settlement rovers will be brought that aredesigned to transport the base components to the desired area and construct the base. Since these rovers are already designed for the integration of the separate parts that make up the base one of them can also be used to pick up the ML, which will land close to the base (within 7.5 $km$), and bring it to the base.

Once landed, the ML will communicate its position so that an optimal route from its location to the base can be planned that contains the minimum amount of obstacles. The rover can then follow this route, couple with the ML, pull it to the base and connect it to the other base modules. The ML's six wheels will make it possible for the rover to drag it across the surface of Mars. If the ML were to become stuck in a ditch or rocky outcrop, it would be possible for the crew members to board the rover and allow it to carry them to the base, leaving the stranded ML behind. The ML will be berthed to the base by the robotic hand of the other settlement rover. While one of the rovers maneuvers the ML into position, the other rover will facilitate the connection between the side door of the ML and the adjacent base module. The connection will use a specially fitted passageway and will be airtight to allow the crew to go from one module to the other without the need for a space suit.

## 12.12 Conclusion

In this chapter some subsystems exclusive to the ML were investigated and discussed. Since these subsystems also depend on the characteristics of the atmosphere of Mars, first a model to simulate Mars's atmosphere was made based on two isothermal layers. Then the flight path angle

at which the ML enters the atmosphere was computed at -2.9° such that it performs a ballistic entry while meeting the requirements of the maximum g-loads and specified velocity required for the parachute deployment. In this chapter also the structure of the ML was designed and the materials were selected. Afterwards it was determined that the maximum heat rate during the entry phase equal 12.1 $W/cm^2$. This value was used to size the heat shield at 5.25 $mm$ of PICA ablator and 0.77 $mm$ of Titanium insulator. The parachute and the thruster which the ML will use to decrease the velocity to the impact velocity were also defined, at 38.0 $m$ and using 381 $kg$ of propellant respectively. Finally the landing mechanism for the final touch-down and transport to the base was designed, and its mass is 88.6 $kg$.

This chapter proves that the ML is able to land on Mars using existing technologies and systems. However, a more detail design is necessary for a design that can be successfully applied to this project. For example, a more detailed design of the heat shield and landing mechanism would be necessary for this. A more detailed mass, power and cost budget should be made and iterated. Also, all the subsystems should be qualified and tested in a relevant environment such as a wind tunnel or vacuum room.

# 13 | Risk management and Contingency Analysis

Risk management is an integral part of every design process as it is important to account for all the risks implied by the different design choices made. This chapter will show the steps taken to perform the risk analysis which will result in an overview of how reliable the design is as well as present different methods that can be used to mitigate risks.

## 13.1 Risk identification and mapping

The first step in the risk management procedure is to identify all the risks that the system encounters. Once these risks are identified, they will be given certain weights in terms of likelihood and impact. This means that each risk will have a "score" based on how likely it will occur and on how severe the impact of this risk would be. This is illustrated in Fig.13.1 where the pre-mitigation risk map is shown classifying the risks, while a list of all the risks identified can be found in Tab.13.1.

As can be seen in this table, two groups of risks were identified: system risks and mission risks. System risks refer to all the uncertainties that follow from the designed subsystems while the mission risks are general risks not directly influenced by any of the decisions made or systems designed. All of these risks and the reasons for their classifications will now be shortly explained.

- **SR01** - Some systems might fail due to the vibrations induced during the launch (sensors, computers). The impact of such an event will be classified as *catastrophic* since it might seriously endanger the mission objective, depending on the system that failed. However, all the systems are designed by taking these vibrations into account so it is *unlikely* such an event will happen.
- **SR02** - Several components of this design have not yet been completely verified. Such examples are launcher and the engine. The TRL of all the components used is 5 so it is assumed that they will be ready in time. Therefore the likelihood of this risk is estimated as *unlikely* and the impact as *critical* since it would imply several changes (different propellant, dimensions, tanks and maybe even a different PTV configuration) in the design to account for a different component what would delay the mission significantly.
- **SR03** - Failure of the in-orbit assembly will have a *catastrophic* consequence since the mission will not be realized in this case. Furthermore, it is *possible* that this will happen since 4 dockings (3 tanks and the ML need to be attached to the PTV) need to be performed and they are all crucial for the mission success.

Table 13.1: Risk Identification Table

| **Risk Explanation** | **Risk Code** |
|---|---|
| System Risks | |
| Failure of the spacecraft systems and components due to launch vibrations | SR01 |
| Risk of one of the components not being ready | SR02 |
| Failure to perform in-orbit assembly | SR03 |
| Failure of the sensors | SR04 |
| On-board computer failure | SR05 |
| Failure of the control thrusters | SR06 |
| Failure of the CMGs | SR07 |
| Failure to provide enough power | SR08 |
| Failure to properly unfold the communications antenna | SR09 |
| Failure to provide enough food, water or oxygen | SR10 |
| Failing to keep all the systems at an operating temperature | SR11 |
| Failure of the cooling system | SR12 |
| Failure to provide structural integrity | SR13 |
| Failure to detach the ML from the PTV | SR14 |
| Failure to provide sufficient heat shielding during Mars atm. entry | SR15 |
| Failure to deploy the parachute | SR16 |
| Failure to land within the desired envelope | SR17 |
| Failure to provide enough radiation shielding | SR18 |
| Failure of the SuperDraco thrusters during landing | SR19 |
| Mission Risks | |
| Launch failure | MR01 |
| Launch delay | MR02 |
| Experiencing a low solar flux particle event | MR03 |
| Not achieving the right orbit | MR04 |
| Collision with a meteorite | MR05 |

- **SR04** - Since sensors provide information on spacecraft's current orientation this is considered to have a *critical* impact. However, the Sun sensors, IMUs and the Star trackers used for this purpose have been, throughout the spaceflight history, used on many spacecraft (MRO [74], Skylab [25]) and have been verified [40]. Therefore, it is *unlikely* such a failure will happen.
- **SR05** - Failure of the on-board computer will result in *catastrophic* consequences since it would automatically imply errors in other subsystems such as communications or GNC. On the other hand, once again, such computers are *unlikely* to fail since there is enough experience from previous missions.
- **SR06** - Failure of the thrusters implies that the momentum dumping cannot be performed or that orbit cannot be controlled. Although this would be *critical* for the mission and the thrusters are flight tested, it is *possible* that it will happen.

- **SR07** - The CMGs are used to provide attitude control. In case they fail the consequences can be characterized as *critical* since the thrusters can still be used for that, although not as accurate and with a risk of not having enough fuel. However due to the CMGs being a verified product the likelihood is estimated as *unlikely*.
- **SR08** - Solar panels are another proven technology used on this spacecraft. Thus it is *unlikely* the power requirements will no be met. However, the consequences of this risk would be *catastrophic* since they would impede the work of all the other subsystems that require power and the mission would not be successful.
- **SR09** - It is *possible* for this failure to occur, thereby implying that the communication with the ground will be limited. However, since the main objective can still be met the impact is classified as *disruptive*.
- **SR10** - If the required supplies for throughout the trip are miscalculated it is possible, though *unlikely* that a shortage occurs. The impact of such a risk depends on how big this shortage is. However, since all calculations were carefully performed it is assumed that if the shortage does occur it's impacts will only be *disruptive*.
- **SR11** - While probability wise this risk is classified as *unlikely*, impact-wise it is regarded as *critical* since it can cause errors in some temperature sensitive systems within the vehicle (sensors, computers, batteries, etc.) which can then further result in some major issues.
- **SR12** - Failure of the cooling system implies that the fuel will not be stored at the required temperature (80 $K$). This event could result in *catastrophic* consequences such as the tanks exploding. This risk is categorized as *possible* since the cooling system is very complex.
- **SR13** - Many statistical and historical data is available when designing the structure (data from Apollo, ISS, MRO, MSL). However, there is always a possibility of an unexpected event in which the structure would have to account for some additional loadings so it is *possible* that the structural integrity criterion will not be met. In addition to this, if it does happen, the consequences will be *catastrophic*.
- **SR14** - Docking mechanisms are not considered as new technology. However, it is still *possible* that such a mechanism fails, especially considering that at least 4 of such systems will be installed on the PTV. If this does happen, the impact will be *catastrophic* since the ML will not be able to bring the people to Mars and the PTV is not designed to do that.
- **SR15** - One of the major issues during the entry phase in general is the heat dissipation. This is an even bigger problem considering that it is a heavy (6.8 $t$), manned vehicle landing on a planet with very thin atmosphere [114]. This risk is thus considered *likely* to happen, while at the same time implying *catastrophic* consequences.
- **SR16** - The parachute is a critical part of the entry and descent phase. Not managing to deploy the parachute would imply failing to decrease the velocity of the ML which would have a *catastrophic* impact on the mission. However parachutes have been used many times (Apollo, MRO, MSL) and such an event is thus classified as *unlikely*.
- **SR17** - Not landing within the desired range might result in some *critical* consequences, as there is a danger of landing onto a too steep or rocky surface or too far away from the

Mars base. Once again, since such a heavy vehicle (6.8 $t$) has not performed a ballistic entry at Mars before it is *possible* for this event to occur.

- **SR18** - If it happens that the designed radiation shield is not good enough to prevent the acceptable amount of radiation, this could have *disruptive* consequences since one of the main mission aspects is to keep the crew safe. With bad shielding it is possible that the crew starts suffering from health issues such as cancer what does not compromise the mission directly but does imply consequences in the long term. Since no manned mission was ever exposed to such a high radiation for such a long time this risk is *possible*.

- **SR19** - Failure of the SuperDraco thrusters can also have *catastrophic* consequences as they are a crucial part of the landing phase. The SuperDraco has already been tested on ground, but not in the space environment (see Sec. 12.9), so this event is still *possible*.

- **MR01** - This is a risk mainly correlated to the choice of the launcher. Having that the launcher considered for the Mars One mission is the Falcon Heavy, and that there is not much historical data on which the launch success rate can be estimated this risk is *possible* and would imply *catastrophic* consequences as it translates into a mission failure.

- **MR02** - Any delay in the launch window can change the $\Delta V$ required and therefore the amount of fuel to be carried on board as well. However, most of the delays are usually due to unsuitable weather conditions that will be allowed to delay the mission 7 days at most. With a 7 days delay the additional $\Delta V$ that is only 0.07 $km/s$. This risk can thus be considered *minor* for the mission as well as *very likely* since exact future atmospheric conditions are almost impossible to predict.

- **MR03** - Low solar flux particle events (SPE) could result in a very high dose of radiation (at least 5 times as high as in normal conditions) [2],[115]. Although such events do not happen very often, it is *possible* one might occur during the year that it takes to perform the journey. However, while the probability of this happening is not very high, the impact can be *critical* since an efficient shielding against such an event requires detailed research. Otherwise the people would suffer from health issues such as cancer or skin diseases.

- **MR04** - If the correct orbit is not achieved the whole mission is endangered and the consequences can be *catastrophic*. This can happen due to inaccurate assumptions made during the trajectory calculation and orbit determination. Since this is another mission aspect in which there is a lot of experience and available historical data it is classified as *possible*.

- **MR05** - This is an unpredictable event that is *possible* to happen since the spacecraft might not be able to react quickly enough to avoid the body in time. The impact of this collision would be *catastrophic*.

To summarize the final classification Fig. 13.1 is shown to indicate all the risks and their importance. This risk map is also used to identify the most critical risks. These risks can be seen on the map as the ones placed in the upper right corner with a *likely* or *very likely* likelihood and a *critical* or *catastrophic* impact.

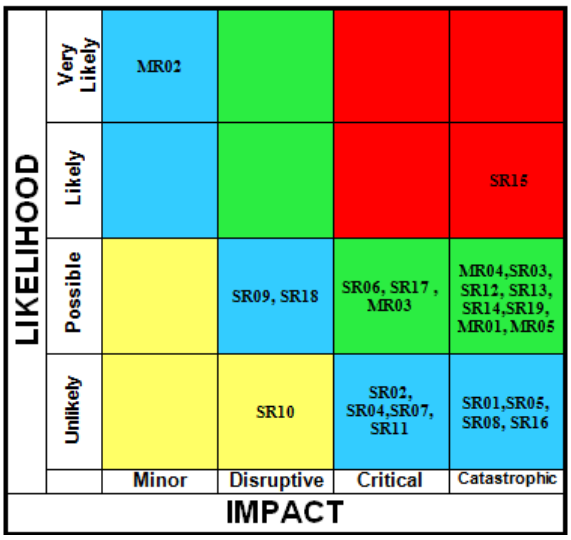


Figure 13.1: Pre-mitigation Risk Map

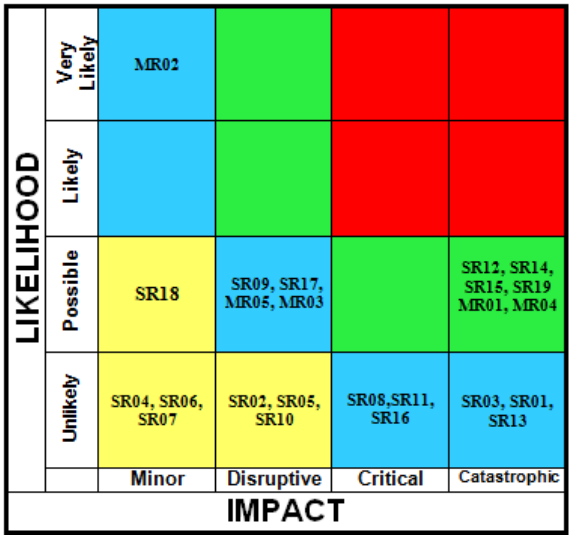


Figure 13.2: Post-mitigation Risk Map

## 13.2 Risk mitigation

Having identified all the risks, several methods were used to account for these in the design and mitigate the consequences. The methods used to perform this are first explained in this section and the mitigated risks are then once again mapped to demonstrate how this technique made the final design more reliable. Risks are mitigated by decreasing the severity of the impact and/or the probability of the impact occurring.

### Mitigation Methods

- **Safety margins** - Unpredictable circumstances can be accounted for by designing with a safety factor. In most of the cases throughout the report some contingencies were used depending on how critical the subsystem is. This method of mitigation usually works by decreasing the likelihood of the risk occurring. The following risks were mitigated with this method:
  -SR06 with 10% safety margin for the force for which the thrusters are sized;
  -SR08 with 20% margin for the array area calculation;
  -SR10 with 30% additional life supplies;
  -SR13 with varying safety margins depending on the load in question (as explained in Ch. 7);
  -SR15 with 20% safety margin for the thickness of the heat shield.

- **Redundancy** - Redundant items were often used throughout the design process in order to account for failures of different components. In this case if a certain component failed a back up is available. This principle decreases the severity of a certain risk by providing back up. It was used to mitigate the following risks:
  -SR03 - additional docking ports will be added and the possibility of having a space tug that performs the assembly will be investigated
  -SR04 - all the sensors have a redundant component;
  -SR05 - an additional back up computer will be present;
  -SR06- an additional pair of thrusters is placed per axis;
  -SR07 - one additional CMG is added to the subsystem;

-SR03 - some emergency propellant is included to maneuver away if failure is about to happen.
-MR03 - special material is applied to the crew quarters decreasing the SPE caused radiation by 78 % (see Ch. 6) -MR05 - an additional structural plate was added to the structure in order to account for any collisions that might happen throughout the transfer phase.

- **Contingency** - Developing contingency plans in case of an alternative outcome is another way of decreasing the severity of certain scenarios happening. One can investigate other aspects of the mission that are still considered risky (more likely to fail) and proceed with creating plans that are to be executed in case of a certain risk occurring. One such example is the SR02 risk. If the component is not yet verified and flight tested by the launch date, the consequences can be mitigated by having a plan that accounts for this happening and defines the exact steps to be taken in such and event. This way the issue is more easily and quickly solved so the consequences can be less severe. Other risks for which this is particularly useful are: SR16, SR17 and MR04. These contingency plans will be discussed later in Sec. 13.3.

Some of the risks from the Tab. 13.1 are not mentioned in the mitigation methods above. This is since these risks either cannot be mitigated as they are very unpredictable and there is nothing that directly can be done in order to decrease the impact severity of such risks. These risks are MR01 and MR02.

Finally, certain risks (SR01, SR09, SR11, SR12, SR14, SR19) are identified were not dealt with in this conceptual design phase. While it is possible to verify the performance of all the subsystems (related to these risks) by doing tests, these tests should be determined and follow a certain procedure. This is why these risks are pointed out in the recommendation section in order to be accounted for in the later design phases.

## 13.3 Contingency Analysis

As mentioned previously, it is important to develop contingency plans in order to decrease the impact of certain risks.

**One of the components is not yet ready** is one of the possible scenarios. All the spacecraft components are interdependent and the number and the sequence of the in-orbit assembly for example depends on the size of different parts.Thus in case something is not ready many changes need to be implemented on the design. In order to avoid canceling the mission or missing the launch window completely periodic checks on how far all of the components are developed need to be made. If up until a certain point in the design process the certain component is still not available it is good to make an alternative configuration complying to a different part that satisfies the mission requirements. Optimally this part will have similar characteristics so that the not many changes need to be made for the alternative design.

**Not achieving the right orbit** is another risk whose consequences can be mitigated using a contingency plan. This event is most likely to occur if the engine for some reason does not provide the desired $\Delta V$ or if the right timing to perform maneuver was missed. In both cases there might be a possibility of still getting into the right orbit at the cost of more fuel spent. Whether this is possible will have to be quickly inspected. The idea is then to use the GNCS

(that is the DSN software) and recalculate the trajectory. With this information the additional amount of propellant can be determined and it can be concluded whether such a maneuver will still make the mission possible. In order to enable this contingency plan additional propellant will need to be carried to allow for an extra $\Delta V$. This propellant can be launched within the third tank that still allows for additional propellant.

**Failure to deploy the parachute** is most likely going to result in catastrophic consequences. However, it might be possible to develop a plan that includes firing the thrusters earlier to decrease the speed rather than using the parachute for that purpose. This suggestion needs to be verified and additional fuel might need to be carried on board but considering how severe the impact of such a failure can be, this is a relevant point in designing for reliability.

**Failure to land within the desired envelope** can have different impacts on the mission depending on where exactly the ML has landed. In case it lands on a very steep surface the consequences can be catastrophic. Even if out of bounds of the envelope, however, the ML can still land on a favorable surface. In this case there is a question on how to perform the base integration if the ML lands too far. If it is not possible to transport the ML over such a big distance a plan of action should be determined so the crew know how to deal with such situation. What could be done in this case is that the crew abandons the lander as fast as possible and navigates towards a certain location from where the rover can provide transportation to the base, life supplies and radiation shelter. This way although the ML is not integrated with the base, the crew can continue the Mars colonization as long as they follow the established plan. This represents just a basic idea of the plan and more details on how exactly the people would navigate on the surface of Mars and how to shield from potential storms and radiation need to be specified in the further design.

## 13.4 Conclusion and Recommendations

This chapter showed how the major system and mission risks were identified and classified. Different methods of mitigating some of these risks were also identified. On the other hand other risks were not yet dealt with and need to be reconsidered and accounted for in the following design phases. Furthermore, only major risks were identified. In order to have a complete overview of the system reliability and the most critical design areas it is recommended to examine all the systems in more detail and identify other possible risks. Although impact-wise they might be minor, if the frequency turns out to be high enough to cause mission failure these risks need to be dealt with using a risk mitigation method.

Finally, as previously mentioned, the contingency plans only contain the basic objective. A precise plan needs to be specified in order to determine how and in what order the necessary steps need to be performed, so as to decrease the severity of the risks as much as possible.

# 14 | Operations and Logistics

## 14.1 Operations and logistics

The operations and the logistics are an important part of the Mars One mission and will be elaborated in more detail in this section. An overview of all the required operations and logistics during the Mars One is given in a flow diagram in Fig.14.1. Only the operations which were not discussed earlier and will not be discussed in further sections, will be explained in this section.

The manufacturing, assembly and integration phase will be explained in the production plan section (see section 18.1). The transportation of the entire vehicle to the launchpad will also be discussed in that section. In Fig. 14.1 it can also been seen that the propellant tanks, PTV, ML and the launcher should be brought to the Vehicle Assembly Building (VAB). This is the building which provides space and tools to assemble all the main systems such as the PTV, ML and tanks to the Falcon Heavy. This building will be located close to the launch platform. If the Falcon Heavy will be launched at the Kennedy Space Center, the VAB of the NASA can be used.

The crew needs to be prepared and trained for the mission. The crew should be able to withstand the high g-loads during the launch phase and the landing phase, the should also be able to command and handle the PTV and the ML and finally they should know how to build up the Mars base. The training of the crew will be done by the Mars One foundation [116].

The operations and logistics of the Mars One mission should also contain a ground control center to provide communication with ML, PTV and the crew. The ground control should also keep track of all the parameters measured by the spacecraft, for example check if the pressure inside the crew cabin does not decrease. The Mission Control Center (MCC-H) in Houston was been used as ground control for the Space Shuttle missions and will probably also been used for the Constellation program. It would beneficial towards the cost if the Mars One mission can use the NASA MCC-H or another already existing ground control building, otherwise a new ground control center should be built. In between transports, a private base will be required to maintain contact with the Mars base 24/7. As mentioned earlier in the communication subsystem chapter (see 9) the maximum data rate received from one PTV will be equal to 81 $Mbit/s$. So at the end of the complete mission with three PTVs in orbit, the data rate will be equal to 243 $Mbit/s$. The ground control should be able to process all these data.

A more detailed explanation of the launch operations and the launch schedule can be read in section 14.4. In section 14.5 some more detailed discussion of the assembly phase and its operations can be found.

## 14.2 Hardware

The spacecraft contains multiple systems cooperating to bring the astronauts safely to Mars. These systems are summarized in Fig. 14.2 for the PTV, and Fig. 14.3 for the ML. Essentially all the hardware systems work together through the main computer. This computer contains all flight and control data required for the mission.

## 14.3 Software

In the spacecraft, computer systems are required to operate the hardware, perform tasks for the crew and assist the crew in their tasks. The main software systems are displayed in Fig. 14.4, where they are categorized by the main hardware they are involved with.

## 14.4 Launch Schedule

SpaceX, the company behind the Falcon Heavy launcher used in this mission, plans to perform up to twelve launches per year [117], giving an average time of one month per launch. Considering that SpaceX technology will be used, a similar amount of time will be required for the preparation of each launch. The reason for the long time between launches is primarily due to the extensive testing required before each launch and the size of the rocket, which necessitates the careful assembly and transportation of all the rocket components.

For the case of the launch window in 2026, five launches will be required to bring the different mission components into LEO for in-orbit assembly. Therefore, a plan for the launch schedule of the different parts is required, as they cannot be launched simultaneously. The first Falcon Heavy launch will carry the PTV living module and propulsion system into the assembly orbit. The second, third and fourth launches will each take fuel tanks into LEO for assembly. The fourth and final launch will also include the ML containing the crew, ahead of the final phase of the in-orbit assembly of the PTV described in more detail in Sec. 14.5.

In order to take advantage of the minimum energy transfer launch window, the PTV must depart LEO on the 11th of October 2026 as shown in Tab. 4.3. In order to meet this deadline, the process of launching all the components into LEO must be started well in advance of the required departure date. Assuming a required time of one month per launch and a further two weeks for the final assembly and testing prior to departure, the first rocket needs to be launched by the 27th of May 2026. Subsequent rockets will be launched after the first one in a monthly interval. The procedure involved with each rocket launch can be seen in Fig. 14.1.

## 14.5 In-Orbit Assembly and Integration

The launch sequence has been designed to maximize the safety of the astronauts and ease of assembly. The first Falcon Heavy launch carries the fully stocked up PTV living module. After arrival in the assembly orbit the solar panels are deployed. In LEO one solar panel is sufficient for the assembly phase, so the two closest to the active modules will remain folded to minimize risk. A detailed description of the power subsystem can be found in Ch. 11.

The following two Falcon Heavy launches carry fuel tanks which will move toward and assemble with the previously launched PTV main module. Lastly, the astronauts and the ML are launched together with the final fuel tank. Launching the astronauts last has the advantages of lowering the time of the astronauts waiting in space and finishing the risky assembly maneuvers without endangering the astronauts.

After docking with the lander all systems are checked and after it has been decided that the mission is safe to continue, first burn is initiated. Solar panels were designed to survive this maneuver.

### 14.5.1 Rendezvous

The PTV is the first module to be inserted into orbit. Once the orbit is correct, the module only needs to maintain this orbit, other modules will actively perform the rendezvous. For this phase a space tug was considered to maneuver the modules into position. However, the modules would still require active spin control, so no large benefit is gained here. Also, the cost of developing and launching a space tug is estimated to be between €350 million and €500 million [118].

Instead, ADCS systems are attached to every module. Small thrusters are used to apply a $\Delta V$ to move the module towards the PTV. The Falcon Heavy launcher can bring the payload to an orbit which will be slightly different from the planned orbit. That is, the apogee from the real orbit may deviate from the apogee of the planned orbit by 10 $km$ and the perigee from the real orbit may deviate from the perigee of the planned orbit by 10 $km$ [42]. From the Vis Viva equation, Eq. 14.1 can be derived. This equation yields a $\Delta V$ of 20 $m/s$ that is needed to maneuver between the two points.

$$\Delta V = \sqrt{\mu_{earth}(\frac{2}{r} - \frac{1}{a-10})} - \sqrt{\mu_{earth}(\frac{2}{r} - \frac{1}{a+10})} \tag{14.1}$$

With Tsiolkovsky's rocket equation the required propellant mass for this maneuver can be calculated, using a specific impulse of 240 $s$ gives a propellant mass of 259 $kg$ per module. A 20 $kg$ battery containing 2 $kWh$ of energy will be sufficient to operate all ADCS equipment and a small communication system for communication with the spacecraft.

### 14.5.2 Docking

Two types of docking ports will be implemented; one docking port connecting the PTV and the ML, and three ports connecting the propellant tanks to the PTV.

#### PTV-ML connection

The docking port will connect the Mars Lander to the PTV. The ML is the last module to connect to the PTV, and also the most important since the astronauts come with the ML. The docking port needs to be big enough to fit an astronaut in a space suit since the astronauts have to be able to transit from the ML to the main module of the PTV through a hatch. Also it needs to transfer electrical power and data. Finally, the hatch needs to be closed for the separation maneuver performed after arrival in Mars orbit.

A good choice for a docking mechanism is the NASA Docking System (NDS), displayed in Fig. 14.5. NASA has been developing this system, also named 'Low Impact Docking System',

since 1996, to simplify operations and reduce risks [119]. Benefits of this system include flexible mission implementation, system level redundancy, reduced mission and life cycle cost.

### PTV-tank connection

The second connection connects the propellant tanks to the PTV. This connection has to accommodate the transfer of propellant and electrical power. (Similar to Space Shuttle docking port, see Fig. 14.6b, but modified and simplified such that no human hands will be required to assemble.) Also, struts will have to be added to secure structural integrity. These struts (Again, similar to Space Shuttle struts, see Fig. 14.6a) can be mechanical hooks that fold from the PTV, and connect to the propellant tanks after the first connection is made. This kind of connection has not been assembled in-orbit before.

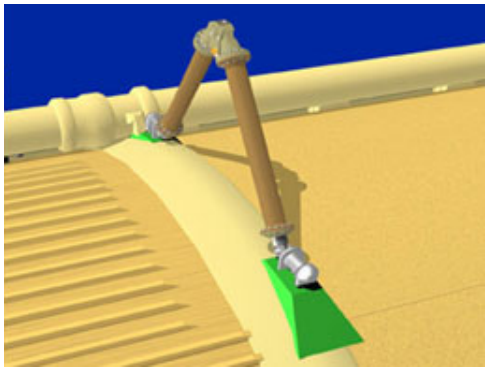

(a) Space Shuttle tank docking strut [120]

(b) Space Shuttle tank docking port

Figure 14.6: Space Shuttle docking mechanisms[121]

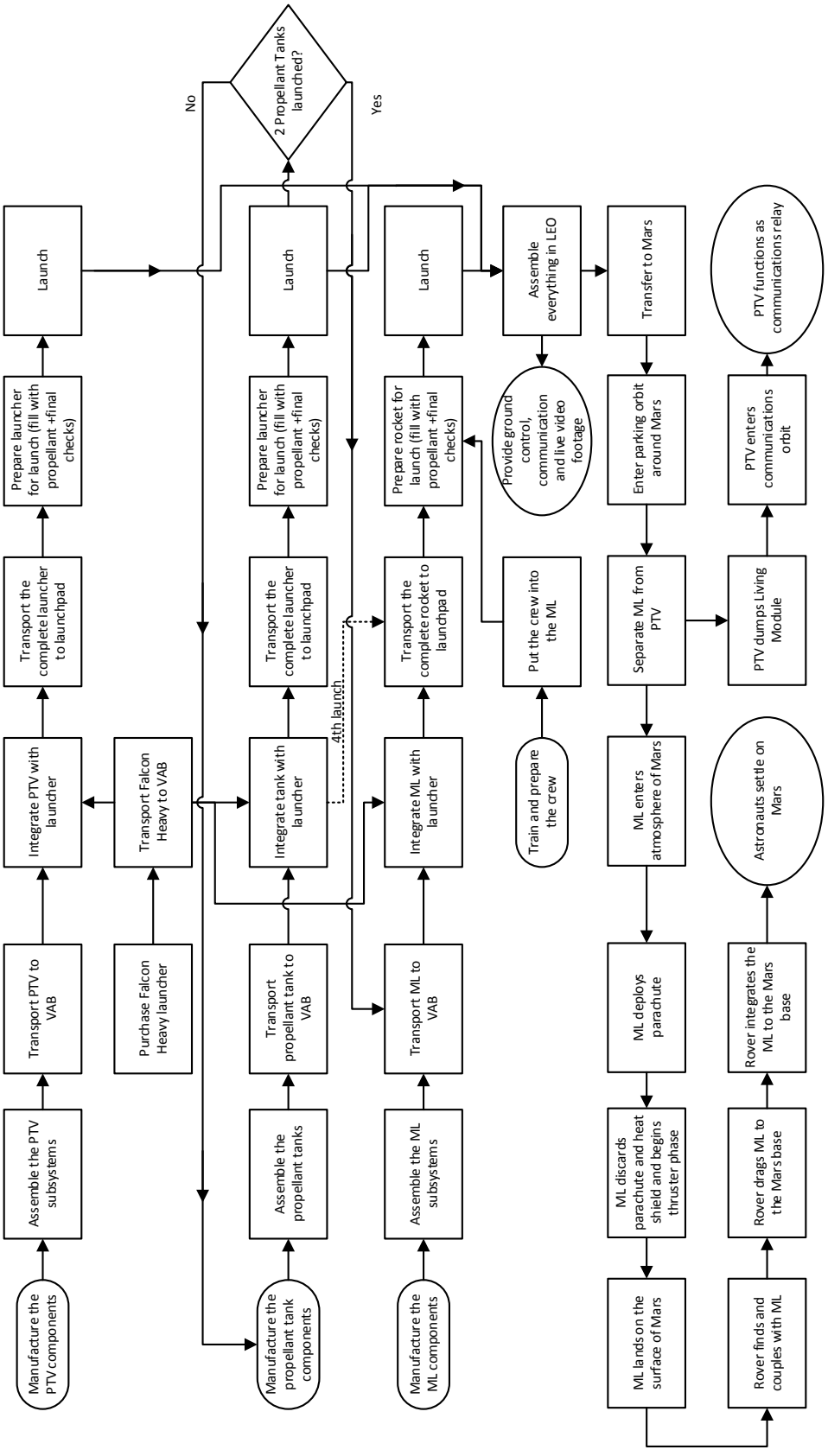


Figure 14.1: Flow diagram of the operations and logistics

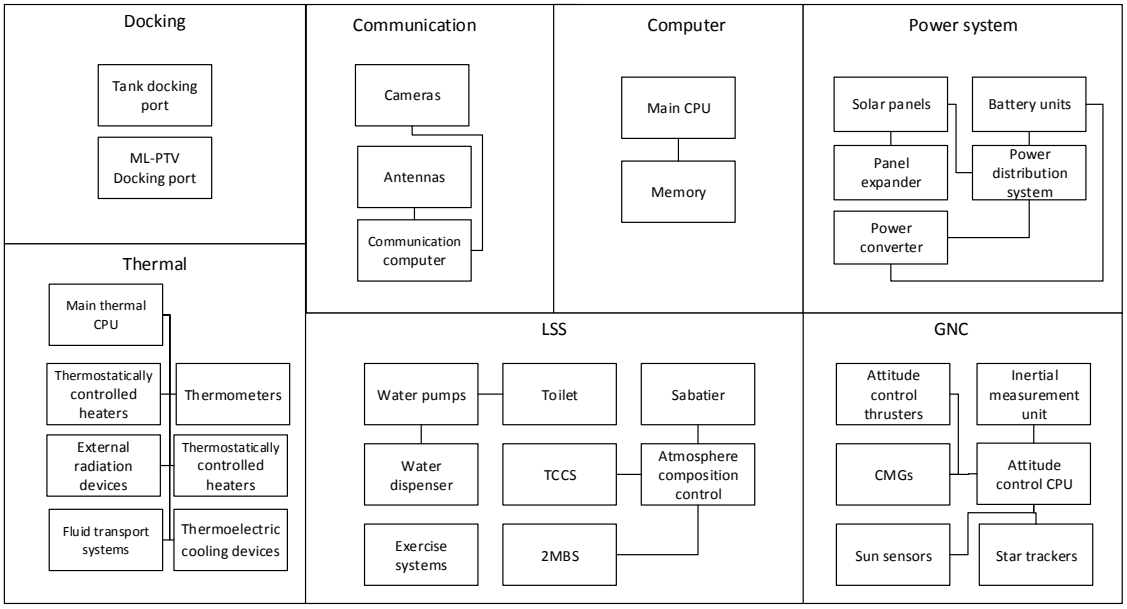


Figure 14.2: PTV hardware diagram

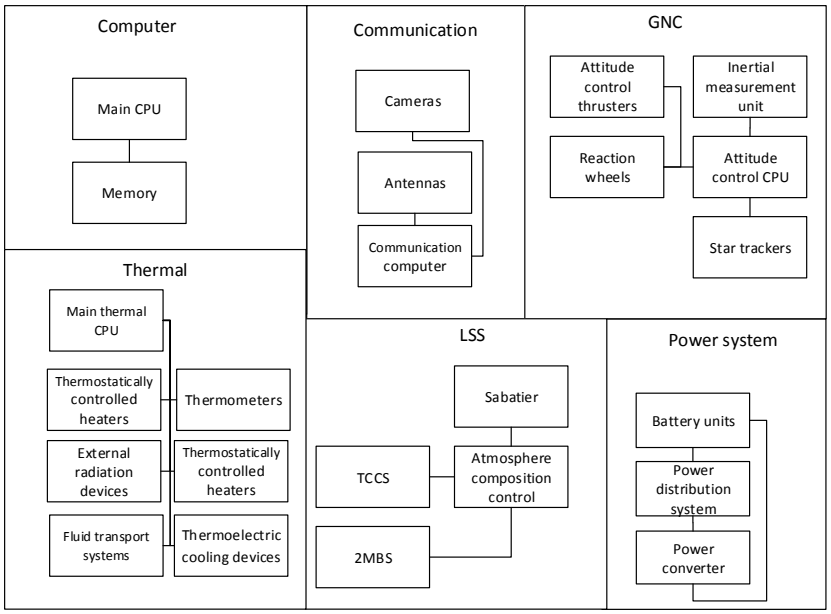


Figure 14.3: ML hardware diagram

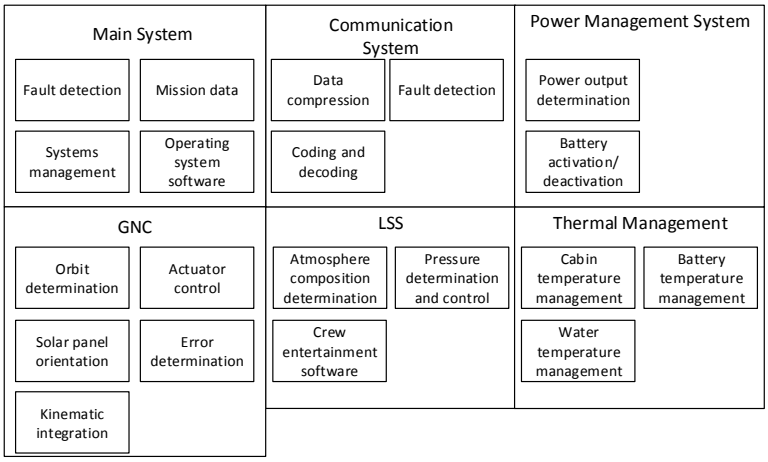


Figure 14.4: Software diagram

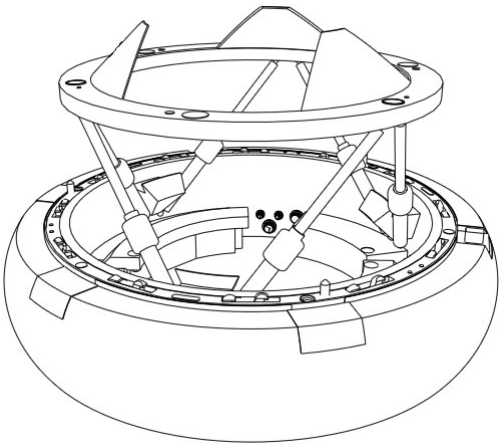

Figure 14.5: NASA Docking System

# 15 | Sustainability Approach

In this chapter the approach of the design with respect to sustainable development will be discussed. Before this can be described, it is desirable to take a look at the definition of sustainable development. Sustainable development is defined as "a development that meets the needs of the present without compromising the ability of future generations to meet their needs" [122]. One could argue whether it is sustainable to bring people to Mars, but the design of the mission proposed in this report contains several sustainable aspects.

The trajectory and departure date were optimized with respect to a minimal $\Delta V$, so a minimal of propellant. In this way the exhaust gases, the total mass and the number of launches is minimized. This makes it fuel efficient. Another sustainable aspect of the Mars One mission is that the PTV and ML will have multiple functions and still can be used after transporting the crew to the Martian surface. The PTV will stay in orbit around Mars and will be reused as a communication satellite to allow good communication between the Mars base and the ground station on Earth. The complete ML, except for the discarded heat shield and the parachute, will be used as part of the base for at least 20 years. In this way less material or base modules need to be produced and transported to the Martian surface.

All the subsystems were designed with a focus on maintaining the standard of the sustainable development. Solar panels that only need the free energy of the sun are used as a power source and no nuclear power sources are used in the PTV or ML. Another example is the the life support subsystem which recycles the $CO_2$ in the cabin into $O_2$ which can be breathed by the crew.

The detailed design of the Mars base is not a part of this report. However, this mission opens up the possibility of building a Mars base, so it is worth mentioning that the base which will be built is sustainable. The goal is to have a self-sustainable base that can function without supply missions, and therefore will produce as little waste as possible. [123]. This self-sustainable base can also be used as an educational example to show the rest of the world how a small number of people can live together in a sustainable way.

The scientific community has speculated about the possibility of the survival of bacteria and other micro-organisms in the Martian atmosphere. In order to be sustainable the risk of contamination of the Mars environment should be avoided. Clean room facilities must be used to make the ML and PTV sterile before they come into contact with the Martian atmosphere (see 18.1). One of the requirements, set to save costs, is to use as much off-the-shelf hardware and technology as possible. This requirement can improve the sustainability of the project as less resources need to be spent on the development and production of new parts. These new parts will likely be developed and produced more inefficiently than existing ones.

# 16 | Cost and Market Analysis

It is clear from the extreme magnitude and complexity of the Mars One project that an accurate cost estimation is crucial to avoid project funding overrun and schedule delays. However, since this project is also first-of-its-kind, it becomes increasingly difficult to estimate the costs involved. The main reason for this difficulty is the lack of directly applicable historical cost data, which is used heavily for ordinary missions but is nonexistent for pioneering missions such as Mars One. Considering these limitations, this chapter aims to present the most relevant cost estimation methods and historical data, which can give a first order cost estimate. This first order estimate is considered to be very important as it helps on limiting the mission cost in later design stages by making the cost itself a driving design variable. Additionally, in order to asses the financing possibilities of the project, a market analysis is presented afterwards.

## 16.1 Parametric Cost Estimation

For the cost estimating purposes of this mission, the **Parametric** cost estimating method will be used, as it is most suited for the Phase A design stage and provides good estimates using Cost Estimating Relationships (CER's) based on relevant historical cost data.

### Main Cost Drivers

**Mass** is traditionally a standard cost driver in the aerospace industry. It is an insightful cost driver because it usually describes the size and often the performance of a component. Furthermore, because mass is a key engineering parameter in design, a mass estimate is usually available early in the design process.

**Quantity** of units produced can influence the cost in many ways. The simplest relationship is one applicable to small quantities and assumes that the average cost is the same regardless of production quantity. On the other hand, in case of higher production quantities, a more complex relationship can be introduced which takes into account learning curve effects. Since the proposed Mars One mission design is currently planned as a Mars transportation system for three transfers, the quantity relationships will consider three units produced.

## 16.2 TRANSCOST Model

The specific parametric cost estimating method that will be used is the TRANSCOST method developed by TransCostSystems [124], which is based on CER's developed from historical data. The CER's can be used to calculate a cost estimate for individual mission segments. Furthermore, as mass is one of the main input parameters for the CER's, the transcost system specifies certain mass margins to use depending on the inheritance-development level of the design. As

this is considered to be a first-of-its-kind mission, a mass margin of 15% is introduced for the current Phase A level design.

### 16.2.1 Man-Year (MYr) Cost Definition

The TRANSCOST model [124] introduces the Man-Year (MYr) effort as a costing value in order to make use of the costs of projects performed in different countries in different time periods, with different currencies, different inflation rates and different conversion rates to the US Dollar. All the CER's of the TRANSCOST cost estimating method express the costs in terms of MYr (symbol H is the effort expressed in MYr in the CERs) and therefore they need to be translated to actual monetary value, of the aerospace industry and currency under consideration. Therefore, european MYr values will be used along with the euro as relevant currency. To obtain the relevant conversion factor, historical data from [124] (Fig. 16.1) is considered, which gives the MYr value of the european aerospace industry from 1960 to 2002. From that data the MYr value of 2013 is extrapolated and used to convert to euros all the MYr estimates from the TRANSCOST method.

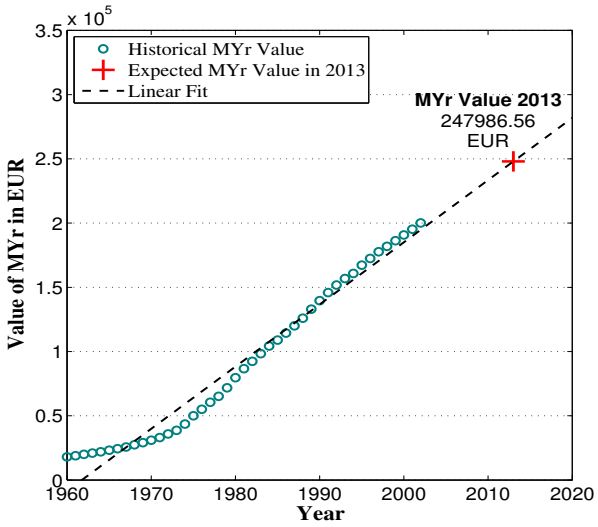


Figure 16.1: MYr value history for the European aerospace industry

### 16.2.2 Development Costs or Non-recurring Cost (NRC)

The development or non-recurring costs includes all activities from detailed design to hardware implementation and verification, when all test models are built, including prototype and protoflight units. The cost estimation methods include the mass of the respective system (M) as the main input. However, they must be supported by three estimated technical development cost factors $f_1, f_2, f_3$ in order to produce accurate results. A more detailed explanation of the factors can be found in [124]; for this mission they are:

- $f_1$ - Development Standard Factor
- $f_2$ - Technical Quality Factor
- $f_3$ - Team Experience Factor

#### Liquid Propellant Engines with Turbo-pumps

For the development of the turbo pump liquid propellant engine used for the PTV propulsion the TRANSCOST method proposed the following CER which gives the MYr effort:

$$H_{EL} = 145 \cdot M^{0.565} \cdot f_1 \cdot f_2 \cdot f_3 \tag{16.1}$$

$f_1$=1 - State of the art, verified technology and components
$f_2$=0.8 - Low level of qualification and development factors
$f_3$=0.8 - Team has performed similar projects

#### Crewed Space Systems

This TRANSCOST CER presented in Eq. 16.2, which is used to estimate the PTV cost, is of preliminary nature and is applicable to a range of manned space systems such as:

- Inter-orbital Space Vehicles with crew cabin
- Crew transfer and maintenance vehicles
- Lunar lander systems
- Space station systems

$$H_{VS} = 1220 \cdot M^{0.37} \cdot f_1 \cdot f_3 \tag{16.2}$$

$f_1$=1 - State of the art, verified technology and components
$f_3$=0.8 - Team has performed similar projects

#### Crewed Ballistic Re-entry Capsules

For the cost estimation of the ML the following CER used for ballistic re-entry capsules is used as it is directly applicable to the Mars One ML system.

$$H_{VC} = 275 \cdot M^{0.48} \cdot f_1 \cdot f_2 \cdot f_3 \tag{16.3}$$

$f_1$= 1 .2- New design with some new technology, components and materials
$f_2 = (N \cdot T_M)^{0.15}$ - Where N is the crew number and $T_M$ is the maximum mission design lifetime
$f_3 = 1.1$ - Partially new project activities for the team

### 16.2.3 Unit Production Costs or Recurring Costs (VRC)

VRC costs are recurring cost types, which occur during production of every unit. They typically decrease over time due to the learning curve effect. In the following CERs the parameter $f_4$ represents the learning curve factor and $n$ represents the number of units produced.

#### Engines with Cryogenic storable propellants

$$F_{EL} = 3 \cdot n \cdot M^{0.535} \cdot f_4 \tag{16.4}$$

Where $f_4 = 0.9$ and $n = 3$.

#### Crewed Space Systems

This production cost estimation includes the cost of all crewed components of the spacecraft. i.e. both the ML and the PTV.

$$F_{VS} = 0.16 \cdot n \cdot M^{0.98} \cdot f_4 \tag{16.5}$$

where $f_4 = 1$ and $n = 3$

### 16.2.4 Ground Segment and Operations Cost

Since this Mars mission is considered to be a long-term highly complex and high-risk manned mission, ground segment and operations costs are expected to reach significant amounts. The TRANSCOST method offers an estimating method which covers vehicles such as the Shuttle Orbiter, the European HERMES Project and the Japanese HOPE vehicle.

#### Crewed Vehicle Operations cost

It is clear that crewed vehicle operations are usually much higher than of unmanned vehicles. The costs do not include only in-robot activities, which depend on the crew number and the mission time in orbit but also on the cost of the crew staff itself, its ground support and training. Consequently, the operations costs, with $f_4 = 0.9$ follow from:

$$C_{ma} = 75 \cdot T_m^{0.5} \cdot N_a^{0.5} \cdot L^{-0.8} \cdot f_4 \tag{16.6}$$

Where:
$T_m$ - Mission duration in orbit (days)
$L$ - Launch rate per year
$N_a$ - number of crew members

### 16.2.5 Cost overview conclusions and recommendations

The project segment costs for 3 Earth-Mars transfers over a period of 10 years that have been calculated using the TRANSCOST method can be seen in Tab. 16.1, whereas Fig. 16.2 visualizes the relative cost distribution.

Table 16.1: Overview of mission segment costs in Billions €

| Mission Segment | Cost |
|---|---|
| Launch | 1.44 |
| Development | 14.56 |
| Production | 0.94 |
| Operations | 1.16 |
| Reserve | 5.43 |
| **Total** | **23.55** |

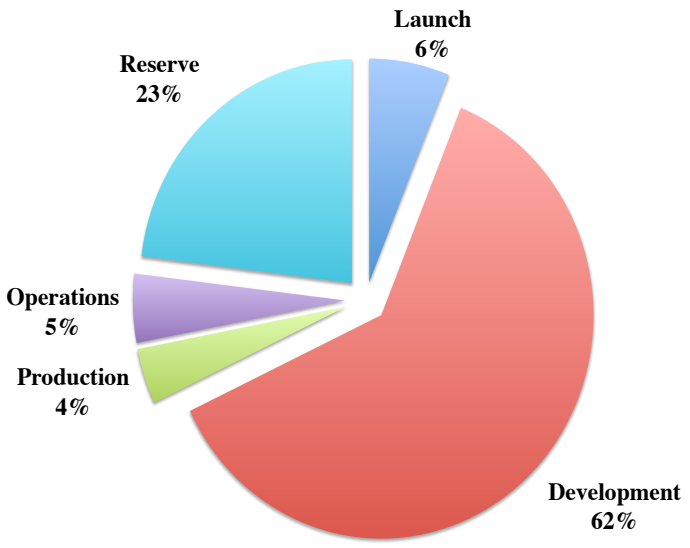


Figure 16.2: Overview of project segment relative costs

**Launch** The launch costs calculations are based on the use of the SpaceX Falcon Heavy launcher, for which SpaceX estimates a launch cost of 125 M$ (conservative estimate).

**Development** It is clear from the table that development costs constitute the largest cost of the project and is thus identified as a critical mission segment where cost reduction methods should be applied. Possibly by using off-the-shelf technology (e.g., Red Dragon by SpaceX) and adapting it to the mission needs.

**Operations** Operations cost for a crewed mission are traditionally much higher than unmanned mission, as mentioned previously. However, by excluding any complex experiments on board and possible secondary missions, the operations costs could be kept to a minimum.

## 16.3 Market Analysis

The Mars One project is unique, requiring a unique funding method. As shown in the previous section, €23.55 billion will need to be generated for the mission to be feasible. This section will consider some of the possible sources of income that need to be secured in order to meet the costs of the project.

### 16.3.1 Mars One for Investors

The first step in finding investors is an analysis of the project itself; what can Mars One offer to investors?

**Scientific research** The astronauts could perform research requested by both scientific and commercial institutions and sell the results. This would require scientific equipment to be brought as additional payload. In a later phase, there may even be a possibility to send samples back to Earth. NASA spent $2.5 billion on the Mars Science Laboratory [125], a machine designed to analyze rocks and do radiation and atmospheric measurements. The additional cost of carrying out these tests would be considerably less for Mars One. However, space agencies would not always be eager to delegate their scientific research as they also place a high value on the technological innovation that comes from developing missions like the MSL.

**Video footage** This footage, which will be recorded 24 hours a day on board the PTV, ML and Mars base, and the rights to publish the footage can be sold to external companies. If the Mars One initiative becomes very popular this could provide a large stream of income as, for example, FIFA earned $4 billion from tv rights for the 2010 World Cup in South Africa [126].

**A ticket to Mars** Interested individuals have, in the past paid up to $20 million for a short stay in the International Space Station[127], so there could be people willing to pay large sums for the opportunity to be among the first humans to set foot on Mars. However, the idea of a one-way trip to Mars will be harder to sell and the selling of a space ticket would also put severe restrictions on the selection of the astronauts, considering that the personalities of the astronauts and customers need to be compatible.

**Advertisements** Any advertisement placed on the PTV or ML will be permanent and will be shown every time a camera records it. If the mission is successful, it can be expected that a significant fraction of the world population will see some of the footage. The advertisements can thus be sold for a lot of money. Big companies are eager to spend money on marketing. For example, a thirty second commercial in the Super Bowl costs $3.8 million [128].

**Personal promotion** High net worth individuals are always looking for new ways to boost their image and take pleasure in spending large amounts of money to show off their wealth. Activities include supporting a soccer club [129] or writing one's name on a two mile piece of land [130]. Mars One offers a unique opportunity for someone to make a name for themselves. People can be approached for this and, depending on their wishes, additional materials may need to be included in the payload.

### 16.3.2 Investors for Mars One

Secondly, what can investors offer to Mars One?

**Financial backing** Financial backing will provide the main income necessary for funding the program. These resource gives Mars One full control over how it is spent, increasing the flexibility of the project.

**Materials** The providing of materials for the design can significantly reduce cost and design time. This category also includes computer systems, sensors and other on-board equipment.

**Services** Companies can provide services or give discounts for services that will greatly reduce the costs of production, operation, etc. Services will mainly be obtained through maintaining relations with the stakeholders.

### 16.3.3 Supporters

Next, a short overview of the potential supporters of the initiative is given.

**Governments** NASA annually receives $17.7 billion [131] from the U.S. government, whereas ESA gets €3.99 billion from multiple connected countries [132]. Governments can be approached for contributions, but they cannot be counted on since their existing contributions are already under threat. They may also try to influence how the project is operated and executed.

**Space agencies** Mars One will probably have to give space agencies access to all the data and results that are obtained in order to receive support from then. They may also place restrictions or want to have an influence on the project. A logical requirement would be that Mars One has to perform some research for them.

**Scientific institutions** There are many scientific institutions that would be very interested in Mars One, although not many will have the funds to give significant backing. They can be approached for research that they would want done during the mission.

**Companies** Companies may want to advertise in and around the PTV and Mars base. For example, in 2000 Pizza Hut paid $2.5 million to display their logo on a Russian Proton rocket during launch [133].

**Consumers** People with interest in the mission will have to be approached through the entertainment branch. They will be the target group for which companies want to advertise. If advertisement and publicity become a main source of income, this will require a large consumer base. The project will need publicity and, therefore, marketing of Mars One will be needed for it to become widely known.

**Billionaires** There are many billionaires with a large disposable income. If they like the project, or see use in it, they can be a valuable contributor.

**The Mars Initiative** A public funding programme with the sole intention of funding a manned Mars mission [134], the Mars Initiative will award a prize to the first group to set humans on Mars. In 2012 they gathered $2000, which is not sufficient to make a big impact on the Mars One program. If the Mars Iinitiative grows in size, it could be a useful organization.

### 16.3.4 Competition

Mars One is not the only group seeking to transport people to Mars. Both NASA, ESA and the Russian Space Agency have shown interest in a manned mission to Mars. ESA started the Aurora program, a program aiming at getting a manned Mars mission done in 2033, although it is possible that it will only be a robotic mission. NASA and SpaceX are collaborating on their Red Dragon mission. They are planning to launch this unmanned mission, using a Falcon Heavy launcher and Dragon capsule in 2018, as a preparation for a manned mission [86]. In the long run, China is perparing a manned Mars mission for 2040-2060 .

Multiple alternative proposals have been done, but no other manned Mars landing missions are currently in any serious stage of development. With an eye on funding and publicity, it is vitally important that Mars One is the first to put humans on Mars.

# 17 | Final Design Overview & Conclusions

This chapter aims to present to the reader the final design and the most relevant conclusions, which have been gathered throughout the development of this feasibility study of the Mars One mission. This report concludes the Phase A level design of the transportation function of this mission. Therefore, it is intended that the knowledge obtained and the observations made in this text be used in Phase B and consecutive design phases.

**Challenges** Designing a crewed mission to Mars still proves to be an extremely difficult feat of engineering and would require an immense effort in terms of funding, research and development, production, operations and logistics. The main challenges being the cost and astronaut safety, the Mars One initiative proposes to solve this problem by making the first crewed mission a one-way mission. It is clear from the performed analyses of this text that this approach indeed offers significant advantages in terms of reduced mission cost and complexity. On the other hand, it introduces moral and legal issues which are outside the scope of this technical feasibility study. Consequently, this text shows that the challenges to perform this mission are significant, but not insurmountable.

**Assumptions** A multitude of assumptions were made throughout this report to facilitate the analysis. Most have been verified and validated and are considered valid according to theory. On the other hand, since this is a first-of-its-kind mission, a number of assumptions remain to be proven. This includes assumptions such as that there is no pressing psychological or health issue for the crew to stay in a confined spacecraft during the long transfer time. Or that there are no significant long-term health issues for the crew which will spend their entire life on Mars. The validity of these and other assumptions will need to be researched and validated in the next design steps, and consequently it will be shown whether the design needs to be updated.

## 17.1 Final Design Configuration

As all subsystems have been developed individually, the spacecraft's configuration can be presented in its final version, with all the subsystems integrated and representative of the flight configuration. A sketch of the final design is shown in Fig. 17.1a and Fig. 17.1b, with it's relevant dimensions in millimetres.

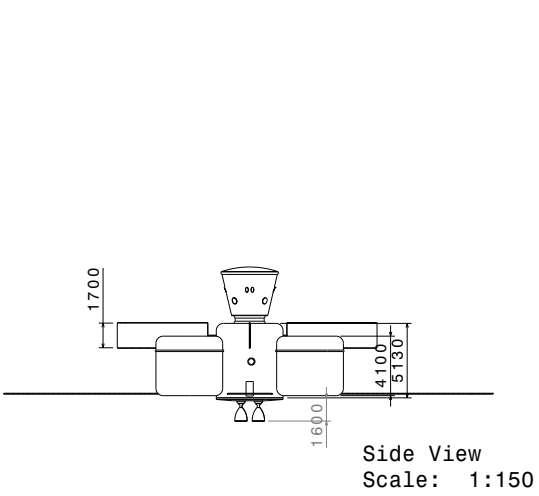


(a) Side view of the PTV & ML assembly

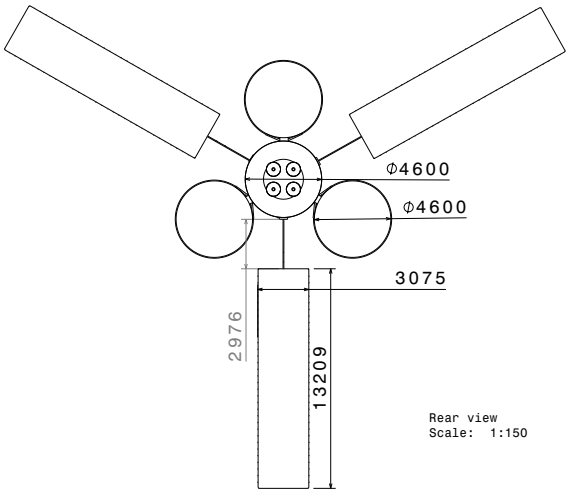


(b) Top view of the PTV & ML assembly

Additionally, Fig. 17.2 shows an isometric view of the spacecraft configuration with deployed solar panels, as during the transfer journey. It can be observed that the ML is connect to the PTV in order to provide additional living space during the journey and the propellant tanks are symmetrically arranged around the PTV to provide mass centralization and advantageous inertia characteristics.

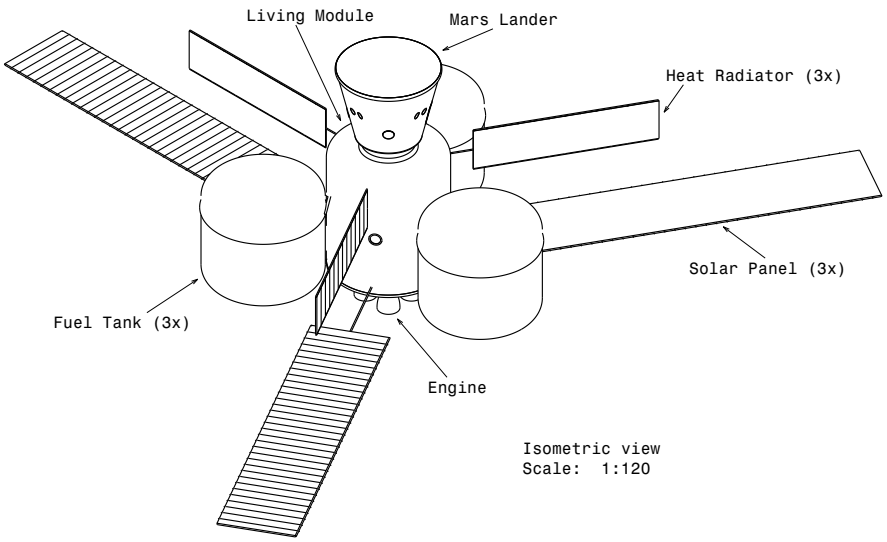


Figure 17.2: PTV Configuration

### Internal Layout

The internal layout of the PTV is of importance because all the necessary subsystems need to be integrated in such a way that they can operate efficiently, not disturb each other, and leave enough living space for the astronauts. The interior configuration of the PTV can be seen in Fig. 17.3, where the crew quarters and all the interior subsystems are shown.

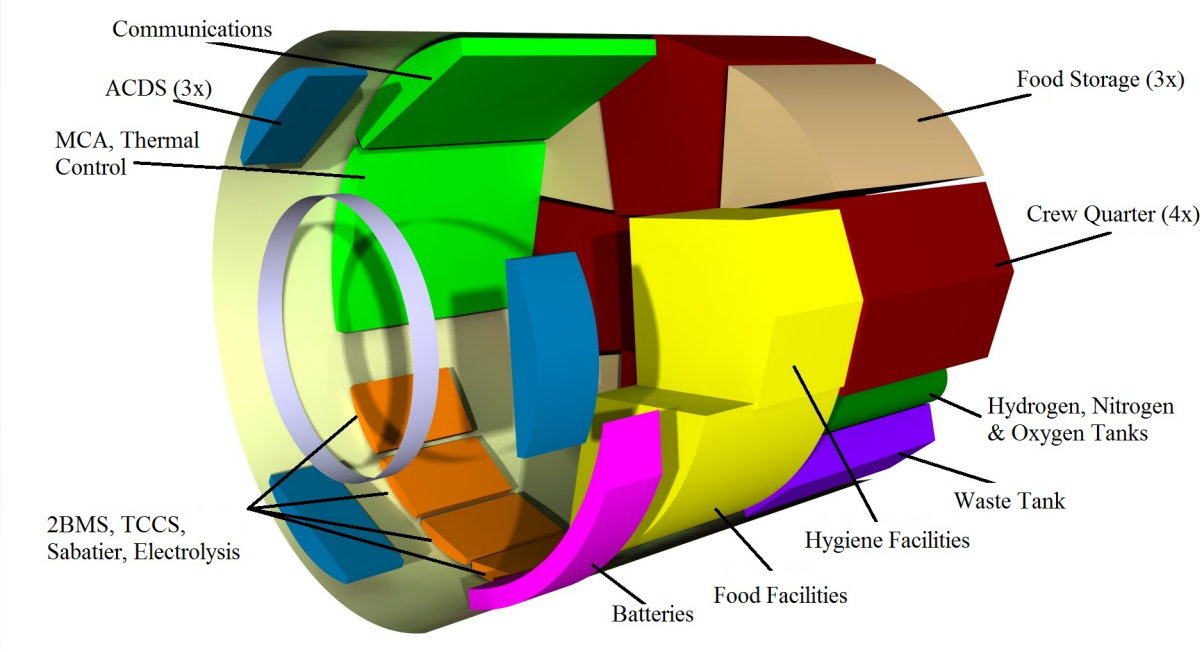


Figure 17.3: PTV internal layout configuration

After having performed this first iteration on the baseline design, the final mass budgets of the PTV, the ML have been obtained. This updated mass budgets also caused the propellant tanks to be resized to account for a different system mass. A summary of this final mass budgets and propellant tank sizes is shown in Tab. 17.1. Fig. 17.4a and Fig. 17.4b show a breakdown of these mass budgets.

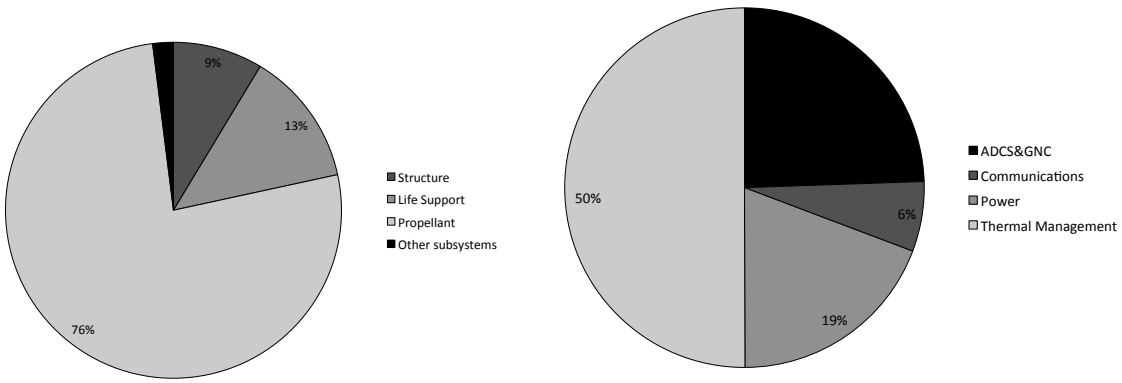


(a) Mass budget breakdown of the PTV + ML (b) Subsystems mass breakdown of the PTV + ML

As can be observed in Tab. 17.1, the ML mass decreased considerably in comparison to the baseline design during the iteration process. The mass that has been saved on the ML is mainly due to the communications, structure, heat shield, environmental control, propellant and navigation & telemetry systems. These subsystems have been designed more efficiently and therefore they used a smaller portion of the mass budget than what was accounted for in the baseline design. On the other hand, the parachute landing system has become larger during the iteration process and has become heavier.

Table 17.1: Final mass budget for the PTV, the ML and the propellant tanks. All values are given in $[kg]$.

| **Subsystem** | **PTV** | **Tank 1** | **Tank 2** | **Tank 3** | **ML** | **Total mass** |
|---|---|---|---|---|---|---|
| Structure | 2390 | 3200 | 3200 | 3200 | 806 | **12796** |
| Propulsion | 743 | - | - | - | 478 | **1221** |
| Life Support | 18720 | - | - | - | 467 | **19187** |
| ADCS and GNC | 477 | - | - | - | 106 | **583** |
| Communications | 130 | - | - | - | 20 | **150** |
| Power | 71 | - | - | - | 387 | **458** |
| Thermal Management | 1014 | 15 | 15 | 15 | 134 | **1193** |
| Parachute | - | - | - | - | 197 | **197** |
| Mobility system | - | - | - | - | 89 | **89** |
| Crew | - | - | - | - | 300 | **300** |
| Propellant | 946 | 49054 | 49054 | 13057 | 1040 | **113151** |
| **Total** | **24491** | **52269** | **52269** | **16272** | **4024** | **149325** |

### 17.1.1 PTV Sensitivity Analysis

In order to test the flexibility of the final PTV design, the requirement of the number of astronauts it must be able to transport was increased from 4 to 6. This increase explores the maximum capacity of the PTV, as 6 is the maximum number of people that can be transported, as stated in the requirements. The volume of living space per astronaut was kept constant in order to avoid compromising on the living conditions of the crew. The radius of the PTV is constrained by the size of the Falcon Heavy payload fairing, resulting in the need for a 2 $m$ increase in the length of the living quarters. This increase in crew capacity will also have a an impact on the life support mass, as 50% more supplies will be required. The structural mass will also increase due to the increased length and the need for extra stringers to withstand the loads experienced by the PTV. This gives a new total mass of 184 $t$, of which 153 $t$ is propellant and fuel tanks.

With the new 6 person configuration of the PTV, the required fuel can still fit in 3 Falcon Heavy launches, but there is no space for the ML in the third launch. Therefore, an extra launch would be required to bring the ML into LEO. The new total length of the PTV, 7 $m$, exceeds the 6.6 $m$ height of the cylindrical segment of the Falcon Heavy payload fairing, meaning that the top of the PTV would have to be cone-shaped in order to fit within the fairing. Beyond these factors, the PTV parameters scale linearly and no significant problems arise when the carrying capacity is increased. The carrying capacity of 4 was selected in order to decrease the cost of the mission and the requirement for a mission every 3 years means that reinforcements will arrive periodically.

### 17.1.2 Subsystem Update

As a result of this design update following the first iteration process, the mass budget values of the PTV and ML have been altered. This means that the subsystem configurations are out of date, as they are based on the baseline values from the previous iteration. However, con-

sidering that the mass values have all been reduced, the subsystems still perform within the system, but are inefficient with regard to their sizing. The next step, as the project moves into Phase B design, is to increase the detail of the design process and iterate it further in order to optimize the definitions of the systems and subsystems. This will result in more optimized subsystems, which can further reduce total system weight and take advantage of the *snowball* effect.

**Parachute** There is, however, one subsystem where the decrease in system mass means that the subsystem requirements are no longer met. For the parachute in the ML, the lighter mass results in shock loads higher than the maximum limit of 5 $g$ during the initial parachute deployment in the descent phase. Therefore, this design must be redesigned ahead of the next expected iteration to ensure that the final design presented in this report is technically suitable for the mission. The new, initial reefed diameter is 20 $m$ and the final, fully inflated, parachute diameter is 29.4 $m$. With this, the shocks experienced by the crew are reduced to below 5 $g$. The rest of the parameters are kept constant and the new final velocity is 94.8 $m/s$, which is slightly lower than the previous value and means that a small amount of fuel will be saved in the next iteration of the thruster descent phase.

### 17.1.3 Final Mission Profile

In order to show a simplified mission profile a flow diagram in Fig. 17.5 is presented. The spacecraft is divided into 4 stages that include different components which need different $\Delta V$ impulses for each mission stage.

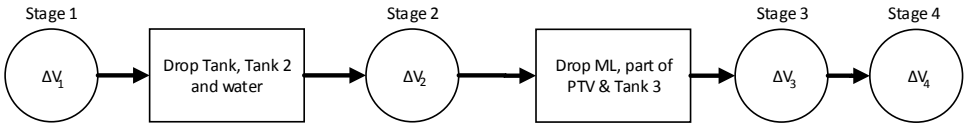


Figure 17.5: Mission profile

Stage 1 includes all components of the spacecraft: The PTV main module, the ML and all 3 propellant tanks. After completing the first $\Delta V$ maneuver tank 1 and tank 2 are discarded. Stage 2 consists of the PTV, the ML and tank 3. All fuel contained in tank 3 is subsequently used for the second $\Delta V$ impulse. After completing the maneuver from the transfer orbit to Mars' parking orbit the ML separates and lands on Mars' surface, and the empty second propellant tank is discarded as well. In addition, 80% of the PTV's structure is discarded such that only the parts necessary for serving as a communications relay station are maintained. Stage 3 now only consists of a short section of the PTV (1 m in length) that includes the communications system, the ADCS system, the power subsystem with the solar panels, the thermal regulation system minus the large radiators, and the small amount of propellant necessary for $\Delta V_3$ and $\Delta V_4$. After completing $\Delta V_4$ the spacecraft finally arrives in the areo-stationary orbit to function as a communications relay station.

**Recommendations** The feasibility study described in this report offers multiple points on which further research is needed. It was seen that due to the restricted amount of time, certain aspects could not be treated with the required level of detail. These points of attention are

discussed in this section.

After the baseline design, the subsystems were designed and one iteration was performed based on this. As, with each iteration the design will become more optimized, increasing the number of iterations results in a more optimized and realistic design. Therefore, for further research on the Mars One project the number of iterations should be increased.

Next to increasing the number of iterations, another important point is the landing phase. The landing phase is a very complex part of the mission, which poses the highest risk of failure. Hence, extra research into the landing phase of the mission is needed to rule out potential problems. Namely the parachute deployment and opening needs be researched in depth. The time in which the parachute needs to be deployed is very limited and opening a huge parachute in this time, as suggested for this mission, is a complex challenge. Furthermore the flight path angle might need to be reevaluated, as the method used for calculation shows a difference of 15% for the verification case. A more sophisticated method is thus beneficial in eliminating uncertainties in this crucial mission phase involving the parachute deployment and unfolding as well as the heat loads.

In addition to the technical aspects mentioned, other non technical aspects needs to be investigated as well. For example the psychological stress on the participants poses a major risk for mission success, which has not been considered in this feasibility study.

All in all, more work on the Mars One project is needed to perform a successful mission. The general idea, though, sending humans on a one way mission to Mars using current technology has proven to be feasible. Therefore, it is advised to stimulate more research on this mission to finally set foot on another planet.

# 18 | Future Developments

The purpose of the Design Synthesis Exercise was to develop a Phase A design of a one-way manned mission to Mars, which is performed for the PTV and the ML. Now it is time to look into further development. This chapter shows the post-DSE activities. First the production plan is discussed where the manufacturing, assembly and integration of the PTV and ML are explained. Second, the project development is discussed, since between the Phase A design and the final product multiple steps need to be taken. Finally, a Gantt chart summarizes all future activities.

## 18.1 Production plan

In this section the manufacturing, assembly and integration plan (MAI plan), also known as the production plan, shall be discussed. This MAI plan is necessary to organize the complete production phase of the Mars One mission. The MAI plan contains a time ordered outline of the entire production phase. Since the production plan is a part of the future planning of the project, it can be seen in the project development flow diagram (see Fig.18.1). The production plan is phase D in the project development flow diagram and will be discussed here in more detail.

In such a big project as the Mars One mission it is impossible to produce the complete system by only one manufacturer and without any assembly or integration. This is mostly due to the the PTV and ML size, different materials, time limit and the economic risks require the assembly process. In the past the work share of big systems like space- and aircraft was often divided into multiple contractors. Three different stages of Saturn V were for example produced by three different manufactures [135]. These manufacturers can outsource some parts to other companies. This process will also be applied to the Mars One mission. For example SpaceX, the manufacturer of the Falcon Heavy, shall not necessarily produce the PTV. This can be done by other companies who have more experience or can produce it at a lower cost. Even the production of the subsystems of the PTV can be divided among several companies if this decreases the cost.

NASA estimates the total time required for the manufacturing, assembly and integration of one Orion capsule around 14 months. The qualification of the spacecraft takes another 2 months [136]. These values can also be used to estimate the manufacturing, assembly and integration time of one ML or PTV.

Throughout the whole production phase a clean room should be available. A clean room provide an environment with a minimum of dust, pollutants and micro-organisms. The availability of clean room facilities is important because the Mars One mission should not contaminate

Mars. Another reason why clean rooms should be used is that they prevent that dust, pollutants and micro-organisms damage systems of the spacecraft.

### 18.1.1 Manufacturing

The manufacturing phase will start after the finalization of the design phase. The manufacturing phase of all the parts will take place in parallel to decrease the production time. All produced parts should be sufficiently tested on several tests like material strength, vibrations, etc. After these tests are performed the parts can be qualified. Quality management should also be implemented in the manufacturing process such that the the quality of each product can be assured. To assure the quality the AS9100 standards shall be used [137]. During the manufacturing phase, lean manufacturing shall be implemented as much as possible. This way the enterprise shall eliminate waste as much as possible. For example the manufacturers shall apply the Just-in-Time method such that the stocks shall be decreased and that no companies have to wait for their supplies. For the Mars One mission this means that the propellant tanks shall be just finished when the first propellant tank tests will be executed, not several months before, because that will also increase the costs[138]. The Just-in-Time method is mainly applicable for mass production, but can also be applied to the Mars One mission to a lesser extent.

### 18.1.2 Assembly and Integration

Subassembly of smaller parts can take place parallel with the production phase, but the main assembly and integration will be after the production phase. It will be labor intensive and time consuming work due to the size of the systems. A part of the assembly of the Mars One mission will take place in orbit around the Earth which will increase the risks. During the assembly phase all the components should be brought together. The transportation of such systems may not be underestimated and even the production of a transportation vehicle for PTV can be necessary if no other existing transportation vehicle can be used. For example the NASA had to built the Crawler-transporters to transport the Saturn rockets during the 1960's. To produce these vehicles the NASA had to spent $ 14 million in 1965 dollars [139].

### 18.1.3 Suppliers

The Mars One company already contacted multiple suppliers to manufacture all necessary parts and systems for the mission. The list of possible suppliers can be found below [140].

- Astrobotic Technology: space robotics and mobility systems, such as the Mars rover
- ILC Dover: high-performance flexible materials, such as space suits
- MDA Corporation: information systems, such as radars and GPS receivers
- Paragon Space Development: life support and environmental control
- Space Exploration Technologies, also known as SpaceX: launchers and spacecraft, such as the Falcon Heavy and Dragon capsule
- Surrey Satellite Technology: small satellites, telecommunication and navigation
- Thales Alenia Space: pressurized vessels and cargo modules

## 18.2 Project Development

In this section, the project development is discussed. With use of *ECSS Space Project Management* [141], the following phases are identified.

- **Phase 0** Identification and analysis of the mission in terms of needs, expected performance, dependability and safety goals. Some possible system concepts are identified and a preliminary project management set-up is made.
- **Phase A: Feasibility** The needs of Phase 0 are finalized and solutions are proposed, by quantifying the critical elements, establishing a Function Tree and exploring multiple possible system concepts. The concepts are being compared against the needs and the technical and industrial feasibility is estimated. Costs, schedules, organization, utilization, production and disposal are identified for every concept and finally, a final concept is chosen.
- **Phase B: Preliminary Definition** Technical solutions for the concept chosen in Phase A are defined, a system requirements review is conducted and the feasibility of the concepts is confirmed. All subsystems are designed. An assessment is made of manufacturing, production and operating costs.
- **Phase C: Detailed definition** A detailed study of the preliminary design is performed. Confirmation of set-up, test and qualification conditions is initiated. Procurements are started. Phase E preparations start.
- **Phase D: Production/Ground Qualification Testing** All products and components of the system are designed in full and the system is validated. Production, assembly, integration and verification of all parts is conducted.
- **Phase E: Utilization** This phase is divided into two sub-phases: First, an overall test in-space is performed. In the second sub-phase, the utilization takes place. Operations reviews are executed which can contribute to improvements during operation and can show the urge of redevelopment of certain parts.
- **Phase F: Disposal** The complete project is reviewed in order to improve future missions and a final cost analysis is made.

For a more extensive description of these project phases, the reader is referred to [141].

Since this is a manned mission to Mars with the intention to establish a permanent colony, no disposal of the systems can be performed: after the mission, the PTV will be used as a communication relay and the Mars Lander will be a part of the Mars base. However, a disposal plan for the PTV for its end-of-life time when it is functioning as a relay should be considered and improvements can be found for future vehicles.

In Fig. 18.1, the flow diagram for the future project development is shown. Since Phase A is already performed at this point, the diagram starts at Phase B. This diagram is valid for both the PTV and the Mars lander.

Mars One aims to launch the first manned mission in 2023. However, as explained before, in chapter 4, the first mission will depart from Earth orbit on the 11th of October 2026 in order to utilise an energy efficient trajectory and allow enough time for the development of the PTV

and ML and the unmanned supplies missions to Mars.

## 18.3 Gantt Chart

Looking at the development of the Dragon lander of SpaceX as a reference, a schedule is made for the PTV and Mars Lander. The Dragon lander project was initiated at the end of 2004, the first tests started in 2010, the first unmanned mission was in 2012 and the first manned mission is expected to be in 2015 [142]. In total, 11 years are needed until the first manned mission. Orion, a manned spacecraft of NASA, is currently under development [136]. The different phases of Orion are shown in Tab. 18.1.

When it comes to the development times of Orion and Dragon it is indeed possible to have

Table 18.1: Orion Development Schedule [136]

| **Phase** | Duration |
|---|---|
| Phase A | October 2007 - October 2008 |
| Phase B | October 2008 - August 2009 |
| Phase C | August 2009 - August 2010 |
| Phase D | August 2010 - October 2015 |

the first manned mission in Mars in 2026. According to the Orion development schedule, the Gantt Chart for the PTV and ML is developed. For this Gantt Chart, the PTV and the Mars Lander will be developed parallel as well. The Gantt Chart is shown in Fig. 18.2. Phase A is not explained further, since it is already performed at this point. Phase B will last 11 months and is assumed it will start right after the end of the DSE. Since the PTV and ML are two complex systems, a lot of manpower is needed as well as a good overview of the process. The design process of the subsystems will run parallel to the finishing the final preliminary design for a short period. It is expected that the preliminary design will be finished in June 2014. Phase C will last one year, where about 60% of the time is scheduled for developing the final design. The remaining time is needed for verification and production plans. Procurements will start right after the final design is finalized. The next phase, Phase D, will start in June 2015 and will last 6 years. During this phase, all subsystems, parts and compartments of the PTV and ML will be produced, assembled and tested on ground.

Finally, in June 2021, the first launch with test vehicles will be launched in orbit around Earth and an in-space test will be conducted. A test PTV will be assembled in space and a test Mars lander will perform a re-entry procedure. It will not perform an actual re-entry, since the lander is not build for the Earth atmosphere and will probably burn up. No practice mission to the Moon is performed either, since the lack of an atmosphere means that the ML would not be able to land. However, the docking/detaching maneuvers will be tested. After the successful tests, the unmanned mission to Mars will take place. These unmanned PTVs will bring the supplies and Rovers to Mars according to Mars One's plans. Finally, on the 11th of October 2026, the first manned mission will leave the Earth orbit. Right after the first manned PTV has departed, the preparations for the second mission start. Preparations include all the on-ground preparations, launch and in-orbit assembly. The departure of the second mission is planned for the 10th of December 2028 and the third mission will depart on the 10th of February 2031. After arrival at Mars, each PTV will function as a communication relay. They should be able

to function at least for two years, but they are designed to function for at least 10 years. In Fig. 18.2, the Gantt Chart can be found.

Technically, the described process is feasible. With enough resources, men can be transported to Mars within this brief time frame. The major issue in execution will be the collection of the resources. An enormous amount of funding is required to even start development, which would be now. Funding methods have been described in section 16.3, and a serious research will need to be done to guarantee a stable source of income.

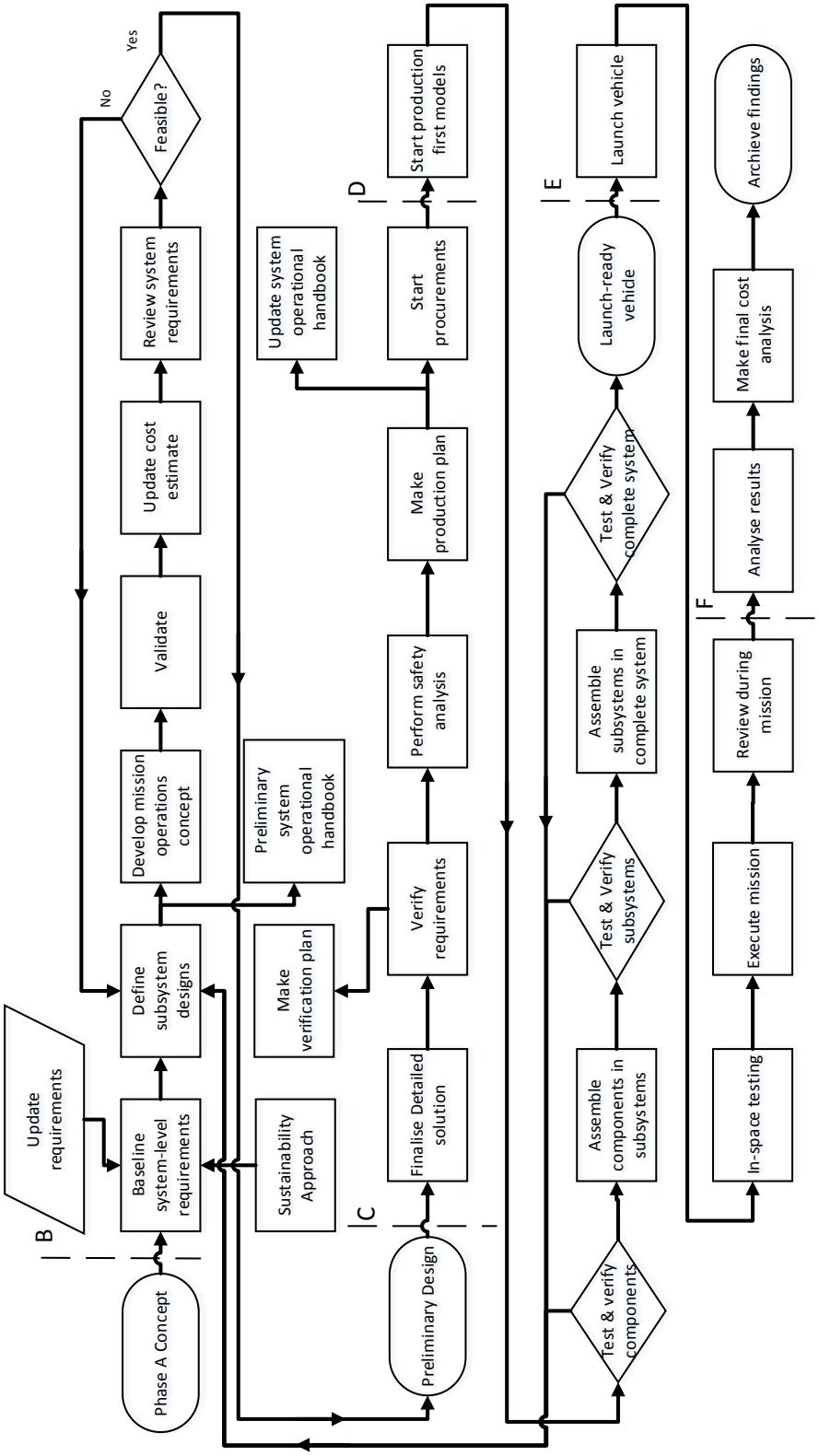


Figure 18.1: Project Development Flow Diagram

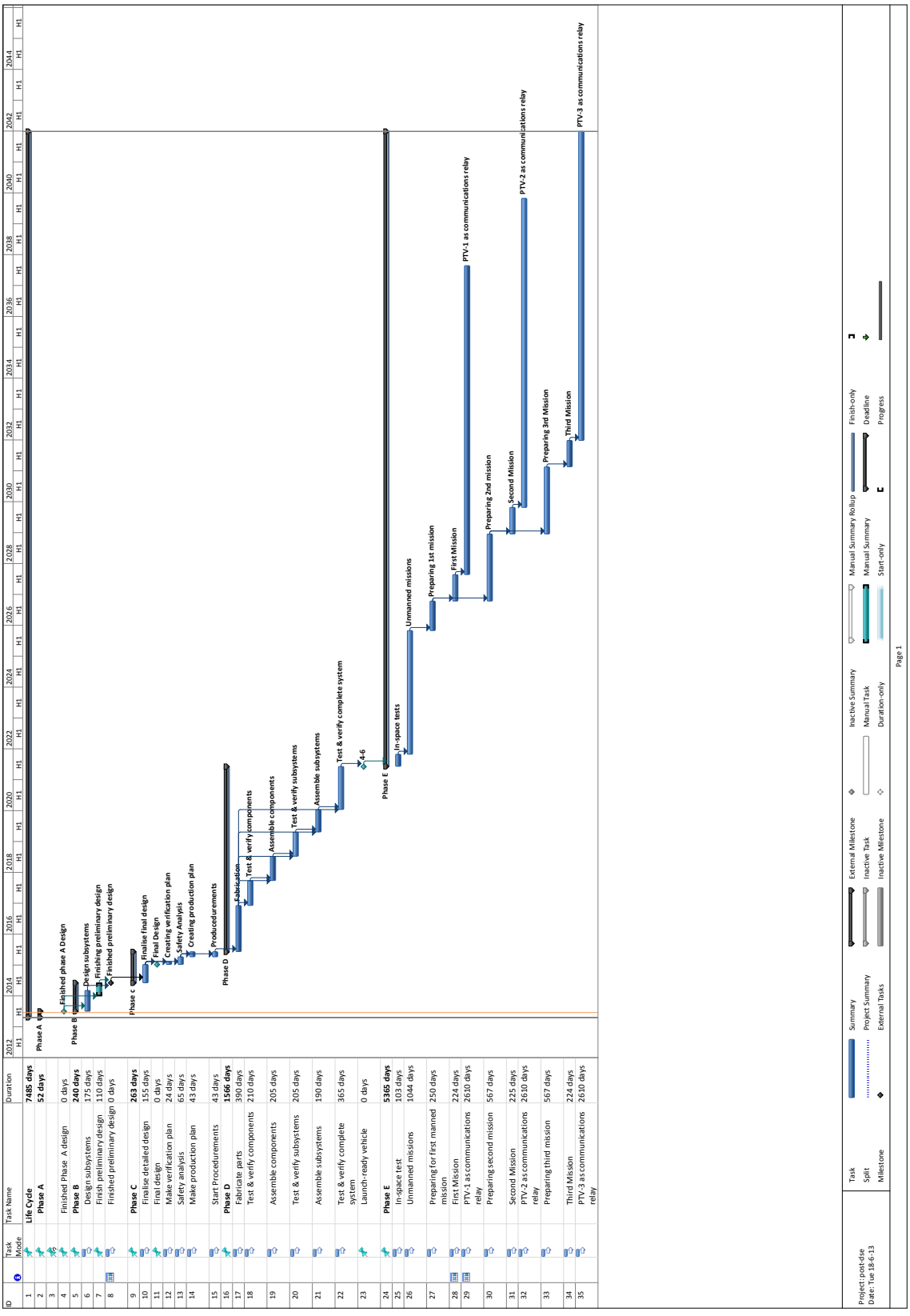


| ID | Task Mode | Task Name | Duration |
|---|---|---|---|
| 1 | | Life Cycle | 7485 days |
| 2 | | Phase A | 52 days |
| 3 | | Finished Phase A design | 0 days |
| 4 | | Phase B | 240 days |
| 5 | | Design subsystems | 175 days |
| 6 | | Finish preliminary design | 110 days |
| 7 | | Finished preliminary design | 0 days |
| 8 | | Phase C | 263 days |
| 9 | | Finalise final design | 155 days |
| 10 | | Final design | 0 days |
| 11 | | Make verification plan | 24 days |
| 12 | | Safety analysis | 65 days |
| 13 | | Make production plan | 43 days |
| 14 | | Start Procedurements | 43 days |
| 15 | | Phase D | 1566 days |
| 16 | | Fabricate parts | 390 days |
| 17 | | Test & verify components | 210 days |
| 18 | | Assemble components | 205 days |
| 19 | | Test & verify subsystems | 205 days |
| 20 | | Assemble subsystems | 190 days |
| 21 | | Test & verify complete system | 365 days |
| 22 | | Launch-ready vehicle | 0 days |
| 23 | | Phase E | 5365 days |
| 24 | | In-space test | 103 days |
| 25 | | Unmanned missions | 1044 days |
| 26 | | Preparing for first manned mission | 250 days |
| 27 | | First Mission | 224 days |
| 28 | | PTV-1 as communications relay | 2610 days |
| 29 | | Preparing second mission | 567 days |
| 30 | | Second Mission | 225 days |
| 31 | | PTV-2 as communications relay | 2610 days |
| 32 | | Preparing third mission | 567 days |
| 33 | | Third Mission | 224 days |
| 34 | | PTV-3 as communications relay | 2610 days |
| 35 | | | |

Figure 18.2: Gantt Chart Future Developments

# Bibliography


[1] "Saturn V Fact Sheet," http://history.msfc.nasa.gov/saturn_apollo/documents/Third_Stage.pdf, December 1968, viewed on 17/06/2013.

[2] Borggräfe, A., Quatmann, M., and Nölke, D., "Radiation protective structures on the base of a case study for a manned Mars mission," *Acta Astronautica*, Vol. 65, No. 9, 2009.

[3] Cucinotta, F., "Radiatian Risk Acceptability and Limitations," http://three.usra.edu/articles/AstronautRadLimitsFC.pdf, viewed on 13/06/2013.

[4] Tito, D. A., Anderson, G., and Carrico Jr, J. P., "Feasibility Analysis for a Manned Mars Free-Return Mission in 2018," http://www.inspirationmars.com/, March 2013, viewed on 14/06/2013.

[5] Trinh, H. P., "Liquid Methane/Liquid Oxygen Injector for Potential Future Mars Ascent Enginers," http://archive.org/details/nasa_techdoc_20000004538, January 1999, viewed on 01/07/2013.

[6] Curtis, H., *Orbital Mechanics: For Engineering Students*, Butterworth-Heinemann, Dec. 2004.

[7] Horneck, G., Facius, R., Reichert, M., Rettberg, P., Seboldt, W., Manzey, D., Comet, B., Maillet, A., Preiss, H., and Schauer, L., "HUMEX, a study on the survivability and adaptation of humans to long-duration exploratory missions, part I: lunar missions." Jan 2003.

[8] Humble, R., Henry, G., and Larson, W., *Space Propulsion Analysis and Design*, McGraw-Hill, 1995.

[9] Zandbergen, B., *Thermal Rocket Propulsion*, 2010.

[10] Musk, E., "Liquid propellant energetic properties: Now test firing our most advanced engine, the Merlin 1D-Vac, at 80 tons of thrust," September 2012.

[11] Kokan, T. S., Olds, J. R., Seitzman, J. M., and Ludovice, P. J., "Characterizing high-energy-density propellants for space propulsion applications," *Acta Astronautica*, Vol. 65, 2009.

[12] Salerno, L. J. and Kittel, P., "Cryogenics and the human exploration of Mars," *Cryogenics*, Vol. 39, 1999.

[13] Smith, T., Klem, M., and Fisher, K., "Propulsion Risk Reduction Activities for Non-Toxic Cryogenic Propulsion," *AIAA*, Vol. 8680.

[14] Massee, M., "XCOR Aerospace Begins Test Firing of Methane Rocket Engine," http://www.xcor.com/press-releases/2007/07-01-16_XCOR_begins_methane_engine_testing.html, January 2007, viewed on 25/06/2013.

[15] Holladay, J., Brooks, K., Wegeng, R., Hu, J., Sanders, J., and Baird, S., "Microreactor development for Martian in situ propellant production," *Catalysis Today*, Vol. 120, 2007.

[16] Zandbergen, B., "Liquid propellant energetic properties," June 2013.

[17] "Oxygen Vapor Pressure Graph," http://encyclopedia.airliquide.com/images_encyclopedie/VaporPressureGraph/Oxygen_Vapor_Pressure.GIF, viewed on 13/06/2013.

[18] "Methane Vapor Pressure Graph," http://encyclopedia.airliquide.com/images_encyclopedie/VaporPressureGraph/Methane_Vapor_Pressure.GIF, viewed on 13/06/2013.

[19] Honour, R., Kwas, R., O'Neil, G., and Kutter, B., "Thermal Optimization and Assesment of an On-Orbit Long Duration Cryogenic Propellant Depot," *AIAA*, Vol. 630, January 2012.

[20] of Energy Lawrence Berkeley National Laboratory, D., "Science of Silica Aerogels," http://energy.lbl.gov/ecs/aerogels/sa-thermal.html, viewed on 17/06/13.

[21] Fortescue, P. and Stark, J., *Spacecraft Systems Engineering*, Wiley, 2nd ed., 1995.

[22] Chow, L., Kapat, J., Wu, T., Sundaram, K., and Ham, C., "A Reliable, Efficient and Compact Reverse Turbo Brayton Cycle (RTBC) Cyrocooler for Storage and Transport of Hydrogen in Spacecraft and Space Vehicle Applications," Tech. rep., University of Central Florida, 2006.

[23] Mulqueen, J. e. a., "Cryogenic Propellant Storage and Transfer Technology Demonstration: Prephase A Government Point-of-Departure Concept Study," Tech. rep., NASA, 2012.

[24] Wilson, A., *Jane's Space Directory*, Alenia Spazio Satellite Systems, 1997.

[25] Larson, W. J. and Pranke, L. K., *Human Spaceflight - Mission Analysis and Design*, McGraw-Hill, 2002.

[26] Jones, H., "Design Rules for Life Support Systems," viewed on 26/06/2013.

[27] Gardner, B., Erwin, P., Thoresen, S., Granahan, J., and Matty, C., "International Space Station Major Constituent Analyzer On-orbit Performance," *AIAA*, Vol. 3633, July 2012.

[28] Ruff, G. and Urban, D., "A research plan for Fire Prevention, Detection, and Suppression in Crewed Exploration Systems," *AIAA*, Vol. 314, January 2005.

[29] Perry, J., Cole, H., and El-Lessy, H., "An Assessment of the International Space Station's Trace Contaminant Control Subassembly Process Economics," .

[30] Broyan, J., Borrego, M., and Bahr, J., "International Space Station USOS Crew Quarters Development," *SAE International Journal of Aerospace*, Vol. 1, 2009, pp. 92–106.

[31] "The Space Shuttle Extravehicular Mobility Unit," http://www.nasa.gov/pdf/188963main_Extravehicular_Mobility_Unit.pdf, viewed on 28/05/2013.

[32] Dismukes, K., "Food for Space Flight," http://spaceflight.nasa.gov/shuttle/reference/factsheets/food.html, April 2013.

[33] Lange, K. and Lin, C., "Crew And Thermal Systems Division," https://taskbook.nasaprs.com/peer_review/prog/old/ALSREQ96.html, July 2013, viewed on 01/07/2013.

[34] Mateos, A., "Space Debris and its Effects on Spacecrafts," http://people.tamu.edu/~amateos/Documents/Extended_Essay_Arturo_Mateos_2009.pdf, 2009, viewed on 17/06/2013.

[35] "Hypervelocity Impact Technology," http://ares.jsc.nasa.gov/ares/hvit/basic.cfm, June 2013, viewed on 11/06/2013.

[36] Musgrave, G., Larsen, A., and Sgobba, T., *Safety design for space systems*, Butterworth-Heinemann, 2009.

[37] "Engineering Toolbox: Fibers in Polymer Composites," http://www.engineeringtoolbox.com/polymer-composite-fibers-d_1226.html, June 2013, viewed on 11/06/2013.

[38] "3M Nextel Textiles," http://www.layogev.co.il/Download/3M-Branches/Aviation-Space/Isolation-A-11.6.pdf, September 2009, viewed on 17/06/2013.

[39] Jiang, H., "Debris Shielding Technology Progress," http://swfound.org/media/50876/Jiang_DebrisShielding.pdf, October.

[40] Larson, W. and Wertz, J., *Space Mission Analysis and Design*, Microcosm Inc. and Kluwer Academic Publishers, 2nd ed., 2001.

[41] Callister, W. and Rethwisch, D., *Materials science and engineering: an introduction*, John Wiley & Sons New York:, 2007.

[42] "Falcon 9 User's Guide," http://www.spacex.com/Falcon9UsersGuide_2009.pdf, 2009, viewed on 06/06/2013.

[43] Megson, T. H. G., *Aircraft structures for engineering students*, Butterworth-heinemann, 2012.

[44] Callister, W. and Rethwisch, D., *Materials science and engineering: an introduction*, John Wiley & Sons New York:, 2007, viewed on 1/07/2013.

[45] Karn, P., "Space Shuttle Propulsion," http://www.nasa.gov/centers/marshall/multimedia/photogallery/photos/photogallery/shuttle/shuttle.html, July 1997, viewed on 23/06/2013.

[46] Williams, R., "NASA Space Flight Human-system Standard," 2011.

[47] Hyder, A., Wiley, R., Halpert, G., Flood, D., and Sabripour, S., *Spacecraft Power Technologies*, Imperial College Press, 2000.

[48] Viscio, M., Viola, N., Gargioli, E., and Vallerani, E., "Conceptual design of a habitation module for a deep space exploration mission," *Journal of Aerospace Engineering*, August 2012.

[49] Zulovich, J., "Active Solar Collectors for Farm Buildings," http://extension.missouri.edu/publications/DisplayPub.aspx?P=G1971, 2012, viewed on 14/06/2013.

[50] Kokoropoulos, P., Salam, E., and Daniels, F., "Selective Radiation Coatings Preparation and High Temperature Stability," *Solar Energy*, Vol. 3, 1959, pp. 19–23.

[51] Petersen, H., Zevenbergen, P., Benthem, B., and Sudmeijer, K., "AE4S20 - Satellite Thermal Control," 2013.

[52] "DVB-S2 Technical Presentation," http://www.advantechwireless.com/wp-content/uploads/DVB-S2-theory.pdf, viewed on 29/05/2013.

[53] Lebedevinskǐ, S. and et al, "High Efficiency Power Klystrons," *Elektronnaya Tekhnika*, , No. 1, 1977, pp. 41–51.

[54] Boeing, "Galaxy XIII/Horizons-1," http://www.boeing.com/boeing/defense-space/space/bss/factsheets/601/galaxy_xiii_horizons_1/galaxy_xiii_horizons_1.page, viewed on 17/06/13.

[55] "Spacecraft (SC) preliminary mass estimation allocation," http://www.lr.tudelft.nl/?id=29336&L=1, viewed on 17/06/13.

[56] NASA, "Galileo Legacy Site," http://solarsystem.nasa.gov/galileo/, viewed on 01/07/2013.

[57] Gill, E., "AE2101 Communications I+II," 2011.

[58] Karn, P., "Mars Pathfinder X-band Downlink Budget," http://www.ka9q.net/mpf_budget.html, July 1997, viewed on 21/06/2013.

[59] NASA, J., "DSN Antennas Gain and Aperture Efficiency," http://dsnra.jpl.nasa.gov/Antennas/AntennaGain.html, viewed on 12/06/2013.

[60] Larson, W. J. and Pranke, L. K., *Human spaceflight: mission analysis and design*, McGraw-Hill Companies, 2000.

[61] Bedrossian, N., "International Space Station Attitude Control," http://www.nasa.gov/mission_pages/station/research/experiments/274.html, viewed on 05/06/2013.

[62] Votel, R. and Sinclair, D., "Comparison of Control Moment Gyros and Reaction Wheels for Small Earth-Observing Satellites," *AIAA*, Vol. 26, 2012.

[63] ECP, "Control Momentum Gyroscope," http://www.ecpsystems.com/controls_ctrlgyro.htm, viewed on 12/06/2013.

[64] Noomen, R., "Flight and Orbital Mechanics: Interplanetary flight," October.

[65] Seidelmann, P. K., Archinal, B., A'hearn, M., Conrad, A., Consolmagno, G., Hestroffer, D., Hilton, J., Krasinsky, G., Neumann, G., Oberst, J., et al., "Report of the IAU/IAG Working Group on cartographic coordinates and rotational elements: 2006," *Celestial Mechanics and Dynamical Astronomy*, Vol. 98, No. 3, 2007, pp. 155–180.

[66] Zandbergen, B., "Aerospace Design and Systems Engineering Elements I," June 2011.

[67] Weck, O., "Space Systems Product Development: Attitude Determination and Control," 2001.

[68] Yoon, H. and Tsiotras, P., "Spacecraft adaptive attitude and power tracking with variable speed control moment gyroscopes," *Journal of Guidance, Control, and Dynamics*, Vol. 25, No. 6, 2002, pp. 1081–1090.

[69] "Space Station Live Exploration," http://spacestationlive.nasa.gov/exploremcc.html, June 2012, viewed on 07/06/2013.

[70] Oberg, J., "Why the Mars probe went off course," *IEEE Spectrum*, Vol. 36, No. 12, 1999, pp. 34–39.

[71] "Encyclopedia Astronautica-Hydrazine," http://www.astronautix.com/props/hydazine.htm, March 2013, viewed on 10/06/2013.

[72] Jackson, B. and Carpenter, B., "Optimal placement of spacecraft sun sensors using stochastic optimization," *Aerospace Conference, 2004. Proceedings. 2004 IEEE*, Vol. 6, IEEE, 2004, pp. 3916–3923.

[73] "Mars Reconnaissance Orbiter Arrival," http://www.nasa.gov/pdf/143619main_mro-arrival.pdf, March 2006, viewed on 04/06/2013.

[74] "Mars Reconnaissance Orbiter Guidance and Control system," http://mars.jpl.nasa.gov/mro/mission/spacecraft/parts/gnc/sensors/, May 2013, viewed on 04/06/2013.

[75] "ISS Soyuz Undocking," http://www.nasa.gov/mission_pages/station/structure/elements/soyuz/landing_timeline.html, October 2010, viewed on 20/06/2013.

[76] Mooij, E., "AE4870B - Re-entry Systems," November 2011.

[77] Wertz, J. and Larson, W., *Reducing Space Mission Cost*, Space Technology Library, 1996.

[78] Zandbergen, B., "AE2203: Propulsion & Power, Part: Aerospace Vehicle Electrical power systems," July 2011.

[79] Gaddy, E., "CIGS Cells for Space," http://www.solar-technology.nl/assets/presentaties/Dutch-Space-Gijs-Oomen.pdf, Januari 2011, viewed on 14/06/2013.

[80] LaMonica, M., "Solar Junction claims cell efficiency record," http://news.cnet.com/8301-11128_3-20053851-54.html, April 2011, viewed on 14/06/2013.

[81] Grahne, M. and Cadogan, D., "Inflatable Solar Arrays: Revolutionary Technology?" January 1999.

[82] "Compressive strength of unidirectional fiber composites with matrix non-linearity," *Composites Science and Technology*, Vol. 52, No. 4, 1994, pp. 577 – 587.

[83] Zandbergen, I. B., "Electrical Supply Systems, AE2203-11 lecture notes," .

[84] C.Kassapoglou, "AE2211-11 lecture notes," .

[85] "DragonLab," http://www.spacex.com/downloads/dragonlab-datasheet.pdf, April 2013.

[86] Grover, M. R., Sklyanskiy, E., Stelzner, A. D., and Sherwood, B., "Red Dragon-MSL Hybrid Landing Architecture for 2018," *LPI Contributions*, Vol. 1679, June 2012, pp. 4216.

[87] Williams, D., "The Apollo Lunar Roving Vehicle," http://nssdc.gsfc.nasa.gov/planetary/lunar/apollo_lrv.html, November 2005, viewed on 06/06/2013.

[88] "Apollo CM," http://www.astronautix.com/craft/apollocm.htm, April 2013, viewed on 13/06/2013.

[89] Orloff, R., "Apollo by the Numbers: A statistical reference for the manned phase of Project Apollo," Tech. rep., National Aeronautics and Space Administration, 1996.

[90] Mooij, E., "AE4870B - Re-entry Systems: Ballistic Entry," 2012.

[91] Sostaric, R. and Rea, J., "Powered Descent Guidance Methods For The Moon and Mars," *AIAA*, Vol. 6287, August 2005.

[92] NASA, "Mars Atmosphere Model," http://www.grc.nasa.gov/WWW/k-12/airplane/atmosmrm.html, viewed on 20/06/13.

[93] Mendeck, G. F., "Mars Science Laboratory Entry Guidance," August.

[94] Dec, J. and Braun, R., "An Approximate Ablative Thermal Protection System Sizing Tool for Entry System Design," *AIAA*, Vol. 780, January 2006.

[95] Moss, J., Boyles, K., and Greene, F., "Orion Aerodynamics for Hypersonic Free Molecular to Continuum Conditions," *AIAA*, Vol. 8081, November 2006.

[96] Mitcheltree, R., DiFulvio, M., Horvath, T., and Braun, R., "Aerothermal Heating Predictions for Mars Microprobe," *Journal of Spacecraft and Rockets*, Vol. 36, No. 3, June 1999, pp. 405–411.

[97] Edquist, K., "Afterbody Heating Predictions for a Mars Science Laboratory Entry Vehicle," *AIAA*, Vol. 4817, June 2005.

[98] Mooij, E., Huot, J., and Ortega, G., "Entry Trajectory Simulation Using ESA Mars Climate Database Version 4.1," *AIAA*, Vol. 6023, augustus 2006.

[99] Outen, E., "To the Extreme: NASA Tests Heat Shield Materials," http://www.nasa.gov/mission_pages/constellation/orion/orion-tps.html, March 2009.

[100] Venkatapathy, E., Szalai, C. E., Laub, B., Hwang, H. H., Conley, J. L., and Arnold, J., "Thermal Protection System Technologies for Enabling Future Sample Return Missions," .

[101] Chen, Y. K. and Milos, F. S., "Ablation and Thermal Response Program for Spacecraft Heatshield Analysis," *Journal of Spacecraft and Rockets*, Vol. 36, No. 3, May 1999, pp. 475–483.

[102] Ridolfi, G., "Space Systems Conceptual Design: Analysis methods for engineering-team support," April 2013.

[103] Robertson, T., "Comparing Heat Shields: Mars Science Lab vs. SpaceX Dragon," http://blog.linuxacademy.com/space/comparing-heat-shields-mars-science-lab-vs-spacex-dragon/, viewed on 14/06/2013.

[104] Mooij, E., "AE4870B - Re-entry Systems: Planetary Entry and Descent," 2012.

[105] Braun, R. and Manning, R., "Mars exploration entry, descent, and landing challenges," *Journal of spacecraft and rockets*, Vol. 44, No. 2, 2007, pp. 310–323.

[106] Cruz, J., Way, D., Shidner, J., Davis, J., Adams, D., and Kipp, D., "Reconstruction of the Mars Science Laboratory Parachute Performance and Comparison to the Descent Simulation," http://ntrs.nasa.gov/archive/nasa/casi.ntrs.nasa.gov/20130012763_2013012510.pdf, March 2013, viewed on 11/06/2013.

[107] Knacke, T. W., *Parachute Recovery Systems Design Manual*, Para Publishing, 1992.

[108] Edwards, A., Hautaluoma, G., and Morcone, J., "NASA Tests Largest Rocket Parachutes Ever for Ares I," http://www.nasa.gov/home/hqnews/2009/may/HQ_09-113_AresI_Parachutes_Test.html, May 2009, viewed on 30/05/2013.

[109] Inman, D., *Engineering Vibration*, Pearson Education, 3rd ed., 2008.

[110] "Industrial Shock Absorbers," http://www.parker-origa.com/fileadmin/files/internet/AT/Industriepneumatik/PDF_katalog/English/Shocks/Shocks_E_00_complete.pdf, December 2006, viewed on 26/06/2013.

[111] Kassapoglou, C., "AE2211 - Structural Analysis and Design," 2013.

[112] Rao, M. and Gruenberg, S., "Measurement of Equivalent Stiffness and Damping of Shock Absorbers," *Experimental Techniques*, Vol. 26, No. 2, 2002, pp. 39–42.

[113] "Mars One - The Technology," http://mars-one.com/en/mission/technology, June 2012, viewed on 25/06/2013.

[114] "MSL: Remaining Martian Atmosphere Still Dynamic," http://www.nasa.gov/mission_pages/msl/news/msl20130408.html, 2012, viewed on 14/06/2013.

[115] JSC, "Spaceflight Radiation Health Program at JSC," http://srag-nt.jsc.nasa.gov/Publications/TM104782/techmemo.htm, 2013, viewed on 07/06/2013.

[116] "Mars One: Roadmap," http://mars-one.com/en/mission/summary-of-the-plan, viewed on 17/06/2013.

[117] Illoldi, S. and Zee, S., "Draft Environmental Impact Statement (EIS) for the SpaceX Texas Launch Site," http://www.faa.gov/about/office_org/headquarters_offices/ast/environmental/nepa_docs/review/documents_progress/spacex_texas_launch_site_environmental_impact_statement/media/SpaceX_EIS_Hearing_Compatibility_Mode.pdf, May 2013, viewed on 20/06/2013.

[118] Galabova, K. and Weck, O., "Economic case for the retirement of geosynchronous communication satellites via space tugs," *Acta Astronautica*, Vol. 58, No. 9, 2006, pp. 485 – 498.

[119] LaBauve, T., "Low Impact Docking System (LIDS)," February 2009.

[120] "External Tank's bipod fitting," http://www.nasa.gov/centers/marshall/multimedia/photos/2004/photos04-205.html_prt.htm, December 2004, viewed on 24/06/2013.

[121] NASA, http://www.astronautica.us/astronautica_shuttle_sts127.htm, June 2009, viewed on 25/06/2013.

[122] WCED, *Our common future*, Oxford University Press, 1987.

[123] Mars-One, "Is this a sustainable mission?" http://mars-one.com/en/faq-en/22-faq-mission-features/190-is-this-a-sustainable-mission, April 2013, viewed on 21/06/2013.

[124] Koelle, D. E., *Handbook of cost engineering for space transportation systems with TRANSCOST 7.0 - Statistical-Analytical model for Cost Estimation and Economical Optimization of Launch Vehicles*, TCS-TransCostSystems, 2000.

[125] NASA, "FY 2011 Budget Estimate by Section: Planetary Science," http://www.nasa.gov/pdf/428154main_Planetary_Science.pdf, January 2010.

[126] Panja, T., "FIFA Receivers $1.85 Billion for Television Rights to 2018, 2022 World Cups," http://www.bloomberg.com/news/2011-10-27/fifa-receives-1-85-billion-for-television-rights-to-2018-2022-world-cups.html, October 2011, viewed on 18/06/2013.

[127] "Two tickets to space station go for $40 million," http://edition.cnn.com/2003/TECH/space/12/17/iss.tourists.reut/, 2003, viewed on 18/06/2013.

[128] Elliott, S., "Super Bowl Commercial Time Is a Sellout," http://www.nytimes.com/2013/01/09/business/media/a-sellout-for-super-bowl-commercial-time.html, January 2013, viewed on 04/06/2013.

[129] Panja, T., "Sheikh's Millions Keep Manchester City as Top Soccer Spender," http://www.bloomberg.com/news/2010-09-01/sheikh-s-millions-keep-manchester-city-atop-spending-as-rivals-tighten-up.html, April 2013, viewed on 18/06/2013.

[130] Friedman, U., "The Billionaire Sheikh Who Carved His Name Into an Island," http://www.theatlanticwire.com/global/2011/07/billionaire-sheikh-who-carved-his-name-island/40224/, April 2013, viewed on 18/06/2013.

[131] USA, *Budget of the U.S. Government, Budget of the United States Government, Fiscal Year 2013*, USA, 2012.

[132] ESA, "ESA Budget For 2011," http://download.esa.int/docs/DG/ESA_2011_Budget_040111_rev2.ppt, April 2013, viewed on 04/06/2013.

[133] "A rocket with extra pepperoni," http://news.bbc.co.uk/2/hi/science/nature/463041.stm, October 1999, viewed on 18/06/2013.

[134] "The Mars Initiative," http://marsinitiative.org, 2013, viewed on 21/06/2013.

[135] Lawrie, A., "The Saturn V rocket: a new review of manufacturing, testing, and logistics," *AIAA*, Vol. 5031, July 2006.

[136] "Orion Crew Exploration Vehicle," http://www.nasa.gov/pdf/374566main_072809_HSFR_Constellation_Orion.pdf, July 2009, viewed on 28/07/2009.

[137] International., S., "Quality Management Systems- Requirements for Aviation, Space and Defense Organization," http://standards.sae.org/as9100c/, 2009, viewed on 18/06/2013.

[138] Sinke, J., "AE2207 - Production of Aerospace Systems: Lean Manufacturing & Automation," 2013.

[139] Peddie, M., "NASA's Historic Giant Crawler Gets a Tune Up for Modern Times," http://www.wnyc.org/blogs/transportation-nation/2012/sep/05/nasas-big-rig-and-we-mean-really-big-gets-a-tune-up-pics/, viewed on 05/09/2012.

[140] "Mars One: About the Suppliers," http://mars-one.com/en/partners/suppliers, viewed on 17/06/2013.

[141] ECSS, *Space Project Management: Project Phasing and Planning*, ESA-ESTEC, 1996.

[142] "SpaceX Updates," http://www.spacex.com/updates.php, viewed on 20/06/2013.

[143] Stuster, J., "Space Station Habitability Recommendations Based on a Systematic Comparative Analysis of Analogous Conditions," Tech. rep., National Aeronautics and Space Administration, 1986.

# A | Compliance Matrix

| Code | Description | Value | Unit | Check |
|---|---|---|---|---|
| | **Project** | | | |
| PRO.1 | The in-orbit assembly of all transfer vehicle components shall be designed on a conceptual level | [-] | [-] | ✓ |
| PRO.2 | The Piloted Earth-Mars Transfer Vehicle (PTV) and Mars Lander (ML) shall be designed at Phase-A level as defined by ESA [141] | [-] | [-] | ✓ |
| PRO.3 | A market analysis shall be performed to find funding sources and possible secondary missions to recover parts of cost | [-] | [-] | ✓ |
| PRO.4 | The feasibility study shall be performed within the planned DSE project time frame | 10 | weeks | ✓ |
| PRO.5 | The project shall be executed with respect to stakeholder needs | [-] | [-] | ✓ |
| PRO.6 | All systems shall have a technology readiness level of at least 5 as defined by ESA | [-] | [-] | ✓ |
| | **Orbit** | | | |
| SYS.AS.1 | An Earth orbit suitable for system in-orbit assembly shall be designed | [-] | [-] | ✓ |
| SYS.AS.2 | A proper Mars orbit shall be designed such that ML can decouple from the PTV | [-] | [-] | ✓ |
| SYS.AS.3 | A descent trajectory suitable for descent to the Mars surface shall be designed for the ML | [-] | [-] | ✓ |
| SYS.AS.4 | The orbit shall provide Earth-Mars and Mars-Earth transport | [-] | [-] | ✓ |
| SYS.AS.5 | Transport time shall not exceed the Hohmann transfer time | [-] | [-] | [1] |
| SYS.AS.6 | The PTV shall be launched in a certain launch window | October 2026 | [-] | ✓ |
| | **Control and Navigation** | | | |

[1] Found lowest energy transfer exceeds Hohmann transfer time

| | | | | |
|---|---|---|---|---|
| SYS.CN.1 | The Guidance, Navigation and Control (GNC) system of both ML and PTV shall be autonomous | [-] | [-] | ✓ |
| SYS.CN.2 | The Guidance, Navigation and Control (GNC) system shall be manually controllable | [-] | [-] | ✓ |
| | **Operation** | | | |
| SYS.1.1 | The flight environment for the proposed mission shall be investigated and specified | [-] | [-] | ✓ |
| | **Launcher** | | | |
| SYS.2.1 | The launcher carrying the crew shall be rated for human flight | [-] | [-] | ✓ |
| SYS.2.2 | The launcher carrying the crew and the spacecraft shall be able to insert them into the desired orbit | [-] | [-] | ✓ |
| | **PTV** | | | |
| SYS.3.1 | The PTV shall keep the payload safe | [-] | [-] | ✓ |
| SYS.3.1.1 | The PTV shall provide structural integrity | [-] | [-] | ✓ |
| SYS.3.2 | The PTV shall transport the ML and the payload to Mars | [-] | [-] | ✓ |
| SYS.3.2.1 | The PTV shall be able to control its attitude | $< 0.1$ | deg | ✓ |
| SYS.3.2.2 | The PTV shall be able to determine its position | $< 0.1$ | deg | ✓ |
| SYS.3.2.3 | The PTV shall be able to control its orbit | [-] | [-] | ✓ |
| SYS.3.3 | The PTV shall be compatible for integration with the launcher and the ML | [-] | [-] | ✓ |
| SYS.3.4 | The PTV shall be able to provide communication to Earth ground | [-] | [-] | ✓ |
| | **Mars Lander** | | | |
| SYS.4.1 | The ML shall be compatible for integration with the launcher and the PTV | [-] | [-] | ✓ |
| SYS.4.2 | The ML shall host a crew of 4 people | [-] | [-] | ✓ |
| SYS.4.3 | The ML shall provide life support for the crew | [-] | [-] | ✓ |
| SYS.EN.1 | The ML shall be able to descend from orbit around Mars to the Martian surface | [-] | [-] | ✓ |
| SYS.EN.1.1 | The ML shall land upright | [-] | [-] | ✓ |
| SYS.EN.1.2 | The ML shall impact the Mars surface with a low velocity [105] | $< 2.5$ | m/s | ✓ |
| SYS.EN.1.3 | The ML shall impact the surface of Mars within a certain angle range [105] | $<35$ | deg | ✓ |
| SYS.EN.1.4 | The ML shall be able to land on a Martian sloped surfaces [105] | $<15$ | deg | ✓ |
| SYS.EN.1.5 | The ML shall be able to land on a rock of certain height [105] | 50 | cm | ✓ |
| SYS.CN.3 | The ML shall provide a certain landing accuracy to connect with the base | 7.5 | km | ✓ |
| SYS.4.6 | The ML shall be aerodynamically stable | [-] | [-] | ✓ |
| SYS.4.7 | The ML shall provide structural integrity during entry, descent and landing | [-] | [-] | ✓ |
| SYS.4.8 | The ML shall keep the maximum heatflux into the ML during entry low | $<12216$ | $W/m^2$ | ✓ |

| | | | | |
|---|---|---|---|---|
| SYS.CO.1 | The ML shall provide communication before and after entry with the Mars base | [-] | [-] | ✓ |
| SYS.CO.2 | The ML shall provide communication with the Earth ground control | [-] | [-] | ✓ |
| SYS.4.11 | The ML shall not contaminate the Martian environment irreparably | [-] | [-] | ✓ |
| | **Propulsion** | | | |
| SYS.PR.1 | The propulsion system shall provide a high enough $\Delta V$ necessary to perform the journey | 5136 | m/s | ✓ |
| | **Power** | | | |
| SYS.PO.1 | Sufficient amount of electrical power shall be available to support all subsystems | 3.5 | kW | ✓ |
| SYS.PO.2 | A power storage device shall store sufficient power to support all subsystems in case of power generation system failure | 38 | kWh | ✓ |
| | **Communication** | | | |
| SYS.CO.1 | A link budget shall be established in order to facilitate all planned communication | >30 | Mbits/s | ✓ |
| SYS.CO.2 | All operational parameters shall be sent to the ground center | [-] | [-] | ✓ |
| SYS.CO.3 | Solar conjunctions shall be predicted so that the impact of breaks in the communication can be mitigated. | [-] | [-] | ✓ |
| | **Life Support** | | | |
| SYS.LS.1 | The system shall provide shelter to protect the crew during solar particle events | 0.25 | Sv | ✓ |
| SYS.LS.2 | The system shall provide a sufficient amount of food per day per person [143] | 0.62 | kg | ✓ |
| SYS.LS.3 | The system shall provide sufficient amount of water per person per day [143] | 6.4 | kg | ✓ |
| SYS.LS.4 | The system shall control the internal environment | [-] | [-] | ✓ |
| SYS.LS.4.1 | The system shall keep the pressure within a reasonable limit | 0.101 | MPa | ✓ |
| SYS.LS.4.2 | The system shall keep the temperature within reasonable values [46] | 18-27 | °C | ✓ |
| SYS.LS.5 | The system shall provide enough volume (space) for human activity | 12.2 | $m^3$ | ✓ |
| SYS.LS.5.1 | *"The system shall provide the volume necessary for the crew to perform all mission tasks, using necessary tools and equipment to meet mission goals and objectives."*[46] | 49 | $m^3$ | ✓ |
| SYS.LS.5.2 | *The system shall provide the volume necessary to accommodate the expected number of crewmembers.* [46, 93] | 49 | $m^3$ | ✓ |
| SYS.LS.5.3 | The system shall provide individual sufficient volume/space for private quarters [143] | 2.1 | $m^3$ | ✓ |
| SYS.LS.6 | The system shall manage human waste | 2.25 | $m^3$ | ✓ |
| SYS.LS.7 | The system shall have medical care facilities | [-] | [-] | ✓ |
| | **User Requirements** | | | |
| USE.1.1 | The system shall provide transportation capabilities for 4 persons, adjusted to the client wishes and reviewed according to Mars base capacity | [-] | [-] | ✓ |

| | | | | |
|---|---|---|---|---|
| USE.1.2 | After two resupply missions separated by a maximum of three years the base shall be self-sustaining | [-] | [-] | ✓ |
| USE.2.1 | The minimum feasible mission mass shall be investigated | 138740 | kg | ✓ |
| USE.2.2 | The minimum feasible mission volume shall be investigated | 49 | $m^3$ | ✓ |
| USE.2.3 | The minimum feasible mission power required shall be investigated | 3 | kW | ✓ |
| USE.3.1 | Critical failure and single point failure shall be avoided | [-] | [-] | ✓ |
| USE.3.2 | Supply stocks shall be maintained for a minimum of 10 years, after which the base will be self-sustaining | [-] | [-] | [2] |
| USE.SU.1 | The risk of contamination of Mars environment by PTV and ML shall be kept as low as reasonably achievable | [-] | [-] | ✓ |
| USE.SU.2 | The PTV shall be capable of being reused twice | [-] | [-] | [3] |
| USE.SU.3 | The ML shall have multi-purpose capabilities when reaching Mars base | [-] | [-] | ✓ |
| USE.SU.4 | All non-reusable hardware shall be disposed in a sustainable way | [-] | [-] | ✓ |
| | **PTV** | | | |
| USE.5.1 | The PTV shall be able to complete 3 missions | [-] | [-] | [4] |
| USE.PR.1 | The propulsion system shall not compromise mission success and crew safety | [-] | [-] | ✓ |
| USE.PR.1.1 | The propulsion system shall not emit harmful levels of radiation throughout the mission duration | <0.3 | Sv | ✓ |
| USE.PR.1.2 | The propulsion system shall not interact with other subsystems in a way that could result in malfunction of any of the subsystems | [-] | [-] | ✓ |
| USE.CO.1 | All recorded video footage shall be sent to the ground center | [-] | [-] | ✓ |
| USE.CO.2 | The crew shall be able to communicate with the ground center | [-] | [-] | ✓ |
| USE.LS.1 | The crew shall be able to exercise to counteract the effects of microgravity | [-] | [-] | ✓ |

[2]Supplies carried with the PTV are for the transfer time + 30% contingency
[3]PTV designed as single use vehicle, partially reused as a communications relay satellite
[4]PTV designed as single use vehicle

# B | Communication Flow Diagram

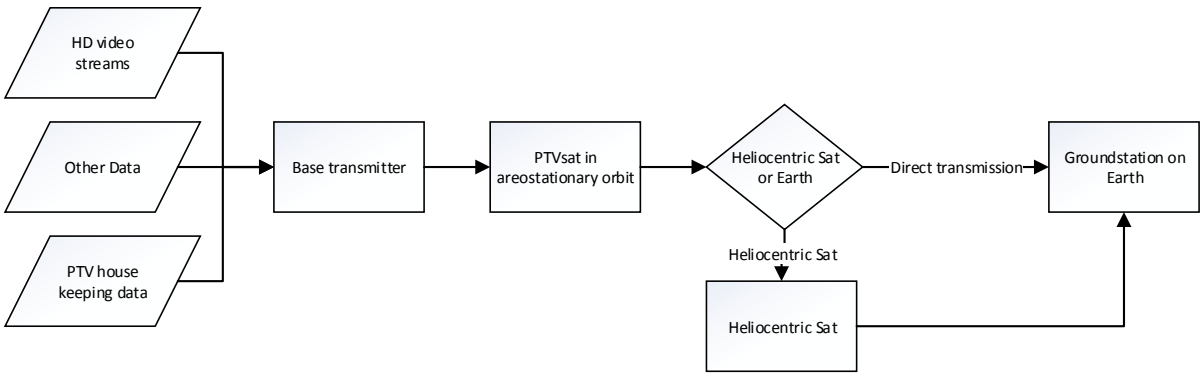


Figure B.1: Communication Flow Diagram

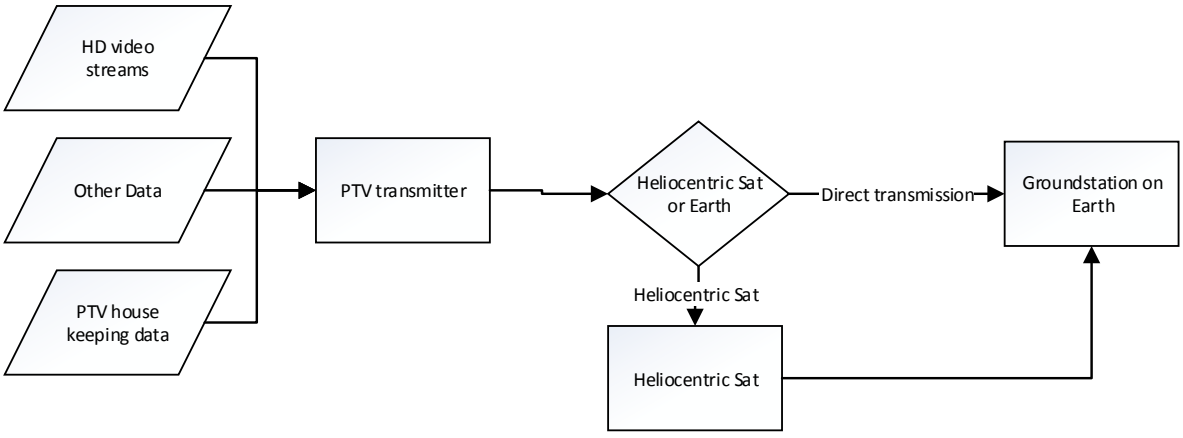


Figure B.2: Communication Flow Diagram PTV